

THE USE OF STATIC FREQUENCY CONVERTER  
FEEDER STATIONS AND A NEW CONTROL STRATEGY  
ENABLING MESH FEEDING FOR 50 HZ AC  
RAILWAYS



by

DELARAM SHARIFI

A thesis submitted to the University of Birmingham for the degree of

DOCTOR OF PHILOSOPHY

Birmingham Centre for Rail Research and Education

School of Engineering

College of Engineering and Physical Sciences

University of Birmingham

September 2020

UNIVERSITY OF  
BIRMINGHAM

**University of Birmingham Research Archive**

**e-theses repository**

This unpublished thesis/dissertation is copyright of the author and/or third parties. The intellectual property rights of the author or third parties in respect of this work are as defined by The Copyright Designs and Patents Act 1988 or as modified by any successor legislation.

Any use made of information contained in this thesis/dissertation must be in accordance with that legislation and must be properly acknowledged. Further distribution or reproduction in any format is prohibited without the permission of the copyright holder.

# ABSTRACT

Railways around the globe are rapidly growing as the passenger numbers surge due to the increasing requirements for connectivity and cleaner methods for transport. To accommodate the current and future demand, new and existing lines are being built and updated. Electrification has been identified as key to achieve sustainable railways, yet solutions have remained unchanged for decades. Although efficient, conventional electrification systems are inflexible and limit the application of multi-source power solutions.

Static Frequency Converters (SFCs) are an alternative to conventional transformer-based electrification systems which provide a more highly interconnected electrification solution, due to their controllability, which potentially allows increased operational flexibility and robustness. Early static converter deployments for 16.7 Hz supplies the potential for dual-end feeding, however, due to the novelty of the SFC technology and its application to railways, a full mesh-feeding solution has not yet been explored.

In this thesis, the author considers the deployment of SFC technologies within the 50 Hz, 25 kV, railway and the application of smart control strategies in deploying the mesh feeding concept. Comparative studies using mathematical models and computational simulations representing the electrification infrastructure and the moving trains have been carried out, in considerable detail, using code written in MATLAB Script.

The mathematical modelling of the traction system is based on a lumped parameter modelling approach. These studies show that the application of SFCs requires lower rated feeder stations and provides increased operational flexibility and fault tolerance, while not suffering from the power quality issues associated with conventional transformer-based systems. In optimised deployments, SFC feeder station ratings and transmission losses can be reduced even further. Additionally, it has been shown that the use of a smart control system for mesh feeding increases flexibility in the locations available for efficient deployment of the feeder stations.

An economic evaluation has demonstrated that SFCs are financially beneficial over a 50-year lifespan, with the novel control system introduced in this thesis proving beneficial, both economically and technically. As the technology is evolving, it is anticipated that economic and operational benefits will increase, and the flexibility associated with SFC solutions is expected to support advances in wider railway electrification, including the deployment of railway smart grids. A roadmap anticipating the wider technology development is therefore also presented.

# ACKNOWLEDGMENTS

What I have learnt during the past few years is that doing a PhD is not only about academic tasks, it is a long and emotionally challenging marathon which requires endurance as well as confidence and above all, it is not achievable alone. Whether it is scientific help, guidance, encouragement, pushes, or even a smile, without people's light, it is impossible to reach the end of the tunnel. What I have taken out of this PhD, is appreciation of the sheer number of beautiful souls I have in my life, who would inspire me to push on, hold my hand when I was about to fall and reassure me when I doubted myself. I will forever remember every drop of their kindness and compassion. It is impossible to mention them all, but it does not mean that I will not try.

First of all, thank you to BCRRE, my second family, where everyone is a sea of energy and encouragement, where nothing is impossible and there is always laughter, hugs and tea, even when the world is dark and stressful.

Thanks to my colleagues at Atkins, for their kind encouragement, support and appreciation of the difficulties of writing up at the same time as working.

Thanks to Dr Paul Weston for his kindness to share his unlimited, eternal wisdom with me, and every other soul who has ever needed it.

Thanks to Professor Felix Schmid, for his incredibly valuable advice throughout my PhD, and for his genuine love and care in teaching, not only in academia, but in how to be a real engineer.

Thanks to Mr Ross MacFarlane, Mr Chris Wilson, Mr Gary Keenor, Mr David Atkey and Mr Alan Hodge for their valuable time and input into the economic analysis Chapter.

Thanks to my supervisors, Dr Pietro Tricoli and Dr Stuart Hillmansen for guiding me through these years and making me a stronger person.

Thanks to my sister, Delafarin, Mrs Rachael Roberts, Dr Narges Mahpeykar and Mr Phil Atkins for keeping me sane and being the glue whenever my confidence was shattered.

Thanks to Mr Sean McCabe and Mrs Mia Kalogjera for doing absolutely everything in their power to make me happy and keep me going, even if what it took was lighting a big fire at every possible opportunity.

Thanks to Mrs Carole Stewart for her warm and loving support and to Mr Roger Stewart for his encouragement and constantly reminding me of the joy of graduation, the space for my photo on his wall of fame and that he wants a copy of my thesis for his book shelf (great ...).

Thanks to my parents, for their unconditional love and support, making me believe that I could do anything I set my mind to, for teaching me never to let society's stereotypes define who I am and for encouraging my love for maths, physics and engineering since I was a child.

And last but not least, thanks to my Fiancé, Dr Edward Stewart, for his infinite love and tireless support at every step of the way, for his patience in going through my panics, doubts and stress many times, for nourishing and inspiring me to thrive, and for his presence, which warms my heart in the coldest, darkest nights.

*“There is nothing in machinery, there is nothing in embankments and railways and iron bridges and engineering devices to oblige them to be ugly. Ugliness is the measure of imperfection.”*

*H. G. Wells*

## CONTENTS

<b>1 INTRODUCTION</b>	<b>1</b>
1.1 HYPOTHESIS	6
1.2 PERSPECTIVES	6
1.3 APPROACH	7
1.4 THESIS STRUCTURE	8
<b>2 REVIEW OF CURRENT RAILWAY ELECTRIFICATION SCHEMES</b>	<b>10</b>
2.1 DC ELECTRIFICATION	11
2.2 AC ELECTRIFICATION	12
2.2.1 <i>Transformers</i>	13
2.2.1.1 Rail Return System	13
2.2.1.2 Booster Transformer System	14
2.2.1.3 Autotransformer System	14
2.2.1.4 Problems Associated With Transformer Systems	15
2.2.1.4.1 Imbalance	15
2.2.1.4.2 Harmonics	17
2.2.1.4.3 Reactive Power Injection	18
2.2.1.4.4 Arcing	18
2.2.1.5 State-of-the-Art Solutions for Transformer-Based Traction Issues	19
2.2.1.6 Power Quality Conclusion	24
2.2.2 <i>Converters</i>	25
2.2.2.1 Structure of Static Converter Feeder Stations	27
2.2.3 <i>PWM Generation</i>	29
2.2.3.1 Inverter Interconnection Control	32
2.2.4 <i>SFCs vs Transformers</i>	34
2.3 CONCLUSIONS	36
<b>3 MODELLING AND CONTROL OF THE AC RAILWAY SYSTEM</b>	<b>38</b>

3.1 MATHEMATICAL MODELLING OF ELECTRIFICATION INFRASTRUCTURE	41
3.1.1 <i>Electrification Infrastructure</i>	42
3.1.1.1 Power Flow Equations	45
3.1.2 <i>Modelling of the AT System</i>	47
3.1.2.1 Effect of ATs on the Admittance Matrix	50
3.1.3 <i>Modelling of the SFC System</i>	51
3.1.4 <i>Power Flow Solution</i>	52
3.2 CONTROL OF SFCs	53
3.2.1 <i>Active Power Control</i>	54
3.2.2 <i>Reactive Power Control</i>	56
3.3 CONTROL METHOD	57
3.3.1 <i>Equal Share of Active and Reactive Power</i>	59
3.4 SUMMARY	61
<b>4 SIMULATIONS OF SFCs FOR AC RAILWAYS AND COMPARISON WITH AT SYSTEMS</b>	<b>62</b>
4.1 INTRODUCTION	63
4.2 LINE CONFIGURATION: TRANSFORMER-BASED ELECTRIFICATION SYSTEM WITH AUTOTRANSFORMERS	63
4.3 LINE CONFIGURATION: SFC-BASED ELECTRIFICATION SYSTEM	64
4.4 TRAIN ACCELERATION, SPEED, POWER AND TIMETABLE	66
4.5 ENERGY LOSS AND SYSTEM EFFICIENCY	69
4.5.1 <i>Energy Loss</i>	69
4.5.2 <i>System Efficiency</i>	71
4.6 VOLTAGE LIMITS	72
4.7 DEMONSTRATION WITH SINGLE-TRAIN EXAMPLES	73
4.7.1 <i>Single Train with Constant Power</i>	74
4.7.1.1 Active Power Profile for a Single Train With Constant Power	74
4.7.1.1.1 AT System	74
4.7.1.1.2 Synchronised Control of SFCs	76
4.7.1.1.3 Equally Shared Power Control of SFCs	78

4.7.1.2 Reactive Power Profile for a Single Train with Constant Power	79
4.7.1.2.1 AT System	79
4.7.1.2.2 Synchronised Control of SFCs	81
4.7.1.2.3 Equally Shared Power Control of SFCs	82
<b>4.7.2 Single Train with Variable Power</b>	<b>83</b>
4.7.2.1 Active Power Profile for a Single Train with Variable Power	83
4.7.2.1.1 AT System	83
4.7.2.1.2 Synchronised Control of SFCs	85
4.7.2.1.3 Equally Shared Power Control of SFCs	86
4.7.2.2 Reactive Power Profile	88
4.7.2.2.1 AT System	88
4.7.2.2.2 Synchronised Control of SFCs	89
4.7.2.2.3 Equally Shared Power Control of SFCs	90
<b>4.8 CONCLUSIONS</b>	<b>91</b>

## **5 A STUDY OF THE COMPARATIVE PERFORMANCE OF SFC AND AT SYSTEMS FOR A HEAVILY USED HIGH-SPEED**

<b>RAILWAY</b>	<b>93</b>
5.1 INTRODUCTION	94
5.2 VARIABLE POWER / FULL TIMETABLE CASE	96
5.2.1 Active Power	97
5.2.1.1 AT System	97
5.2.1.2 Synchronised Control of SFCs	97
5.2.1.3 Shared Power Control of SFCs	98
5.2.2 Reactive Power	99
5.2.2.1 AT System	99
5.2.2.2 Synchronised control of SFCs	100
5.2.2.3 Shared Power Control of SFCs	101
5.2.3 Apparent Power	102
5.2.4 Voltage Profiles	104
5.2.5 Power Losses	106

5.2.6 Discussion	108
5.3 WORST-CASE SCENARIO	110
5.3.1 Active Power	111
5.3.1.1 AT System	111
5.3.1.2 Synchronised Control of SFCs	112
5.3.1.3 Equally Shared Power Control of SFCs	113
5.3.2 Reactive Power	114
5.3.3 Apparent Power	116
5.3.4 Discussion	118
5.4 CONCLUSIONS	119
<b>6 ANALYSIS OF THE EFFECT OF THE NUMBER OF, AND DISTANCE BETWEEN, SFC FEEDER STATIONS ON SYSTEM PERFORMANCE</b>	<b>121</b>
6.1 INTRODUCTION	122
6.2 NUMBER OF FEEDER STATIONS AND THEIR ARRANGEMENT	124
6.3 LOAD AND CONTROL CONFIGURATIONS	126
6.4 RESULTS	127
6.4.1 Maximum Apparent Power	127
6.4.1.1 Constant Power	127
6.4.1.1.1 Constant Power – Synchronised Control SFC System	128
6.4.1.1.2 Constant Power – Equally Shared Active and Reactive Powers	129
6.4.1.1.3 Constant Power – Comparison of Synchronised and Equally Shared Active and Reactive Powers	129
6.4.1.2 Variable Power	131
6.4.1.2.1 Variable Power – Synchronised Control SFC System	131
6.4.1.2.2 Variable Power – Equally Shared Active and Reactive Powers	132
6.4.1.2.3 Variable Power – Comparison of Synchronised and Equally Shared Active and Reactive Powers	133
6.4.2 Transmission Losses	135
6.4.2.1 Constant Power	135
6.4.2.1.1 Constant Power – Synchronised Control SFC System	135

6.4.2.1.2 Constant Power – Equally Shared Active and Reactive Power	136
6.4.2.1.3 Constant Power – Comparison of Synchronised and Equally Shared Active and Reactive Powers	137
6.4.2.2 Variable Power	138
6.4.2.2.1 Variable Power – Synchronised Control SFC System	138
6.4.2.2.2 Variable Power – Equally Shared Active and Reactive Power	139
6.4.2.2.3 Variable Power – Comparison of Synchronised and Equally Shared Active and Reactive Powers	140
<i>6.4.3 System Efficiency</i>	<i>141</i>
6.4.3.1 Constant Power	141
6.4.3.2 Variable Power	142
6.5 CONCLUSIONS	143
<b>7 ECONOMIC ANALYSIS</b>	<b>145</b>
7.1 INTRODUCTION	146
7.2 EVALUATION OF BENEFITS	148
7.3 SCENARIOS CONSIDERED	151
7.4 COST ANALYSIS	151
7.5 COST ANALYSIS USING DISCOUNTING TECHNIQUE	157
7.6 CONCLUSIONS	160
<b>8 RAILWAY SMART GRID TECHNOLOGY ROADMAP</b>	<b>162</b>
8.1 INTRODUCTION	163
8.2 POWER ELECTRONICS	166
8.3 SFCs	166
8.4 RENEWABLE ENERGY	168
8.5 ENERGY STORAGE	169
8.6 SMART GRID	170
8.7 CONCLUSIONS	171
<b>9 CONCLUSION</b>	<b>172</b>
<b>10 REFERENCES</b>	<b>179</b>



# LIST OF TABLES

TABLE 1 ELECTRIFICATION PARAMETERS	43
TABLE 2: TRANSFORMER POSITIONS ALONG THE LINE	64
TABLE 3: SFC POSITIONS ALONG THE LINE	66
TABLE 4 CLASS 390 PENDOLINO PARAMETER VALUES USED FOR DAVIS EQUATION	67
TABLE 5 SUMMARY OF RESULTS FROM THE STUDY ON TRANSFORMER-BASED AND SFC-BASED SYSTEMS	109
TABLE 6 SUMMARY OF RESULTS FROM THE WORST-CASE SCENARIO STUDY ON TRANSFORMER-BASED AND SFC-BASED SYSTEMS	119
TABLE 7 LOCATION AND SEPARATION OF SFCs FOR THREE-SFC ARRANGEMENTS	124
TABLE 8 LOCATION AND SEPARATION OF SFCs FOR FOUR-SFC ARRANGEMENTS	124
TABLE 9 LOCATION AND SEPARATION OF SFCs FOR FIVE-SFC ARRANGEMENTS	125
TABLE 10 LOCATION AND SEPARATION OF SFCs FOR SIX-SFC ARRANGEMENTS	125
TABLE 11 LOCATION AND SEPARATION OF SFCs FOR SEVEN-SFC ARRANGEMENTS	125
TABLE 12 COLOUR CODING FOR NUMBER OF SFC FEEDER STATIONS	127
TABLE 13 CAPITAL COSTS FOR INSTALLATION OF AT AND SFC SYSTEMS	154
TABLE 14 OPERATIONAL COSTS FOR AT AND SFC SYSTEMS	155

# LIST OF FIGURES

FIGURE 1 SINGLE-PHASE CONNECTION	16
FIGURE 2 V-V CONNECTION	19
FIGURE 3 SCOTT CONNECTION	20
FIGURE 4 LEBLANC CONNECTION	21
FIGURE 5 DIAGRAM FOR A CYCLO-CONVERTER	26
FIGURE 6 MODULAR MULTI-LEVEL CONVERTER CIRCUIT DIAGRAM WITH HALF-BRIDGE SUBMODULES	29
FIGURE 7 GENERAL SCHEMATIC DIAGRAM FOR THE LUMPED PARAMETER MODEL	45
FIGURE 8 POWER FLOW EXAMPLE	46
FIGURE 9 SCHEMATIC DIAGRAM OF AT SYSTEM BASED ON THE LUMPED PARAMETER MODEL	48
FIGURE 10 SCHEMATIC DIAGRAM OF AT CONNECTIONS	49
FIGURE 11 SCHEMATIC DIAGRAM OF THE SFC SYSTEM BASED ON THE LUMPED PARAMETER MODEL	52
FIGURE 12 SCHEMATIC DIAGRAM FOR TWO SUBSTATIONS FEEDING A LOAD	53
FIGURE 13 SCHEMATIC OF THE COMMUNICATION SYSTEM BETWEEN THE FEEDER STATIONS	58
FIGURE 14 BLOCK DIAGRAM OF THE CLOSED-LOOP CONTROLLER FOR DETERMINATION OF THE REFERENCE VOLTAGES OF THE FEEDER STATIONS — ACTIVE POWER	60
FIGURE 15 BLOCK DIAGRAM OF THE CLOSED-LOOP CONTROLLER FOR DETERMINATION OF THE REFERENCE VOLTAGES OF THE FEEDER STATIONS — REACTIVE POWER	60
FIGURE 16 AT SYSTEM ARRANGEMENT OF THE LINE	64
FIGURE 17 ARRANGEMENT OF SFC FEEDER STATIONS	65
FIGURE 18 TIME-DISTANCE GRAPH OF TRAIN SERVICE	68
FIGURE 19 SFC EFFICIENCY CURVES PLOTTED FOR PF 0.9 AND PF 1	71
FIGURE 20 SINGLE-TRAIN WITH CONSTANT POWER, ACTIVE POWER PROFILE FOR THE AT SYSTEM SCENARIO	75

FIGURE 21 SINGLE-TRAIN WITH CONSTANT POWER, ACTIVE POWER PROFILE FOR THE SYNCHRONISED CONTROL SFC SYSTEM SCENARIO	77
FIGURE 22 SINGLE-TRAIN WITH CONSTANT POWER, ACTIVE POWER PROFILE FOR THE EQUALLY SHARED CONTROL SFC SYSTEM SCENARIO	79
FIGURE 23 SINGLE-TRAIN WITH CONSTANT POWER, REACTIVE POWER PROFILE FOR THE AT SYSTEM SCENARIO	81
FIGURE 24 SINGLE-TRAIN WITH CONSTANT POWER, REACTIVE POWER PROFILE FOR THE SYNCHRONISED CONTROL SFC SYSTEM SCENARIO	82
FIGURE 25 SINGLE-TRAIN WITH CONSTANT POWER, REACTIVE POWER PROFILE FOR THE EQUALLY SHARED CONTROL SFC SYSTEM SCENARIO	83
FIGURE 26 SINGLE-TRAIN WITH VARIABLE POWER, ACTIVE POWER PROFILE FOR THE AT SYSTEM SCENARIO	85
FIGURE 27 SINGLE-TRAIN WITH VARIABLE POWER, ACTIVE POWER PROFILE FOR THE SYNCHRONISED CONTROL SFC SYSTEM SCENARIO	86
FIGURE 28 SINGLE-TRAIN WITH VARIABLE POWER, ACTIVE POWER PROFILE FOR THE EQUALLY SHARED CONTROL SFC SYSTEM SCENARIO	88
FIGURE 29 SINGLE-TRAIN WITH VARIABLE POWER, REACTIVE POWER PROFILE FOR THE AT SYSTEM SCENARIO	89
FIGURE 30 SFC SINGLE-TRAIN WITH VARIABLE POWER, REACTIVE POWER PROFILE FOR SYNCHRONISED CONTROL SFC SYSTEM SCENARIO	90
FIGURE 31 SINGLE-TRAIN WITH VARIABLE POWER, REACTIVE POWER PROFILE FOR THE EQUALLY SHARED CONTROL SFC SYSTEM SCENARIO	91
FIGURE 32 ACTIVE POWER FOR THE AT SYSTEM WITH FULL TIMETABLE AND VARIABLE POWER	97
FIGURE 33 ACTIVE POWER FOR THE SYNCHRONISED CONTROL SFC SYSTEM WITH FULL TIMETABLE AND VARIABLE POWER	98

FIGURE 34 ACTIVE POWER FOR THE EQUALLY SHARED POWER SFC SYSTEM WITH FULL TIMETABLE AND VARIABLE POWER	99
FIGURE 35 REACTIVE POWER FOR THE AT SYSTEM WITH FULL TIMETABLE AND VARIABLE POWER	100
FIGURE 36 REACTIVE POWER FOR THE SYNCHRONISED SFC SYSTEM WITH FULL TIMETABLE AND VARIABLE POWER	100
FIGURE 37 REACTIVE POWER FOR THE EQUALLY SHARED POWER SFC SYSTEM WITH FULL TIMETABLE AND VARIABLE POWER	101
FIGURE 38 APPARENT POWER FOR THE AT SYSTEM WITH FULL TIMETABLE AND VARIABLE POWER	102
FIGURE 39 APPARENT POWER FOR THE SYNCHRONISED SFC SYSTEM WITH FULL TIMETABLE AND VARIABLE POWER	103
FIGURE 40 APPARENT POWER FOR THE EQUALLY SHARED POWER SFC SYSTEM WITH FULL TIMETABLE AND VARIABLE POWER	103
FIGURE 41 NODAL VOLTAGE PROFILE FOR THE AT SYSTEM WITH FULL TIMETABLE AND VARIABLE POWER	104
FIGURE 42 NODAL VOLTAGE PROFILE FOR THE SYNCHRONISED SFC SYSTEM WITH FULL TIMETABLE AND VARIABLE POWER	105
FIGURE 43 NODAL VOLTAGE PROFILE FOR THE EQUALLY SHARED POWER CONTROL SFC SYSTEM WITH FULL TIMETABLE AND VARIABLE POWER	105
FIGURE 44 TRANSMISSION POWER LOSS FOR THE AT SYSTEM WITH FULL TIMETABLE AND VARIABLE POWER	106
FIGURE 45 TRANSMISSION POWER LOSS FOR THE SYNCHRONISED SFC SYSTEM WITH FULL TIMETABLE AND VARIABLE POWER	107
FIGURE 46 TRANSMISSION POWER LOSS FOR THE EQUALLY SHARED POWER SFC SYSTEM WITH FULL TIMETABLE AND VARIABLE POWER	107

FIGURE 47 ACTIVE POWER FOR THE AT SYSTEM SCENARIO WITH FULL TIMETABLE AND CONSTANT MAXIMUM	
POWER	111
FIGURE 48 ACTIVE POWER FOR THE SYNCHRONISED SFC SYSTEM WITH FULL TIMETABLE AND CONSTANT	
MAXIMUM POWER	113
FIGURE 49 ACTIVE POWER FOR THE SHARED SFC SYSTEM WITH FULL TIMETABLE AND CONSTANT MAXIMUM	
POWER	113
FIGURE 50 REACTIVE POWER FOR THE AT SYSTEM WITH FULL TIMETABLE AND CONSTANT MAXIMUM POWER	115
FIGURE 51 REACTIVE POWER FOR THE SYNCHRONISED SFC SYSTEM WITH FULL TIMETABLE AND CONSTANT	
MAXIMUM POWER	115
FIGURE 52 REACTIVE POWER FOR THE SHARED SFC SYSTEM WITH FULL TIMETABLE AND CONSTANT MAXIMUM	
POWER	116
FIGURE 53 APPARENT POWER FOR THE AT SYSTEM WITH FULL TIMETABLE AND CONSTANT MAXIMUM POWER	
	117
FIGURE 54 APPARENT POWER FOR THE SYNCHRONISED SFC SYSTEM WITH FULL TIMETABLE AND CONSTANT	
MAXIMUM POWER	117
FIGURE 55 APPARENT POWER FOR THE SHARED SFC SYSTEM WITH FULL TIMETABLE AND CONSTANT	
MAXIMUM POWER	118
FIGURE 56 MAXIMUM APPARENT POWER FOR CONSTANT POWER LOADS USING THE SYNCHRONISED CONTROL	
SFC SYSTEM	128
FIGURE 57 MAXIMUM APPARENT POWER FOR CONSTANT POWER LOADS USING THE EQUALLY SHARED	
CONTROL SFC SYSTEM	129
FIGURE 58 MAXIMUM APPARENT POWER FOR CONSTANT POWER LOADS USING BOTH SFC CONTROL	
STRATEGIES ('●' SYNCHRONISED, 'x' EQUALLY SHARED)	130

FIGURE 59 MAXIMUM APPARENT POWER FOR VARIABLE POWER LOADS USING THE SYNCHRONISED CONTROL SFC SYSTEM	132
FIGURE 60 MAXIMUM APPARENT POWER FOR VARIABLE POWER LOADS USING THE EQUALLY SHARED CONTROL SFC SYSTEM	133
FIGURE 61 MAXIMUM APPARENT POWER FOR VARIABLE POWER LOADS USING BOTH SFC CONTROL STRATEGIES ('●' SYNCHRONISED, 'x' EQUALLY SHARED)	134
FIGURE 62 TOTAL TRANSMISSION ENERGY LOSS FOR CONSTANT POWER LOADS USING THE SYNCHRONISED CONTROL SFC SYSTEM	135
FIGURE 63 TOTAL TRANSMISSION ENERGY LOSS FOR CONSTANT POWER LOADS USING THE EQUALLY SHARED CONTROL SFC SYSTEM	136
FIGURE 64 TOTAL TRANSMISSION ENERGY LOSS FOR CONSTANT POWER LOADS USING BOTH SFC CONTROL STRATEGIES ('●' SYNCHRONISED, 'x' EQUALLY SHARED)	137
FIGURE 65 TOTAL TRANSMISSION ENERGY LOSS FOR VARIABLE POWER LOADS USING THE SYNCHRONISED CONTROL SFC SYSTEM	138
FIGURE 66 TOTAL TRANSMISSION ENERGY LOSS FOR VARIABLE POWER LOADS USING THE EQUALLY SHARED CONTROL SFC SYSTEM	139
FIGURE 67 TOTAL TRANSMISSION ENERGY LOSS FOR VARIABLE POWER LOADS USING BOTH SFC CONTROL STRATEGIES ('●' SYNCHRONISED, 'x' EQUALLY SHARED)	140
FIGURE 68 SYSTEM EFFICIENCY FOR CONSTANT POWER LOADS USING BOTH SFC CONTROL STRATEGIES ('●' SYNCHRONISED, 'x' EQUALLY SHARED)	141
FIGURE 69 SYSTEM EFFICIENCY FOR VARIABLE POWER LOADS USING BOTH SFC CONTROL STRATEGIES ('●' SYNCHRONISED, 'x' EQUALLY SHARED)	142
FIGURE 70 CAPITAL AND CUMULATIVE ANNUAL OPERATION COST	157

FIGURE 71 CAPITAL AND CUMULATIVE ANNUAL OPERATION COST WITH CURRENT DISCOUNT RATES (3.5%)	159
FIGURE 72 CAPITAL AND CUMULATIVE ANNUAL OPERATION COST WITH HISTORIC DISCOUNT RATES (7.5%)	160
FIGURE 73 POTENTIAL ROADMAP FOR THE ADOPTION OF A RAILWAY SMART GRID	165

## ABBREVIATIONS

Name	Description
AC	Alternating Current
APQC	Active Power Quality Conditioner
AT	Autotransformer
ATF	Autotransformer Feeders
BT	Booster Transformer
CAPEX	Capital Expenditure
CD	Carrier-Disposition
DC	Direct Current
GPS	Global Positioning System
GTO	Gate Turn-Off
HBRPC	Half-Bridge RPC
HELM	Holomorphic Embedding Load-Flow Method
HPQC	Hybrid Power Quality Conditioner
IGBT	Insulated-Gate Bipolar Transistors
IGCT	Integrated Gate Commutated Thyristor
LQI	Linear Quadratic Integrator
MMC	Modular Multi-level Converters
MOSFET	Metal Oxide Semiconductor Field-Effect Transistors

NPC	Neutral-Point Clamped
NPV	Net Present Value
NSC	Negative-Sequence Component
OCS	Overhead Contact System
OHL(E)	Overhead Line (Electrification)
OPEX	Operating Expenses
PI	Proportional Integral
PR	Proportional Resonant
PSC	Positive-Sequence Component/ Phase-Shifted Carrier
PWM	Pulse-Width Modulation
RC	Return Conductor
RPC	Railway Power Conditioner
SFC	Static Frequency Converter
STATCOM	Static Synchronous Compensator
SVC	Static VAR Compensator
TCS	Thyristor-Controlled Susceptance
THD	Total Harmonic Distortion
VSI	Voltage Source Inverter

# VARIABLES

Name	Definition and Units
A	Mass resistance coefficient of mechanical resistance (N)
B	Mechanical resistance coefficient, braking force (N s/m, or kg/s)
C	Aerodynamic resistance coefficient (N S <sup>2</sup> /m <sup>2</sup> , or kg/m)
CF	Cash Flow (£)
D	Drag (N)
e	Error
f	Acceleration (m/s <sup>2</sup> )
F	Force (N)
g	Standard acceleration due to gravity (m/s <sup>2</sup> )
I	Current (A)
$K_i$	Integral Gain
$K_p$	Proportional gain
M	Mass (g)
P	Active Power (W)
Q	Reactive power (var)
R	Resistance ( $\Omega$ )
S	Apparent power (VA)
T	Tractive effort (N)
V	Voltage (V)

V	Velocity (m/s)
Y	Admittance (S)
Z	Impedance ( $\Omega$ )
A	Gradient (rad or $^\circ$ )
$\eta$	Efficiency (%)

# 1 INTRODUCTION

From relatively early in the existence of the railway, electrical power was identified as a viable means of powering locomotives, with the German inventor Werner von Siemens demonstrating the first electric railway in 1879, using third-rail current collection at 150 V DC. Volk's Electric Railway in Brighton opened in 1883 as a novelty using the same technology and still operates in 2020 (Schmid et al., 2017). The City and South Railway (now part of the London Underground's Northern Line) was the first commercial electric railway, starting operation in 1890; however, it was originally designed as a cable-hauled railway with electric traction. The first railway designed from the ground up to be electrically powered was the Liverpool Overhead Railway, running first in 1893 (RSSB, 2007).

Due to the limitations of the electric machines available at the time, these railways were DC-powered, albeit using differing voltages and current collection arrangements (525 V DC from a third rail for the Liverpool Overground, 50 V DC through the running rails for Volk's Electric Railway, from 1883 to 1886, then later 160 V through an off-side third rail, and 500 V DC by means of an inside track third rail for the City and South Railway). In an attempt to prevent further fragmentation of the railway network, the government mandated the use of 1500 V DC overhead lines as the standard for railway electrification, but compliance with this was limited. The Southern Railways, in the period up to World War II, adopted a 660 V DC and 750 V DC third-rail system and used this to great effect to extend their network south of London, effectively as a metro. The Network was later converted to 750 V DC.

Post-war, the government accepted the existence of both third rail DC and overhead lines and the nationalised British Railways expanded electrification of the network using all three technologies. This co-existence was short lived, however, and in 1956 British Railways adopted 25 kV AC overhead line electrification as the standard for all new projects, except for those which were extensions or improvements of existing systems.

During the British Rail era in the 1970s, large sections of the intercity mainlines were electrified, with the West Coast Main Line being completed in 1974, Great Eastern Main Line being completed in 1980, and the East Coast Main Line being electrified in two parts – from 1975–1978 running from London to Royston and from 1984–1991 extending electrification of the line as far as Edinburgh.

Currently, railways worldwide are enjoying a period of growth and experiencing a surge in both the number of passengers and the volume of freight carried. In many countries, this means putting additional strain on already heavily loaded infrastructure. In addition to growth through the construction of extra lines, there is a push to achieve greater capacity utilisation on the existing network. The UK Railway Technical Strategy and Rail Sector Deal describe an improvement in railway capacity as one of ‘The Four C’s’, alongside carbon, customer and cost. For heavily used lines, electrification has been identified as an essential tool in attaining improvements in all four of these areas.

Currently, efforts are underway to electrify both the Great Western Main Line and the Trans-Pennine Line (as part of the wider Northern Hub initiative). Electrification does not stop at electrifying existing railway lines and there are new electrified lines being built around the UK and elsewhere in the world, such as High Speed 2 in the UK, and the Lyon–Turin LGV currently in place between France and Italy.

In addition to the high-level objective described above, the drive for electrification of the railways has come from three major motivations:

- **Power** – Electric trains are, in general, more powerful and responsive than their diesel counterparts due to the efficiencies present in electrical motors compared to their diesel counterparts, in particular their ability to generate full torque at 0 RPM. Most modern diesel trains (such as the British Rail Class 68 or 220) are diesel–electric trains, using the diesel engine purely as an electrical generator and electric motors for traction.
- **Logistics** – Electric trains are not limited in range by the volume of fuel they can carry, or in power by the rating of the diesel engine. Due to this, electric locomotives are used almost exclusively on the highest-speed passenger lines, where high power is essential. In addition, not having to carry large fuel loads and their simpler drive trains in comparison to a diesel (or diesel–electric) train mean that the trains are lighter and consequently produce less track wear.
- **Environmental** – Electric trains have the significant advantage that they are decoupled from their power supply, meaning that a railway network powered by fossil fuels can be converted easily to more environmentally friendly power generation, with no need to reconfigure the

trains, while diesel trains also require dedicated infrastructure for fuelling, along with the environmental impacts of diesel exhausts.

In addition to this, there are benefits from electric trains having their power sources away from the traction unit, particularly for usage within the tight confines of underground systems or long tunnels. This also provides the additional benefit of reducing noise pollution from the trains for residents living near the rail network.

In February 2018, the UK government announced a target to phase out diesel-only trains by 2040 (Rail Industry Decarbonisation Taskforce, 2019) as part of the UK's wider commitments, to the 2016 Paris Climate Agreement within the United Nations Framework Convention on Climate Change (United Nations, 2015). While shorter or lightly loaded railway networks, or those with limited passenger numbers, may benefit from vehicle-borne traction sources, such as batteries or hydrogen to replace the diesel units, mainline operation will undoubtedly adopt electrification to meet these targets. In order to do this, the rail industry will need to make extensive use of renewable energy as the primary source supplying the electrification infrastructure.

There are, however, limitations associated with the use of renewable power to feed the railway network. The railway network represents a heavy and constantly varying demand, while renewable energy sources are individually of lower rating than conventional generation, and notoriously intermittent and unpredictable. Renewable energy sources are another area undergoing extensive development and continuous improvement with the government's backing (DECC, 2016). However, in order to use renewable sources to power the current railway, it is necessary to combine multiple (lower-rated) renewable energy inputs. Support from the national grid in bulk generation is still required. Furthermore, in order to obtain the greatest possible benefit from the use of renewable energy sources, energy storage units must be integrated into the power network and used to compensate for the unpredictable nature of renewable resources.

Where there are multiple lower-rated energy supplies, energy storage units, and with the potential for electric traction to be used for regenerative braking, it is appropriate to consider the formation of a railway smart grid (Pilo De La Fuente et al., 2014).

In order to achieve a smart grid, the railway infrastructure must be capable of being fed by multiple power inputs. With the current transformer-based railway infrastructure, the presence of the neutral sections, which are required to allow feeding from different phase combinations and to avoid synchronisation issues, effectively divides the network into multiple smaller networks. An efficiently utilised smart grid infrastructure, by contrast, requires a highly connected (ideally monolithic) and controllable network (Steele et al., 2019). While technologies to overcome this limitation exist (Pilo De La Fuente et al., 2014; Pilo et al., 2015), they would increase the complexity of the railway power network and associated costs.

Considering the continued push towards electrification, however, it is important to consider other infrastructure technologies and to install the most beneficial systems from the beginning or when renewals are required. Static Frequency Converters (SFCs) have been identified as a potential technology to replace transformer feeder stations for railway electrification. While the use of converters has been common practice on Central European railways using 16.7 Hz, the 50 Hz railways have not yet adopted this technology extensively. The use of SFCs eliminates the requirement for neutral sections, as well as enabling controllability of the feeder stations on the network (Behmann, 2013). These features pave the way for the integration of multiple variable power sources into the system, enabling the implementation of a railway smart grid without the complexities imposed by conventional transformer-based systems.

The author of this thesis describes investigations undertaken in order to establish the suitability of SFCs for use in 50 Hz railways and the potential for the development of smart control strategies in order to enable mesh feeding amongst SFC feeder stations on the line. The topic is considered from the perspective of technical implementation and feasibility; an evaluation of the costs associated with the deployment and operation of such systems is also provided.

## 1.1 HYPOTHESIS

The researcher explores the hypothesis that the use and configuration of SFC feeder stations on a line, in combination with the associated control strategy, can reduce the overall cost of railway electrification and operation, and provide additional benefits around operational robustness and flexibility.

The hypothesis is explored from two perspectives. Initially, the effect of the control strategy on the operation of an SFC-based system is considered in order to investigate the appropriate capacity rating of the individual SFC units. Secondly, the effects of the number and spacing of SFCs along the line on the required rating and overall efficiency of the system are considered. These elements are then combined in an analysis of initial and operational costs in order to evaluate the suitability of SFC systems for railway applications, and the creation of a technology roadmap demonstrating how SFCs (and their development) will facilitate the implementation of a railway smart grid.

## 1.2 PERSPECTIVES

This thesis addresses the potential for SFC-based railway electrification systems from two perspectives:

1. The control strategies that can be applied to an existing configuration of feeder stations.
2. The sizing and spacing of a network of SFC feeder stations.

In the first investigation, different control strategies are applied to an SFC-based system in order to manage the distribution of loading of the individual SFCs. Synchronised control is the currently accepted control method where each SFC supplies an amount of power inversely proportional to the distance of the load from the feeder station and this is used as a baseline solution. Equally shared control manages the network of SFCs to balance the whole network load continuously across all feeder stations. The investigation compares SFC performance, using both strategies, to that of an equivalent state-of-the-art AC transformer system in order to identify the potential reduction in the rated capacity of each individual feeder station.

While the first investigation aims to maximise comparability with existing infrastructure, the second investigation considers how SFC-based system efficiency can be improved at the design stage. It

considers the effects that the number of SFCs, and their spacing along a line, can have on the overall system efficiency and the required rating of each SFC. Additionally, where precise geographical positioning of a feeder station may be challenging, this investigation considers the use of a control system to improve flexibility in the positioning of each feeder station. This exploration is undertaken for both of the control strategies explored in the first investigation.

### 1.3 APPROACH

A number of specific tasks have been considered in order to address the investigations described in Section 1.2.

- Mathematical and computational modelling of Autotransformer (AT)- and SFC-based railway electrification systems to develop a platform to explore the operation of these systems.
- Demonstration of the ability to share both active and reactive power between multiple feeder stations on a 50 Hz/25 kV OLE system will show the feasibility of different control strategies.
- Comparison of SFCs with the latest AC transformer systems for 50 Hz to identify any potential advantages or disadvantages of each system.
- Investigation into the effects of the distance between SFCs on their required ratings and the overall system efficiency.
- Analysis of the capital and operational cost of the use of SFCs to provide electrical traction power on a rail network.
- Development of a roadmap outlining the key steps to developing SFC technology and its incorporation into a railway smart grid.

## 1.4 THESIS STRUCTURE

Chapter 2, 'Review of Current Railway Electrification Schemes' provides a literature review discussing different arrangements and methods of electrification. It then focuses on AC electrification and the benefits and drawbacks of different arrangements and the issues which need to be considered in order to provide the energy required for the railway network without impairing the utility grid. The structure and the operating methods of SFCs are also discussed.

Chapter 3, 'Modelling and Control of the AC Railway System' describes the mathematical models used to represent the railways' power system for both AT- and SFC-based power networks and includes the arrangements, connections and values of the impedances which form the networks.

Chapter 4, 'Simulations of SFCs for AC Railways and Comparison with AT Systems' describes the method by which the mathematical models of the AC railway for AT and SFC systems have been implemented to represent a realistic scenario of a timetable of trains moving through a railway line in both directions. This chapter includes the arrangement of the AT system as well as that of an SFC network specifically designed for this project. This chapter also includes an example where one train completes a journey in order to demonstrate the behaviour of the power system in a more easily interpretable scenario.

Chapter 5, 'A Study of the Comparative Performance of SFC and AT Systems for a Heavily Used High-Speed Railway', is an investigation into the potential for using SFCs in place of a comparable AT network. The chapter considers the effects of multiple SFC system control strategies applied to the network for a timetable of trains completing journeys in both directions. The chapter considers both the timetabled and worst-case loading scenarios, in order to evaluate and compare the performance of the different technologies and the ratings of the components required.

Chapter 6, 'Analysis of The Effect of the Number of, and Distance Between, SFC Feeder Stations ', presents an investigation into the effects of the spacing and number of SFC feeder stations on the line on the rating of each SFC and the overall system efficiency for both control strategies explored in

Chapter 5. The investigation initially uses a simplified vehicle model to explore the effects of vehicle position within the network, before expanding to a more complex vehicle model to consider the significance of a timetable on the proposed infrastructure.

Chapter 7, 'Economic Analysis', presents a discussion of the significant elements affecting the capital and operating costs of both AT- and SFC-based railway electrification systems. The observations made within Chapters 5 and 6 are used to explore the financial implications of implementing the different SFC design solutions considered.

Chapter 8, 'Railway Smart Grid Technology Roadmap', discusses a vision for how SFCs and their support technologies will evolve and interact along a timeline in order to support the development of a railway smart grid.

Chapter 9, 'Conclusion', presents a summary of the conclusions drawn at each stage of the investigation and brings them together to consider the hypothesis that the use and configuration of SFC feeder stations on a line, and the associated control strategy, can reduce the overall cost of railway electrification and operation.

# 2 REVIEW OF CURRENT RAILWAY ELECTRIFICATION SCHEMES

Reports from Network Rail in 2006 stated that 4928 km (approximately 40%) of the UK Rail Network was electrified and that 60% of all passenger journeys across the network were by electric traction. Of the electrified network, 64% uses the 25 kV AC overhead system (mainly on the mainlines) while 36% uses the 750 V DC third-rail system (mainly on the former Southern Region). These numbers are expected to swing heavily towards 25 kV AC overheads with the coming electrification of the Great Western Railway, parts of the Midland Main Line, Northern Hub and both Crossrail and Thameslink, which all follow both EN 50163:2004 and IEC 60850, thus conforming with the European Union's Trans-European railway interoperability standards. The following sections consider different approaches to railway electrification and the key technologies that support each approach.

## 2.1 DC ELECTRIFICATION

As described above, the first electric railways used, and many of those developed prior to the 1956 adoption of 25 kV overhead in GB, a DC system for traction which was selected largely due to the simplicity of the components required on the vehicle. DC railways operate by creating a DC network alongside or above the running rails from which the vehicles draw their power. The vehicles used comparably simple combinations of switches and variable resistances to control the operation of the vehicle (White, 2010). As the national distribution network is AC, transformers and rectifiers are used to produce the DC network (Hill, 1994).

Commonly used DC networks include +420/-210 V (London Underground), 600 V (older continental tram systems), 750 V (South of England, modern trams), 1200 V (Hamburg, Germany, Metro), 1400 V (Inter-Urban Trams), 1500 V (Eastern and Southern France, Mainline) and 3000 V systems (Belgium, Eastern Europe, Russia, Spain,) (Hill, 1994; Schmid et al., 2017). For the most common voltages, in the 500–750 V range, a typical traction current might be of the order of 2000 A (British Standards, 2010). Although the infrastructure resistance is low, drawing currents of this size at a single location (the train's position) puts a large point load on the network and, as such, the supply points must be situated regularly and close together in order to avoid drops in the supply voltage. This is particularly important in the presence of multiple trains, where multiple loads may be operating in a region simultaneously

(Seimbille, 2014). Another key reason not to use HV AC in metro systems is the insufficient space on the rolling stock for a large and heavy traction transformer. HV AC also requires a larger tunnel cross section.

Due to this need for regular closely spaced supply points, DC networks are most commonly used in metro systems where the overall operating lengths are shorter, and stations and other supporting infrastructure are already present. In metro networks, the operation of vehicles is also generally more frequent (International Railway Journal, 2013). This, combined with careful timetabling, improves the potential for one vehicle to be able to operate using energy regenerated from another (Hillmansen, 2013). This is of particular benefit in DC networks which are rarely capable of regeneration to the grid. This characteristic is primarily based on the cost of the infrastructure required, although inverting substations capable of providing regeneration capability do occur, for example, Southern, a UK train operator, in conjunction with Bombardier as their train supplier (Taylor et al., 2010).

While DC systems are therefore well suited to smaller or more densely populated networks, larger networks, or those where a full regeneration solution is required, tend to be more compatible with AC electrification approaches.

## 2.2 AC ELECTRIFICATION

AC electrification is the preferred method of railway electrification for long distances, high speed and heavy haul railways. In this electrification system, power is taken from the three-phase grid supply and fed into the single-phase AC railway network. The most commonly used arrangement for AC railway electrification uses transformers to convert the high-voltage grid supply to the specific railway's usable traction supply.

Central Europe uses single-phase 15 kV, 16.7 Hz AC while the most popular AC electrification arrangement is now 25 kV 50 Hz worldwide. 25 kV 50 Hz AC was chosen as the standard system in the UK in 1956 (Hill, 1994; Network Rail, 2003).

Railways with 25 kV 50 Hz overhead systems are fed directly from the three-phase utility grid, typically 110kV to 400kV, using two-phase transformers (White, 2008). The current feeding arrangements mainly use transformer-based feeder stations. However, there are several limitations associated with use of the utility grid for transformer-based feeder stations. These limitations will be further discussed in Section 2.2.1.4.

## 2.2.1 TRANSFORMERS

Conventional traction transformers are used as the power supply in most AC railway electrification systems, however, the arrangements of the connections for different transformer-based systems vary greatly, depending on the principles used for each case.

The transformers are fed with three-phase high-voltage feed connections at 132, 275 or 400 kV from the grid and convert it to single-phase 25 kV or 50 kV, depending on the AC rail network (Li, 2010).

Transformers are located along the line in pairs separated by an isolation section and connected to different pairs from the three-phase grid to manage the load imbalance put on the grid. The imbalance problem is one of the biggest issues the transformer-based AC systems suffer from as the railway is one of the biggest loads on the grid but in a single-phase form with point loading that naturally causes imbalance on the three-phase grid supply system (Yu-quan et al., 2011).

These arrangements have evolved over time starting with simple Rail Return (RR) systems, developing into Booster Transformer systems to address voltage drop problems and, relatively recently, progressing into AT systems (Schmid et al., 2017). These are described in detail in the following sections.

### 2.2.1.1 RAIL RETURN SYSTEM

The RR system is the simplest transformer-based electrification arrangement for AC systems. In an RR system, the current is fed to the railway load through the Overhead Contact System (OCS) and 60% is returned through the dedicated Return Conductors (RC), if available, and/or the contacted running rails. A further 40% is generally returned through the Earth and touch voltages can cause a significant

electromagnetic interference surrounding systems, due to the magnetic loop caused by return of the current through the earth (Hillmansen et al., 2016). In this scenario, the transformers are 40–60 km apart and the rails and tracks are typically bonded every 300 m (Network Rail, 2007). The biggest drawback associated with this system is that, as in the RR system about 40% of the current returns through the earth, electromagnetic interference causes disruption to the communication systems nearby (Cozza and Démoulin, 2008).

#### 2.2.1.2 BOOSTER TRANSFORMER SYSTEM

With Booster Transformer (BT) systems, the disadvantages of the current loop and hence the electromagnetic interference are addressed. With BTs located every 3–8 km along the line (Baxter, 2015), the primary side is connected in series with a 25 kV line and the secondary side is connected to the RC and RR lines, hence forcing the return current to flow through the RC line instead of through the rails or the ground (Chen et al., 2016). BTs are essentially 1:1 current transformers (Abrahamsson et al., 2012), which help to reduce interference into co-linear communication and telecommunication systems (Castro et al., 2014; Chen et al., 2011). In a BT system with an RC, there is an increase of about 50% in the total feeding inductance in comparison with a classic RR system. The disadvantage of using BT systems is that for high-load applications, there are considerable voltage drops across the impedance of the feeding catenary due to the heavy currents drawn by larger traction demands, which results in the need for unfeasibly closely placed feeder stations (Feng et al., 2017).

#### 2.2.1.3 AUTOTRANSFORMER SYSTEM

In order to address the requirements of BT systems for close proximity of the ‘current sucking’ transformers, the AT system has been designed. ATs located every 8–10 km can solve the disadvantages of BT transformers and enable the feeder stations to be 50–100 km apart (Alvarez-Alvarado et al., 2018). Another key advantage of AT systems is that the spacing between feeder stations can be increased, due to the power being fed at 50kV and not 25kV, and hence the number of feeder stations can be reduced.

An AT has two symmetrical windings. The feeder wire is connected to the Overhead Line (OHL). The running rails (the middle tap) are connected to the supply transformer and, consequently, the train only sees half the voltage of the system and hence the current is divided between the catenary and feeder wires which reduces the voltage drop between the feeder station and the train (Castro et al., 2014). Another advantage with an AT system is the reduced electromagnetic interference in comparison with both RR and BT systems. The major disadvantages associated with the AT system, however, are that the rating for the capacity requirement for the feeder stations in these systems is considerably larger than that for BT systems, which results not only in greater capital cost but also more expensive maintenance and protection equipment. It also requires more installation space (Kulworawanichpong, 2003).

#### 2.2.1.4 PROBLEMS ASSOCIATED WITH TRANSFORMER SYSTEMS

In all the different arrangements and systems of transformer-based traction systems, there are issues such as; Imbalance, reactive power injection and arcing. Due to the high power rating of the traction substations, these complications cause poor power quality and other harmful influences on the utility network (Shu et al., 2011; Tan et al., 2005). As rail traffic increases, the issue of the power quality induced by railway traction becomes a more critical problem, which requires attention and implementation of preventive solutions.

These issues require special equipment, specific connections or extra margin in the sizing of the feeder stations to compensate and rectify, which consequently makes the system more expensive and less reliable. Some of these issues are mentioned below.

##### 2.2.1.4.1 *IMBALANCE*

Load balance can be named as the most significant problem with transformer-based traction systems for railways. Single-phase traction transformers are extensively used in railway application due to their low cost as well as simplicity in structure (Yu-quan et al., 2011); however, they introduce the imbalance problem into the system, due to putting a large single-phase load on a balanced three-phase system. The connections for a single-phase traction transformer are presented Figure 1.

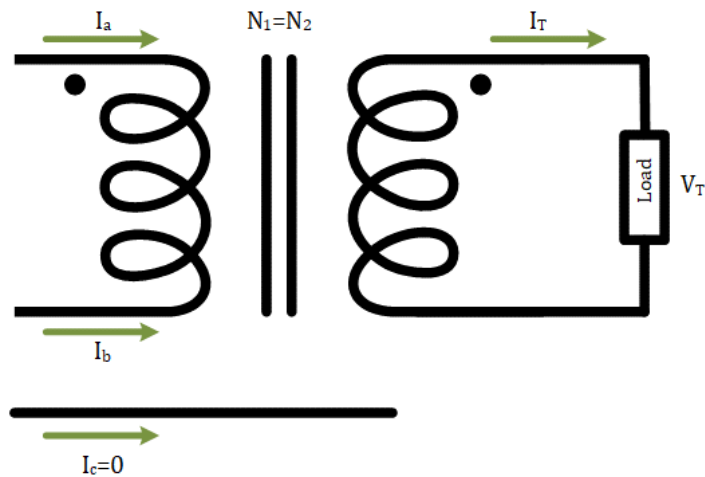


*Figure 1 Single-phase connection*

Voltage imbalance for three-phase systems refers to the lack of symmetry in voltage magnitude or phase angles between the phases (von Jouanne, 2005). There are various definitions for imbalance. According to the NEMA index in the US, imbalance can be defined as “the maximum deviation from average line voltage over the average line voltage”. In Europe, however, the voltage imbalance and its severity is defined as ‘the ratio of the negative sequence voltage over the positive sequence voltage’ in EN 50160 (British Standards, 2010) and IEC 61000-3-13 (International Electrotechnical Commission, 2008; Seiphethlo and Rens, 2010).

There is a specified range of voltages over which the trains can function healthily. These voltage ranges are specified in BS EN 50163 (CENELEC, 2007).

The balance of the utility grid is due to the equal magnitude and equal,  $120^\circ$ , separation between phases. Putting a single-phase load on a three-phase grid results in an unequal voltage drop across different phases which results in imbalance (Kneschke, 1985). Even though the transformers are alternately connected to different pairs of phases on the grid to mitigate the current imbalance due to the unequal and unpredictable traction power requirements of the railway systems, the load would not be evenly distributed over the transformers and consequently disrupts the balance of the system.

Due to the damaging impacts of imbalance on the three-phase grid, strict limits are applied by National Grid standards, in GB and elsewhere, in order to control the imbalance issue and ensure the railway load does not adversely affect other nearby users.

#### *2.2.1.4.2 HARMONICS*

Harmonics are the second biggest problem associated with the current conventional transformer-based traction in railways.

In AC supplied railway traction systems, there has to be AC/DC/AC conversions on the traction unit, in transformer-based systems, to convert the grid supply into a railway traction-usable form. These conversions result in different harmonics flowing into the three-phase grid supply side (Mousavi Gazafzudi et al., 2015). Legacy rolling stock fleets with phase angle-controlled rectifiers and DC traction motors present the greatest problem in terms of low order harmonics. Modern rolling stock with 4-quadrant, usually IGBT based, converters switch at a higher frequency and usually have relatively low, low order harmonic emissions. In an electric train, thyristor or Pulse-Width Modulation (PWM) controlled converters generate harmonic currents flowing through the traction network (catenary). Specially connected transformers can reduce the harmonics injected into the supply system by acting as passive filters (Huang and Chen, 2002; Mazin and Xu, 2009; Zhiwen Zhang et al., 2009). It is also possible to control the harmonics by using special equipment working as active and passive filters. The classic solution to harmonics is tuned passive filters (Peeran and Kusko, 1985), however, the most effective solution is to use shunt active filters. Despite these being the more effective solution, passive filters are still a commonly used solution as active filters are more expensive. In scenarios where there is sensitive equipment involved, active filters will be used. In other scenarios, depending on the sensitivity of the situation, passive filters or a combination of active and passive filters would be used (Quesada et al., 2011). More equipment-based solutions are discussed in Section 2.2.1.5.

Harmonics induced on the grid side by drawing a non-sinusoidal current can damage the grid performance and consequently strict limits on harmonics are applied by National Grid standards in order to ensure the railway load does not adversely affect other nearby users

#### *2.2.1.4.3 REACTIVE POWER INJECTION*

Although PWM AC converters in traction systems reduce the reactive power almost to zero (Konishi et al., 2003), and the compensators for power quality have a unity power factor, there are still issues with reactive power using traction transformers (Wu et al., 2012).

Reactive power compensation cannot be performed separately from the compensation of the Negative-Sequence Component (NSC) induced into the system by imbalance. This is due to the requirement for generating or transferring active and reactive power in order to compensate for NSCs (Mousavi Gazafardi et al., 2015).

The length of the cable lines in power supply systems for railway traction have increased, which results in an increased capacitive effect on the system and, consequently, the terminal voltage is increased and reactive power flown into the distribution system, resulting in reduced power quality (Sun et al., 2012).

The legacy rolling stock fleets with phase angle-controlled rectifiers and DC traction motors present the greatest problem in terms of low Power Factor. The Power Factor with such rolling stock can be as low as 0.6, which is not desirable. Modern rolling stock with four quadrants, usually IGBTs, converters can operate at very close to unity Power Factor.

Non-unity power factor can affect the grid by making the railway transformers appear as inductive loads and consequently strict limits are applied by Nation Grid standards with respect to reactive power injection and Power Factor, to ensure the railway load does not adversely affect the nearby users.

#### *2.2.1.4.4 ARCING*

When a train is going through isolation sections, it is possible for the contact between the pantograph and the catenary wire to cause arcs. Arcs have the potential to cause problems by distorting the currents and voltages which would break the dielectrics by introducing a DC component into the AC system (Liu et al., 2002; Mousavi Gazafardi et al., 2015).

### 2.2.1.5 STATE-OF-THE-ART SOLUTIONS FOR TRANSFORMER-BASED TRACTION ISSUES

The problem of imbalance has been recognised from the early days of AC railway electrification. Connecting a large single-phase load onto a three-phase grid results in an imbalance by creating an NSC equal to the Positive-Sequence Component (PSC) (Barnes and Wong, 1992). Several methods have been investigated, developed and used to address this problem. The ultimate purpose of these methods is to compensate the NSC and reactive power that results from the imbalanced circuit to zero (Kunyu et al., 2018; Chen, 2002; Chen et al., 2004).

These solutions and different methods are described here:

- 1- V-V-type transformers can be used. A V-V transformer is a special connector transformer used in railway applications primarily to solve the imbalance problem. The V-V transformers are connected as presented in Figure 2. The V-V configuration consists of two transformers which have their primary sides connected to different pairs of phases from high-voltage grid connections, i.e., AB and BC. This arrangement is introduced to distribute the load evenly between the phases of the grid. This, however, is not accurately possible with railways as the load is unpredictable and has many dependencies.

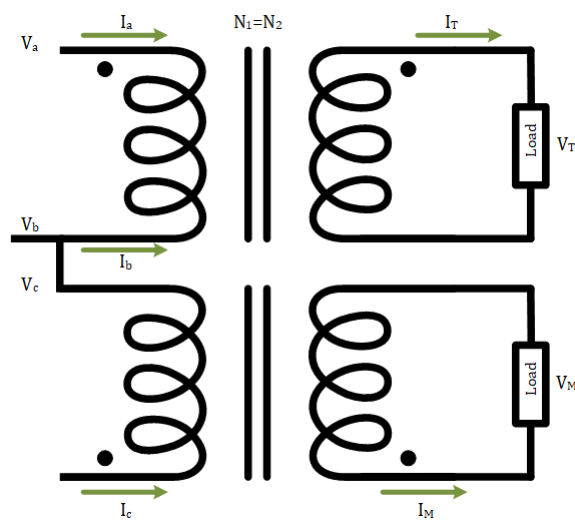
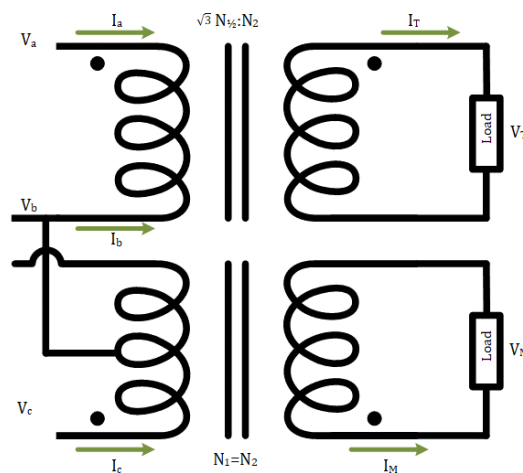


Figure 2 V-V connection

- 2- Balance transformers such as Le Blanc, Scott, MPV and Woodbridge types

The **delta–wye-type transformer** is the most conventional in the power industry, but in the case of traction application, it is not popular. There are several configurations of transformers designed to address the imbalance problem.

The **Scott transformer** configuration consists of two single traction transformers which are usually referred to as M and T transformers. The circuit diagram for Scott transformers is presented in Figure 3. The way the Scott transformers are connected creates a balanced two-phase supply from a three-phase supply which means there are two secondary sides with equal magnitudes of voltage but phase angles  $90^\circ$  apart, where T is leading M. If the loads drawing power from the secondary sides are equal, the system would be balanced but, as mentioned previously, this is highly unlikely in railway applications (Chen, 2002; Huang et al., 2006; Kalantari et al., 2010).



*Figure 3 Scott connection*

Similarly, the **LeBlanc** transformer connection is designed to create balanced two-phase supply systems from three-phase supply systems and vice versa. A LeBlanc transformer has a three-legged core, i.e., the winding of the primary side is designed as a delta ( $\Delta$ ) connection. There are two windings on the secondary side that are usually referred to as T and M. The configuration of a LeBlanc connection is illustrated in Figure 4.

Similar to the Scott transformer configuration, the LeBlanc transformer configuration can reduce the severity of voltage imbalance induced by the single-phase traction loads of the railway (Chen, 1994; Chen and Guo, 1996; Chen et al., 2004; Kalantari et al., 2010).

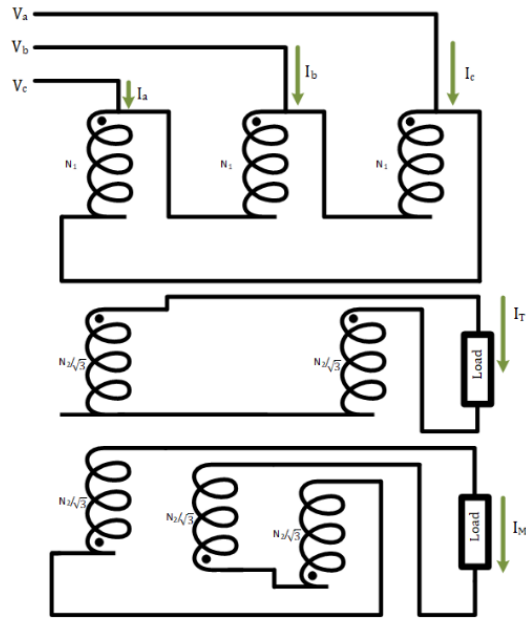


Figure 4 LeBlanc connection

There are several solutions which primarily use different connections and configurations with the basic single-phase transformers. They have been referred to as **configuration-based solutions**:

1- Three-phase trains

Three-phase trains were developed in some countries in the early years of the 20<sup>th</sup> century to achieve a symmetrical load which would eliminate the imbalance issues. These trains used double pantographs connected to two phases and had the third phase connected to the running rails. This technology was adopted widely in Italy and on mountain railways. Although this approach addressed the imbalance issue, it created mechanical problems with using the second pantograph, as well as the dangers and issues of electrifying the running rails on the ground. These serious disadvantages resulted in this solution being dropped, except for some tourist railways (Middleton, 2002).

## 2- Phase-shift technique

The phase-shift method is applied to a traction system in order to compensate for the fundamental NSC of the system. In this method, three adjacent traction transformers are connected between two different phases of the network to share the load between all phases (Li and Yang, 2010). This technique will, however, only work fully when the loads on each pair of the phases are equal. Due to the unpredictable and changing nature of railway loads, this rarely happens, which results in the phase-shift method being only partially effective for tackling the imbalance problem (Peroutka et al., 2009).

## 3- Co-phase system

The co-phase system has been developed recently and is still an immature technology and in the research stages. It uses a combination of both equipment- and configuration-based technologies to address the imbalance problem. In this technique, the contact wire is fed through two phases via an active power compensator while the running rail is connected to the third phase. This configuration has been designed to share the power equally between the phases and consequently prevent asymmetrical currents in the primary side. This method addresses not only the imbalance issues but also harmonics and reactive power issues at the same time. The co-phase method can also potentially remove the isolation sections between traction transformers which would be a great advantage due to the cost of isolation sections, their maintenance and the limits the existence of isolation sections imposes on the speed profile of running trains. The co-phase method consequently has the potential to be a turning point for high-speed railway lines (He et al., 2014; Lao et al., 2015; Shu et al., 2011, 2013; Wong et al., 2012).

Another method of limiting the imbalance and other power quality issues in transformer-based traction systems for railways is the use of special equipment, such as filters, to eliminate harmonics. These **equipment-based solutions** include:

### 1- Static VAR Compensator (SVC)

SVCs are a more common name for Thyristor-Controlled Susceptance (TCS) systems and have been around since the 1970s (Czarnecki et al., 1995; Otto and Gbciv, 1978). They are used to compensate for NSCs and consequently imbalance problems, as well as improving reactive power issues. SVCs can adjust the three-phase impedance connected to the grid supply and thus address the imbalance problem (Chen et al., 1999). It is not possible to improve the power factor values in the system due to the requirement to compensate for the NSCs in traction systems by controlling the active and reactive power in the system (Wu et al., 2012).

### 2- Static Synchronous Compensator (STATCOM)

STATCOMs are converters that can inject a controlled reactive current into a system in order to control the voltage magnitudes as well as reactive power levels (Heydt et al., 2012). STATCOMs are from the same family as SVCs.

### 3- Railway Power Conditioner (RPC)

RPCs were firstly introduced as a railway technical solution in the early 1990s to compensate for NSCs (Takeda et al., 1993). An RPC is made of two back-to-back converters which share a capacitor as a DC link. Using advanced control techniques, RPCs can also help eliminate the reactive power and harmonics issues. The configuration in which the RPCs are connected differs with the type of transformer connection used for each particular instance. The most popular examples of RPCs are accompanied by Scott and V-V transformers. It must be noted that wye-delta transformers are not used with RPCs (Senini and Wolfs, 2002).

The Active Power Quality Conditioner (APQC) (Ishikura et al., 2009), Half-Bridge RPC (HBRPC) (Ma et al., 2013) and Hybrid Power Quality Conditioner (HPQC) (Lao et al., 2018) are other, more advanced, structures from the family of RPCs to address the harmonics, NSC and reactive power issues more adequately. RPC-based solutions are widely used in east Asian railways.

#### 2.2.1.6 POWER QUALITY CONCLUSION

Power quality issues are serious problems in high-traffic railways where the power consumption is high and access to multiple high-rated power generation plants is limited. In scenarios where the railway has little traffic and there are power plants nearby, the power quality problems will not be significant.

The strength of the three-phase grid supply has a strong influence on the impact of adverse power quality problems caused by the railway load. The railway load has a more severe negative impact on power quality problems where the three-phase grid is weak and, consequently, conventional transformer connections on weak three-phase systems are difficult, requiring additional systems to mitigate for the power quality problems.

As for any other engineering problem, selection of the compensation method for power quality issues comes down to the benefit vs cost of the solution. For each scenario and each arrangement of the railway system, there may be a different best solution to address the issues.

Active power filters have been the most effective method to mitigate power quality issues. The use of active power filters enables the transmission facilities to utilise a greater percentage of their total capacity in power transmission in the presence of power quality issues. Although the first active method for NSC and power factor quality compensations was the SVC method, it introduced too much harmonic content into the system. This means that there is another cost added to the cost of the system in order to add filters to compensate for the harmonics introduced with the use of SVCs. This makes RPCs a better solution as there is no harmonics issue with the RPC family of solutions. The future, however, holds greater opportunities for the use of co-phase systems due to the increased implementation of high-speed railways. The use of three-phase rectifiers, a DC link and a single-phase inverter connected to a single-phase transformer feeding the OHL is also a viable solution (Mousavi Gazafrudi et al., 2015).

With all the issues addressed in the previous sections, railway traction systems seem to require new technologies and approaches to address multiple issues at the same time. It must be noted that power quality issues are due to the use of transformers on the line. These issues would be eliminated with the

use of power electronics structures such as static converters. These may involve further investigations of power electronic components already present in railway traction systems.

The following section investigates the options for SFCs, their benefits, drawbacks and potential as the answer for the ultimate solution of future electrification systems.

### 2.2.2 CONVERTERS

While power electronic converters are widely used in different configurations to compensate for the power quality issues associated with transformer-based traction systems, it is possible to use converters as a full substation solution for traction purposes. The railways in Central Europe and North America require frequency conversion to get power from the grid to both their DC and AC railways. The Central European single-phase network, 15 kV, 16.7 Hz is fed by three-phase utility network or single-phase synchronous generators at power stations. A special railway single-phase power grid at 110 kV 16.7 Hz exists in Germany and Austria, and at 132 kV in Switzerland. A DC link normally connects a three-phase converter to an inverter. The four-quadrant inverter generates the single-phase 16.7 Hz voltage (Steimel, 2012). The conversion was traditionally done using converters with rotary parts with synchronous three-phase motors and single-phase asynchronous generators. In these generators, the motor is mechanically coupled with the generator in order to convert the frequency and generate a 16.7 Hz supply. Due to having moving parts, these converters require regular maintenance. There are mechanical oscillations between the motor and the generator pair due to the low frequency required for the rail supply. To extend the service life of these rotary transformers, these oscillations require damping (Krastev et al., 2016).

In Germany, Switzerland, Sweden, Austria and Norway, the use of power electronics frequency converters to replace the conventional rotary converters is well established (Banceanu et al., 2015; Xie and Schmidt, 2004). The North-East corridor in the USA uses SFCs that convert from three-phase 60 Hz to single-phase 25 Hz.

The modern converters use power electronic devices to replace rotary parts. Static converters have been in use since 1994 (Aeberhard et al., 2010) with the use of thyristors in cyclo-converters. A circuit diagram of cyclo-converter topology is presented in Figure 5. Although the controllability of a cyclo-converters reduces voltage regulation issues due to the single-phase load, the low-frequency switching operation of thyristor-based converter produces enough harmonics content to require large reactors to compensate for the harmonics in the output voltage waveforms. Due to the drawbacks of thyristors for static converters, modern converters were developed which use Insulated-Gate Bipolar Transistors (IGBTs), Gate Turn-Off (GTO) thyristors, and Integrated Gate Commutated Thyristors (IGCTs) which operate at high frequencies, in the range of 1 kHz. These converters are known as DC Link Converters. They have the benefits of thyristor-based converters without the harmonics interference which makes them a viable replacement for cyclo-converters. Cyclo-converters are now completely superseded by the new generations of converters. (Gruber and O'Brien, 2014).

These days, IGBTs are used over Metal Oxide Semiconductor Field-Effect Transistors (MOSFETs) due to the better performance of IGBTs, with higher power gains and smaller losses. IGBTs can also function in a higher voltage band with higher junction temperature ranges (Hossain et al., 2017).

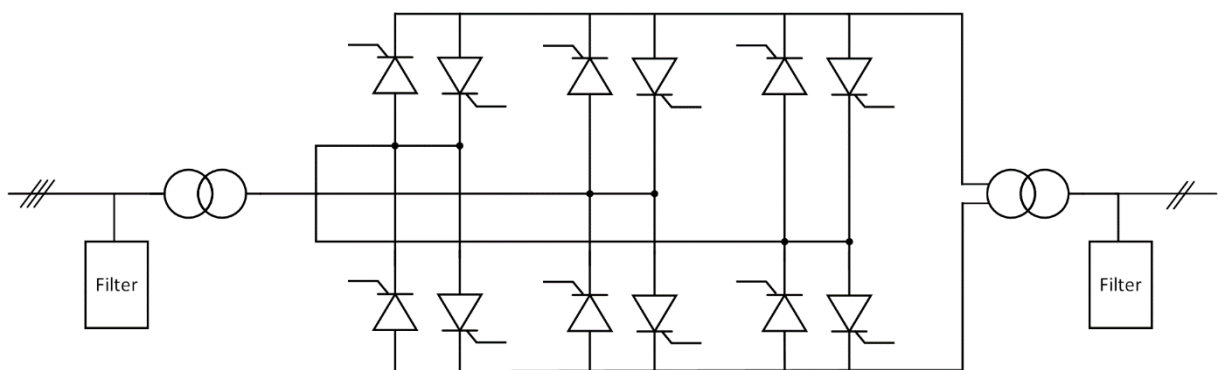


Figure 5 Diagram for a cyclo-converter

In the cases where SFCs have been used extensively for 16.7 Hz applications, the requirement is not only to change the frequency. The converter is required to change three-phase, 110 kV, 132 kV or other voltages, input to 25 kV. In Great Britain, and many other countries, both input and output frequency would be 50 Hz. The only current applications of SFCs on 50 Hz railways are as follows;

- Two 50 Hz railway SFCs on the Bauhinia Line in Central Queensland, commissioned in 2014.
- Two 50 Hz railway SFCs on the Moreton Bay Line, north of Brisbane, commissioned in 2015.
- A 50 Hz railway SFC at Wulkuraka near Ipswich west side of Brisbane, commissioned in 2016.
- A 50 Hz railway SFC Potteric Carr, on the ECML near Doncaster. This also feeds Hitachi's Azuma Depot in Doncaster.
- Two 50 Hz railway SFCs are currently being built in Brisbane.
- Two 50 Hz railway SFCs are currently being built at Hambleton Junction on the ECML, south of York.

The application in Australia is on a 46 km long route where the SFC was installed to address the potential increase in train traffic. Queensland Rail decided to install an SFC to support the existing conventional transformer after extensive technology research in 2006 (ABB, 2017). In the UK, an SFC feeder station was commissioned at Potteric Carr, in 2019, to support a new depot near Doncaster built for Hitachi Rail Europe's new Class 800/801 high-speed trains introduced onto the East Coast Main Line from 2018 onwards under the UK's Intercity Express Programme. For this SFC feeder station, Network Rail has made the connection at 33kV (Mott MacDonald, 2019).

#### 2.2.2.1 STRUCTURE OF STATIC CONVERTER FEEDER STATIONS

Static converters and, specifically, rail application SFCs, are made of power electronic semiconductors. The structure of the SFCs enables connections between independent power grids. SFCs, unlike transformers used in the conventional electrification system for the railways, are active devices. Being an active device means that it is possible to have control over the power flow between the two connected but independent grids. This means that the SFC can produce a balanced current which is almost sinusoidal with an approximately unity power factor (Krastev et al., 2016).

Most SFCs used for substations in AC rail electrification involve a three-phase converter connected to a single-phase converter via a DC link. The DC link consists of capacitors charged to a specified DC voltage level using the three-phase converter side. A filter is required on the DC link to compensate for

the pulsating characteristics cause by the single-phase loads (Ufert, 2016). The DC link voltage can go up to 3.25 kV for two-level H-bridges. It can go up to 6.5 kV for three-level Neutral-Point Clamped (NPC) bridges.

Modular multi-level converters (MMCs) are recent revolutionary middle-voltage devices which enable operation in high-voltage applications with improved quality of the waveforms compared to normal converters (Ladoux et al., 2014).

The use of MMCs has been growing substantially during the past few years in applications in medium- and high-voltage systems. There are difficulties associated with using MMCs, such as the circulating current control system and the DC current control system (Debnath et al., 2015).

MMCs have become the most popular type of converter in HVDC applications (Ding et al., 2008). The MMC topology has significant advantages over that of other converters. MMCs are modular and scalable which provides flexibility in providing different voltage and power levels. MMCs are more efficient than conventional converters, which results in a significant reduction in power loss for medium- and high-voltage applications. MMCs also have a good harmonic performance, which reduces the need for harmonic filters and saves on capital and maintenance cost as well as space. There also is no DC link capacitor required in these topologies; however, there are capacitors in each submodule.

A circuit diagram presenting an MMC with half-bridge submodules is presented in Figure 6. Each half-bridge section is a submodule of the MMC; the submodules can be of different topologies: half bridge, full bridge, clamp-double and five-level cross-connected (Ladoux et al., 2014).

There are, however, some potential disadvantages associated with the use of MMCs: There are arm current and capacitor voltage problems. There is a danger of high short-circuit currents. Due to the increased number of power electronic devices used in MMCs, the reliability of these modules is somewhat decreased in comparison with topologies using a smaller number of power electronic devices (Debnath et al., 2015). These disadvantages are being addressed though, as the technology matures.

There are several topologies suitable for the use of MMCs in transformer-less applications of SFCs for supplying the catenary such as: three 3-level converters in series, IGCTs (Ranneberg, 2007), four 3-level converters in series, six IGBTs, Multi-Level Flying Capacitor Converters (Hemici et al., 2015) and Multi-Level Cascaded H-Bridge Converter.

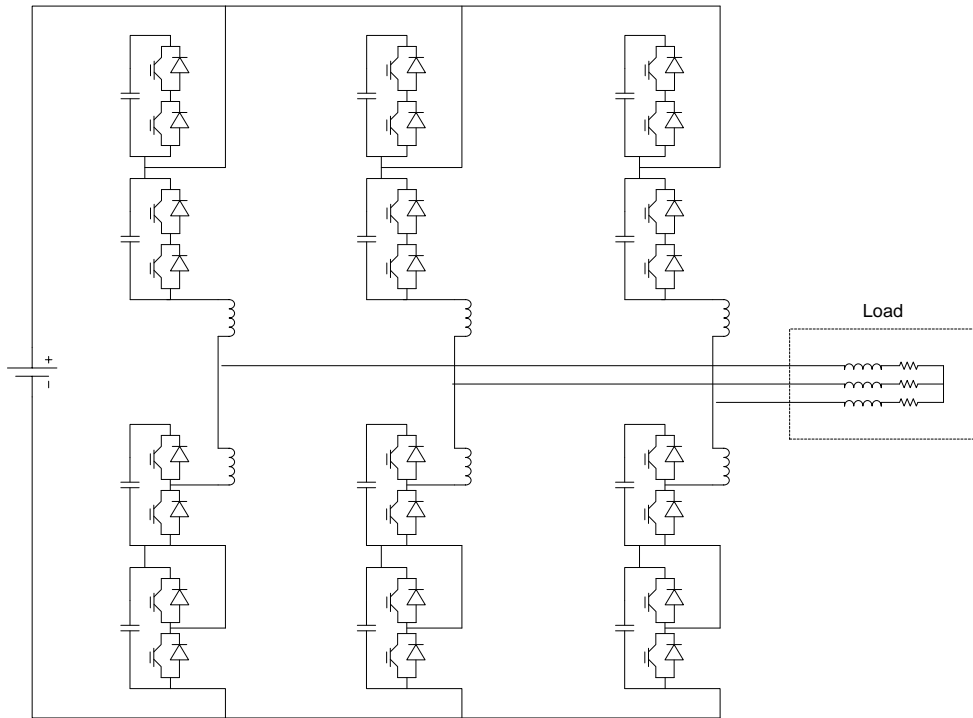


Figure 6 Modular multi-level converter circuit diagram with half-bridge submodules

The submodules are controlled using PWM techniques. There are several different methods of generating the PWM waveforms. Some are described in Section 2.2.3.

### 2.2.3 PWM GENERATION

Different modulation techniques have been developed to control the PWM signals in MMCs. These have different characteristics and advantages and disadvantages.

- **Carrier-Disposition PWM techniques (CD-PWM):** The basis of this technique is the comparison between the reference of the phase of the voltage waveforms and the N number of identical triangular waveforms symmetrically displaced with respect to the zero axes (Hassanpoor et al., 2012; Konstantinou and Agelidis, 2009; Sutherland et al., 2006).

There are disadvantages associated with using the CD technique. The voltage ripples across the capacitors of each module are not distributed equally. This causes harmonic distortion on the AC-side voltages and also large-magnitude circulating currents. To improve the harmonic distortion, a simple or modified carrier rotation technique or a signal rotation technique can be used (Jin et al., 2005; Kang et al., 2004).

- **Subharmonic techniques:** In this method, there are  $2N$  identical carriers per phase-leg, saw-tooth or triangular waveform with  $\theta = \frac{360^\circ}{2N}$  phase shift with respect to each other (Debnath et al., 2015; Konstantinou and Agelidis, 2009).

With an equal number of switching transitions, the phase disposition method has a better line-to-line voltage Total Harmonic Distortion (THD) (Carrara et al., 1992; Mcgrath et al., 2000).

In addition to the methods expressed above, there are a number of modulation techniques which use multiple reference waveforms. Some of these techniques are mentioned below (Siemaszko et al., 2010).

- **Direct Modulation:** In this method, two complementary sine waveforms control the upper and lower voltages of phase  $j$ ; the sine waves are as follows:

$$n_{p,j,ref} = N \frac{\frac{V_{dc}}{2} - v_{j,ref}}{V_{dc}}$$

$$n_{n,j,ref} = N \frac{\frac{V_{dc}}{2} + v_{j,ref}}{V_{dc}}$$

Depending on the number of submodules,  $n_{p,j,ref}$  and  $n_{n,j,ref}$  are the reference waveforms.  $v_{j,ref}$  is the reference output voltage.

The main disadvantage of the direct modulation method is the level of circulating currents. Circulating currents increase the losses and result in the system requiring higher rating value for the components (Ladoux et al., 2014).

- **Indirect Modulation:** In this method, the reference waveforms of the upper and lower arms in phase  $j$  are given by:

$$n_{p,j,ref} = N \frac{\frac{V_{dc}}{2} - v_{j,ref} - v_{reg,j}^{\Sigma} - v_{reg,j}^{circ}}{\sum_{i=0}^N v_{cp,i,j}}$$

$$n_{n,j,ref} = N \frac{\frac{V_{dc}}{2} - v_{j,ref} - v_{reg,j}^{\Sigma} - v_{reg,j}^{circ}}{\sum_{i=0}^N v_{cn,i,j}}$$

where  $v_{cx,i,j}$  is the capacitor voltage of submodule  $i$  in arm  $x$  of phase  $j$ . The phase  $j$  leg and balancing of energy between the arms are done using  $v_{reg,j}^{\Sigma}$  and  $v_{reg,j}^{circ}$ .

- **Phase-Shifted Carrier-based PWM technique (PSC PWM):** In this method, every submodule is controlled independently. The voltage is balanced using averaging control and balancing control. The reference voltages for the upper and lower arms are as follows (Hagiwara and Akagi, 2009):

$$m_{p,i,j} = \frac{\frac{V_{dc}}{2N} - \frac{v_{j,ref}}{N} + v_{a,j} + v_{b,i,j}}{v_{cp,i,j}}$$

$$m_{n,i,j} = \frac{\frac{V_{dc}}{2N} + \frac{v_{j,ref}}{N} + v_{a,j} + v_{b,i,j}}{v_{cp,i,j}}$$

Averaging and balancing control outputs are named  $v_{a,j}$  and  $v_{b,i,j}$ , respectively. The average voltages across capacitors in each leg and individually in each submodule are controlled. The PWM signal is generated by the comparison between the reference voltage signal of the corresponding submodule and the triangular carrier waveform. The carrier waveforms for each leg are generated using subharmonic methods.

The disadvantage of this technique is the substantial increase in complexity as the number of submodules increases. This also causes instability in some operating conditions (Hagiwara et al., 2011). However, this technique is the most comprehensive control technique with respect to both compensating for the disadvantages of other techniques and the overall cost–benefit analysis.

One of the great advantages of using power electronics is the controllability of the magnitude and phase angle of the output voltage. In order to utilise this feature, alongside the PWM methods controlling each of the power electronic components inside a converter, a control system is required to facilitate interconnection between multiple converters at different locations on the line.

#### 2.2.3.1 INVERTER INTERCONNECTION CONTROL

Interconnection between inverters has been extensively used in smart grid applications; droop control has been the predominant facilitator for the interconnection of multiple converters along the line (Kwan Lee et al., 2013).

Much like standalone microgrid applications, the converters used for traction systems are of the Voltage Source Inverter (VSI) type. VSIs can be used to regulate the magnitude and phase angle of voltage as well as the frequency of the output going into the network (Dehbonei et al., 2006; Li, 2009). A voltage control topology enables the system to have instantaneous voltage control as well as peak current protection and overload limitations (Kazmierkowski et al., 2002). Various Reference Frames can be used to execute different control approaches in order to regulate the output voltage and frequency and consequently improve the power quality issues by having appropriate designs for the voltage controllers (Rocabert et al., 2012). Reference Frames are sometimes required to improve the controllers' performance by transforming the control parameters. Selection of the appropriate Reference Frame technique is dependent on the nature of the application (Hossain et al., 2017).

The voltage controller used in VSIs can use different Reference Frames such as:

- **Synchronous Reference Frame:** This type of Reference Frame is also known as Park or d-q Transformation. In this method, electrical quantities are rotated synchronously with the network

frequency in order to be transferred to DC components. A Proportional Integral (PI) controller can be easily deployed to regulate the real and reactive power. The ease of implementation for PI controllers is due to the components being transformed into DC entities (Chen and Guo, 1996; Liu et al., 2019; Zhang et al., 2019).

- **Stationary Reference Frame:** This type of Reference Frame is also known as Clarke and  $\alpha$ - $\beta$  Transformation. In this method, the quantities are transformed into sinusoidal form which makes implementation of PI controllers difficult and a Proportional Resonant (PR) controller is the preferred controller (Blaabjerg et al., 2006).
- **Natural Reference Frame:** This Transformation Frame is also known as abc Transformation. The control strategy for this Transformation Frame requires both linear and non-linear controllers. In this approach, each phase of the three-phase system is controlled individually and consequently allows control of single- and three-phase systems with no transformation techniques required (Blaabjerg et al., 2006; Hossain et al., 2017).

These reference methods are used with the inner loop control method for the converter and hence regulate the output voltage as desired to address power quality issues. There are several controller methods available, depending on the application; they include PI, RP, Dead-Beat, Model Predictive, Hysteresis, H-Infinity, Repetitive, Neutral Network, Fuzzy, Sliding, Linear Quadratic Regulator (LQR) and Linear Quadratic Integrator (LQI) (Hossain et al., 2017). Of these, the PI controller is of most interest in power sharing controls for SFCs. PI controllers are usually paired up with d-q Reference Frame Transformation. The transfer function for the PI controller is as follows:

$$C_{PI}(s) = K_p + \frac{K_i}{s}$$

where  $K_p$  is the proportional gain and  $K_i$  is the integral gain.

Although a PI controller accompanied by a d-q Transformation Frame can result in very accurate control of active and reactive power, with the possibility to achieve zero steady state error, it must be noted that implementation of this approach can be complex due to the requirement for information regarding the

frequency and phase of the system at all times (Abusara et al., 2015; Hornik and Zhong, 2011). Another issue with PI controllers is that they are easily stressed by disruptions and, hence, it is important that in scenarios where PI controllers are implemented, the reaction of the set coefficients in disturbance circumstances is tested.

Power control implementation methods can be divided into two groups, communication-based control and communicationless control. In communicationless control, it is possible to save costs and complexity using the modularity of the converter units (Rocabert et al., 2012). Communicationless controls are, thus, more useful for applications where the converter modules are located in remote areas and do not require accurate active and reactive power control (Hossain et al., 2017). Communicationless control is dependent on knowledge of the network impedance and is not fully reliable with non-linear loads. Communication-based control facilitates accurate power sharing and reliable voltage regulation (Chen et al., 2010). The drawbacks of this method are expensive communication channels and potential disruptions caused by the delay in sending and receiving information on the communication lines. There are several arrangements available for communication-based control systems, such as master–slave, centralised, average load sharing, circular chain, peak value-based sharing, angle droop control and consensus-based droop control (Tayab et al., 2017).

#### 2.2.4 SFCs VS TRANSFORMERS

There are several benefits associated with the use of SFCs. As SFCs can output regulated voltages with no imbalance and reactive power issues, the harmonic contents of the output are negligible. This makes significant savings due to not needing active or passive filters to compensate for the harmonics' distortions. Whether or not additional filters are required on the three-phase or single-phase sides of the SFC largely depends on the characteristics of the three-phase and single-phase networks upstream and downstream of the SFC.

The controllability of SFCs is their strongest feature. SFC feeder stations can be fed with grid connections at voltages as low as 33 kV. Due to this capability, several requirements due to the power

quality issues imposed by the use of transformers on the line will be eliminated. First and foremost, there is no requirement for connection into a very high-voltage grid. SFCs, due to their lack of imbalance problems, have the freedom to connect to lower-voltage lines of the grid network. This not only saves costs on the equipment required for very high-voltage connections, such as expensive switchgears and measurement transformers, but also notably reduces the complexity of the arrangements and hence improves reliability. Being able to have lower-voltage connections also provides increased availability of locations for the SFCs along the railway line. The benefits work significantly towards making SFCs a viable solution despite the power electronic components costs which are currently still high in comparison with conventional transformer systems.

Control of the voltage on the single-phase side of the converter enables synchronisation of the output of multiple converters connected to the same network and therefore creates an environment where the OHLE can be continuous. Furthermore, with no neutral sections on the line, the AC OHL will be continuous and synchronised and hence multiple substations are able to simultaneously contribute into feeding the load on the line. The removal of neutral sections saves on capital costs and maintenance costs; it also enables multiple converters working in parallel to support the same line, as is the case with DC railways. It must be noted that SFCs can control both the output voltage magnitude and phase angle unlike DC railways which are only required to manipulate the magnitude of voltage. This feature enables mesh feeding for AC railways which, both expands the capacity of an existing line with the same rated substations and reduces the required capacity of the feeder station for new electrified lines.

Having control also enables these arrangements to address the power quality issues self-sufficiently. The grid sees the load through the static converters and, consequently, as far as the grid is concerned, as a balanced three-phase symmetrical sinusoidal load. The phase of the supply can also be controlled. These features therefore eliminate the requirement for very high-voltage connections for the SFC feeder stations as well as the need to have neutral sections which are required in transformer-based electrification networks.

A great benefit of SFCs is their modular design. The modular design facilitates a plug-and-play approach in the railway traction environment. SFCs can then be added in smaller sizes in different locations easily, and the capacity of an SFC-based feeder station can be increased or reduced easily. The modularity of the SFC feeder stations facilitates faster rectification of any faults or any maintenance requirements. This means lower labour costs and shorter shutdown periods on mainlines which would save cost in the event of a fault or breakdown, in comparison with conventional transformer-based traction networks.

However, there are some drawbacks associated with the use of SFCs. The transformer-based power systems for railways represent a mature technology which has been used for decades. The transformer-based feeder stations have a longer life span in comparison with the converter-based feeder stations and require cheaper maintenance. It must be noted that this is with respect to current power electronics prices and that costs are estimated to reduce as the technology matures and the demand for power electronic devices increases (Advanced Propulsion Centre UK (APCUK), 2017; Behmann and Schütte, 2012a).

SFC feeder stations have lower internal efficiency in comparison with the equivalent transformer-based feeder stations, which results in greater internal losses (Behmann and Schütte, 2012a).

### 2.3 CONCLUSIONS

A growing number of traction power engineers believe that SFC-based feeder stations are the future of traction power supplies in railway applications (Behmann and Schütte, 2012b) due to the multiple benefits associated with the use of SFCs that address the problems and limitations of the current traction systems using transformers. In 2014, the first inverter for a 50 Hz railway fed from a three-phase 50 Hz grid was put into operation in Queensland, Australia where it operates based on synchronised feeder stations (Brandt et al., 2014). The numerous benefits of controlling the active and reactive power in SFC-based railways have not yet been fully explored. Smart control of SFC-based feeder stations can open doors to more optimised scenarios and greater savings on different aspects of this, new to 50 Hz traction, technology. The research and author of this thesis investigate the possibility of running the feeder stations with synchronised frequencies with closed loop adjusted voltage phase angles and

magnitudes in order to control the percentage of the total load's active and reactive power that each feeder station provides.

# 3 MODELLING AND CONTROL OF THE AC RAILWAY SYSTEM

As described in Chapter 2, with transformer-based railway systems, it is not possible to deploy control strategies where the power demand on each feeder station is managed systematically. However, using SFCs it is possible to manipulate the phase angle and magnitude of the output voltage which enables the load on the railway network to be fed by several feeder stations along the line simultaneously. Current railway systems require a rated power much larger than the typical average consumption for each feeder station, due to the unpredictable nature of the railway with variation of loads, unexpected faults and variability in timetables. Cumulatively, these issues provide unavoidable inefficiencies in the railway system because the feeder stations are required to cater for unpredictable margins and hence incur costs, greater losses and more significant maintenance.

It is possible to use the mesh-feeding capability of SFCs to control the power demand on each feeder station. This leads into the element of this study's hypothesis that states that through sharing the load in an intelligent manner between feeder stations, it is possible to reduce the required feeder station capacities. This study considers the possibility of deploying an intelligent control scenario and its effects on feeder stations. Such effects are assessed and analysed in a scenario where the active and reactive power output requirements from SFC feeder stations are shared equally. It is thought that this approach has the potential to allow a reduction in the rated power requirement for each individual feeder station. It may also have the potential, through such sharing, to overcome the effects of a fault situation on the line and hence prevent greater disruptions as well as reducing the required fault margin on individual SFC feeder stations.

It is impossible to assess the effects of sharing active and reactive power equally without designing and simulating both the control systems and infrastructure of the traction system for these scenarios. Without running simulations, the assessment of the exact effects and benefits of any potential control technique are speculation. Such simulations are based on computational realisations of mathematical models. This chapter describes a number of such models, where implementation is then described in Chapter 4. In order to deliver a comprehensive analysis of deploying a control system on SFC feeder stations, an electrification system consisting of the OHLE, Rail Return, trains and feeder stations for the railway is

modelled. This provides a platform where the functionality of the proposed control system can be examined, tested, modified and analysed.

In the work described in this chapter, mathematical models of the power system for transformer- and SFC-based systems have been developed. In the models the feeder stations and trains are treated as black boxes acting as voltage sources and active loads, respectively. In the next chapter, a realistic timetable of trains is also modelled and combined with the implementation of the traction system model to simulate an operational scenario of a high-speed railway and facilitate analysis of the behaviour of the power systems and their comparison. The mathematical model, described in this chapter, can be viewed in two parts:

1. Simulation of the railway electrification system.
  - a. Transformer feeder stations with ATs on the line
  - b. SFC feeder stations with Rail Return
2. Simulation of different control strategies for the SFC case.

It is not easy to obtain and communicate the information about the location of a train to the control system. Having systems such as Global Positioning System (GPS) in place to find the location of the train as an input to the control system continuously creates limitations, delays and inaccuracy of results. Due to the reasons mentioned above, the control system for this project has been designed in such a way that it does not require information about the location of the trains. In order to achieve this, the designed control system is a central control system. The central control has a means of communicating with all SFC feeder stations on the line and takes information about their complex voltage and current outputs. The control system then calculates the phase angle and magnitude of the output voltage required depending on the control strategy target.

In order to control the contribution of active power from each feeder station, the phase angle of the output voltage must be controlled. Controlling the reactive power is dependent on the magnitude of the output voltage. This is further discussed in Sections 0 and 3.2.2.

Although this method has drawbacks, such as a predicted increase in losses, it is possible to establish a trade-off that considers both the reduction in the capacity requirement of the feeder stations and the positive impact on the requirements for maintenance.

MATLAB software has been used to carry out the described simulations. Although using MATLAB Script is more complex and time consuming than working with other simulation tools, the commercially available software does not support modelling a variable impedance. Simulating variable impedances with respect to time are required to model the movement of the train on the railway line.

### 3.1 MATHEMATICAL MODELLING OF ELECTRIFICATION INFRASTRUCTURE

The models and simulations produced for this PhD thesis consider two scenarios for which the system is analysed. These will be discussed in detail in Section 3.3.1. The proposed control techniques are then implemented, tested and analysed in such a way that the data produced can be compared with conventional arrangements in order to provide a meaningful evaluation of performance.

The electrification system has been modelled using a ‘lumped parameter’ technique. The lumped parameter method is discussed in Section 3.1.1. In this project, the simulation is done in electrical steady state, i.e., the electrical quantities are sinusoidal all the time, but their amplitude and phase change over time. This model is also referred to as a quasi-stationary model (Feldgun et al., 2011).

Three different arrangements have been considered for the electrification system. The AT system, as the most efficient of the current transformer-based systems, has been selected to be used as the base comparison scenario for the SFC-based systems. The arrangements considered are:

- 1- Transformer-based feeder stations feeding isolated sections with ATs.
- 2- SFC-based feeder stations with constant output voltage magnitude and synchronised phase angle.
- 3- SFC-based feeder stations sharing active and reactive power as required by the load between all SFC feeder stations on the line.

The mathematical modelling for these scenarios is described in the remainder of this chapter, while its application as part of a series of wider simulations is described in Chapter 4.

### 3.1.1 ELECTRIFICATION INFRASTRUCTURE

In order to develop a model of a power system, it is important to have information about the impedance of the line between the train and the feeder stations. This property changes as the train moves on the line. The movement of the train is continuous in real life, but a continuous change of the impedance parameters is complex and time-consuming, while not providing critical accuracy; consequently, a lumped parameter model has been used instead. As the location of the load changes and, consequently, the values of impedance connected to either side of the train also change. Using the lumped parameter model, the continuous movement of the trains is discretised. The discretisation of the system facilitates the simulations using the mathematical models that have been developed. In this approach, the location of the train is determined by the nodes on the system, described below, which means that during the movement of the train, its location jumps from one value to the next, rather than changing continuously.

The lumped parameter model is also popularly referred to, in power system studies, as a lumped element model or lumped component model. Such models replace continuous physical entities with discrete approximations, which simplifies the system while approximating its real behaviour. In this case, the continuous impedance of the electrification line has been replaced by discrete impedance blocks representing the impedance of a specific length of the line (Agarwal and Lang, 2005). A system can be made from connected lumped elements which are treated as passive black boxes with terminals.

In order to choose an acceptable distance between the nodes, when designing the lumped model, the voltage drop across this distance is key. It should not be a great percentage of the average nominal voltage as this would cause inaccuracy in further calculations for the power flow analysis of the system. Conversely, choosing too small a value would slow the simulations down hugely and would not add to the overall accuracy. In this case, the voltage drops across a number of distances were calculated and

100 m was chosen as the desirable interval as it provides efficient simulation speed while keeping the calculations sufficiently precise and accurate.

For this calculation, the worst-case scenario of a train accelerating while at a point as far as possible from the feeder station has been considered. This would result in lower train voltages and consequently higher currents. Assuming a 23 kV voltage of the train, and a 5.1 MW max power requirement for the train (see Section 4.4), the current would be:

$$I = \frac{P}{V}$$

$$I = \frac{5.1 \text{ MW}}{23 \text{ kV}} = 221.7 \text{ A}$$

In this case, the voltage drop across 100 m of the OHL would be:

$$V_{drop} = I \times Z$$

The  $Z$  value in this case is calculated based on data taken from the British Rail Standard (CENELEC, 2007) as presented in Table 1. This data has also been used as the base parameters for any other simulation done in this PhD thesis.

*Table 1 Electrification Parameters*

OHL impedance	$0.29 + 0.81j \text{ } \Omega/\text{km}$
RR impedance	$0.19 + 0.48j \text{ } \Omega/\text{km}$
Transformer internal impedance	$4.2j \text{ } \Omega$

In this case, the equivalent impedance of 1 km of the line would be  $0.29 + 0.81j \text{ } \Omega$  and hence one-tenth is used for 100 m of the line. Using the above values:

$$V_{drop} = 221.7 \text{ A} \times 0.029 + 0.081j = 6.4304 + 0.0810j \text{ V}$$

$$|V_{drop}| = 6.4309 \text{ V}$$

The voltage drop is approximately 0.02% of the 25 kV nominal voltage which makes 100 m a sufficiently accurate choice while also being acceptably fast to compute.

There are three types of elements used in the equivalent lumped parameter model of the electrification system:

- A lump element representing an equivalent impedance of 100 m of OHL + RR line. (This is reasonable as the current flowing through the RR is approximately equal to the current through the OHL.);
- A lump element representing the cross-bond impedances for the OHL. These cross-bonds are connected every 4 km, and also at both ends of the feeding sections for the AT system, and at every feeder station for the SFC system;
- A lump element for the internal impedance of the transformer feeder stations (only used in the AT system model). The lumped element used in this case is resistive and inductive (R + L).

Using the lumped parameter model to simulate the electrification system, the system is described by nodes. The line is a bi-directional railway line. This means the electrified lines consist of  $2N$  nodes where nodes 1 to  $N/2$  represent the line in one direction while  $N/2 + 1$  to  $2N$  represent the reverse line.

Figure 7 shows a schematic diagram indicating how the nodes and lumped elements are arranged and the way in which they are numbered. The nodes are illustrated by small circles. The lumped elements for the combined OHL and RR are represented by blue rectangles, and the lumped elements for cross-bonds are represented by orange rectangles. The feeder station is represented by a green circle.

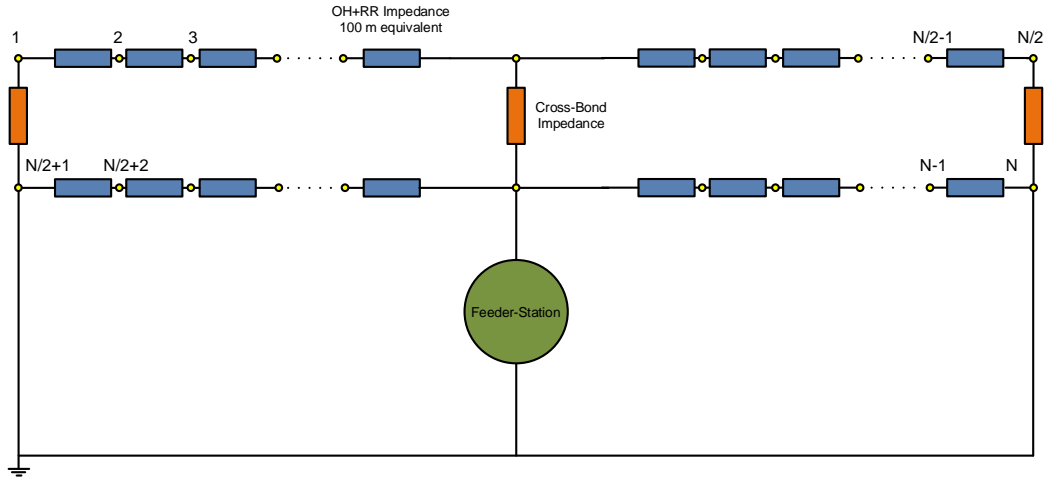


Figure 7 General schematic diagram for the lumped parameter model

### 3.1.1.1 POWER FLOW EQUATIONS

The voltage and current in the power flow equations are represented by matrices in the formats shown below:

$$[V] = \begin{bmatrix} V_1 \\ \vdots \\ V_{N_{nodes}} \end{bmatrix}, [I] = \begin{bmatrix} I_1 \\ \vdots \\ I_{N_{nodes}} \end{bmatrix}$$

The admittance matrix is created based on the impedances between the nodes of the system. The admittance matrix changes size, depending on the number of nodes in the system. A case with 3202 nodes is discussed as an example. This case only has positive feed (+25 kV line), similar to the case of the SFC system explained further in Section 3.1.3. Element  $Y(a, b)$  consists of the value of the admittance connected between nodes  $a$  and  $b$ . Element  $Y(a, a)$  consists of the value of all admittances connected to node  $a$  with the opposite sign to the non-diagonal elements of the matrix. The admittance matrix is a symmetrical matrix, i.e.  $Y(a, b) = Y(b, a)$ .

$$[Y] = \begin{bmatrix} -Y_{1, 1} & \cdots & Y_{1, N_{nodes}} \\ \vdots & \ddots & \vdots \\ Y_{N_{nodes}, 1} & \cdots & -Y_{N_{nodes}, N_{nodes}} \end{bmatrix}$$

The example in Figure 8 shows the case where a feeder station is connected to the node and hence injecting current into the system. Where a train is connected to a node, it draws current from the system, in which case the representative value in the currents vector would be negative. For any node that has no injection or drawing of current, the resultant current would be zero. The location of the train in this model affects the power flow solution by the node number from which it is drawing current. The movement of the train in this model is, as previously described, discrete as the train jumps from one node to the subsequent node.

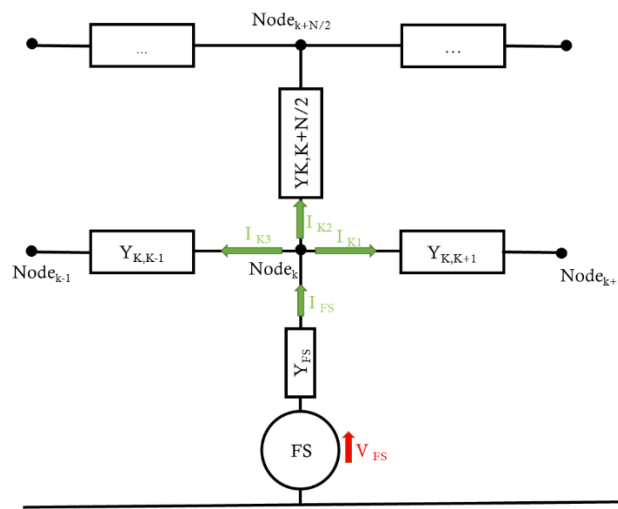


Figure 8 Power flow example

Using Kirchoff's current law for Figure 8, which represents a section of the whole system drawn in Figure 7, it is possible to write the following equations:

$$I_{FS} = I_{K1} + I_{K2} + I_{K3}$$

$$Y_{FS}V_{FS} = Y_{K,K-1}(V_K - V_{K-1}) + Y_{K,K+1}(V_K - V_{K+1}) + Y_{K,K+N/2}(V_K - V_{K+N/2})$$

$$Y_{FS}V_{FS} = V_{K-1}(-Y_{K,K-1}) + V_K \left( Y_{K,K-1} + Y_{K,K+1} + Y_{K,K+N/2} \right) + V_{K+1}(-Y_{K,K+1}) + V_{K+N/2}(-Y_{K,K+N/2})$$

$$\begin{bmatrix} \dots & -Y_{K,K-1} & Y_{K,K-1} + Y_{K,K+1} + Y_{K,K+N/2} & -Y_{K,K+1} & \dots & -Y_{K,K+N/2} & \dots \\ & & \vdots & & & \vdots & \end{bmatrix} \begin{bmatrix} \vdots \\ V_{K-1} \\ V_K \\ V_{K+1} \\ \vdots \\ V_{K+N/2} \\ \vdots \end{bmatrix} = \begin{bmatrix} \vdots \\ \vdots \\ I_K \\ \vdots \\ \vdots \end{bmatrix}$$

As demonstrated above, using Kirchoff's laws, the arrangement of this system is then defined using the admittance matrix  $[Y]$ , the voltage matrix  $[V]$  and the current matrix  $[I]$ . The admittance matrix  $[Y]$  in this case contains admittance values between the nodes. The voltage  $[V]$  and current  $[I]$  are  $N$  by  $1$  matrices containing the complex voltage and current values at each node. The relationship between the current and voltage at each node can then be written as the following equation:

$$[Y][V] = [I]$$

### 3.1.2 MODELLING OF THE AT SYSTEM

This section describes the mathematical model used to represent the AT system. The AT system has been modelled to provide a comparable basis for analysis of the controlled SFC model. The model uses the basic principles discussed in Section 3.1.1. The AT system has been chosen as a comparative transformer-based model as it is the most efficient solution for transformer-based railway electrification to date. The aim of installing ATs on electrified lines is to keep the voltage drop to a minimum and keep a supply voltage as close to 25 kV as possible throughout by minimising the supply current. In the AT system, a dual 25 kV supply is created through a 50 kV supply split by means of a three-winding transformer. The voltage between the catenary and the rails is  $180^\circ$  out of phase in comparison with the voltage between the negative phase and the rails. In order to tailor the system described in Section 3.1.1 to accommodate connected ATs, the admittance, voltage and current matrices are modified.

There are four transformers on the line, placed in pairs in feeder stations. There are ATs on the line every 10 km. The neutral isolated sections are located between the two transformers at each feeder station as well as in the middle of the line where the feeding zone of one transformer ends and another begins. The neutral sections provide isolation between the two transformers, described extensively in Section 2.2.1.

Each of the transformer feeder stations covers 40 km of the line. The transformers are connected between the catenary (also referred to as positive feed) and the rails, and the rails and the RC. In order to make

mathematical interpretation of the model easier, the terms positive and negative feed have been used. It should be noted that the term ‘negative feed’ is potentially, however, misleading. There is no ‘negative feed’ per se as the system is an AC system. The reason it is referred to as a negative feed is that the voltage applied is  $180^\circ$  out of phase in comparison with the voltage of the OHL. With respect to the equivalent circuit of the transformers, the transformers in the mathematical model have been modelled as two voltage sources connected between the rails and the positive feed, and the rail and the negative feed. Each one of these voltage sources supplies 25 kV rms but they are  $180^\circ$  out of phase. The lumped parameter models for both these lines are identical. There are mutual couplings between the catenary and contact conductors, and the same node-based system is applied as explained in Section 3.1.1. There is a cross-bond connection on the OHL wherever an AT is connected to the system as well as at every 4 km. The nodes for the AT scenario are designated as 1–3203 for the positive feed and 3204–6404 for the negative feed. There are neutral sections located to isolate the transformers from one another. These isolation sections do not have any impedances connected between them and, hence, provide disconnection from the traction where the load moves from one transformer zone to another.

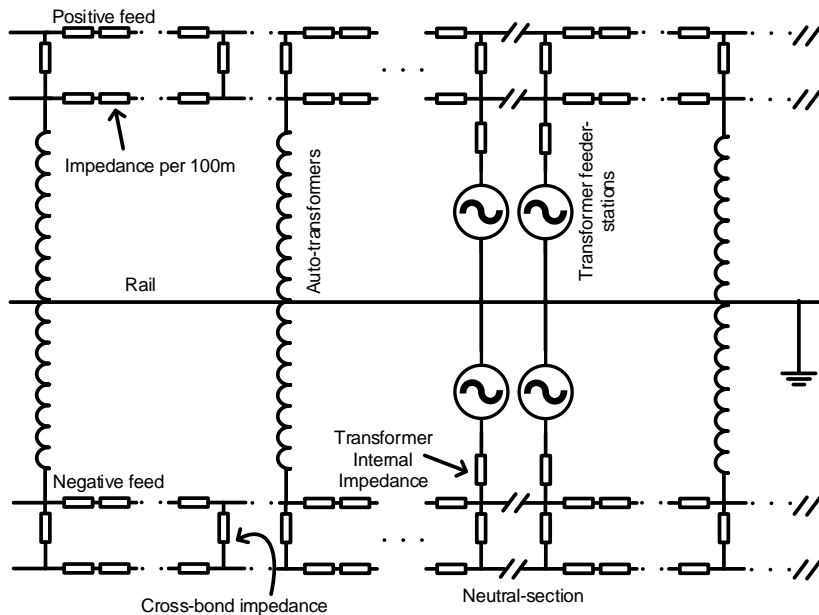


Figure 9 Schematic diagram of AT system based on the lumped parameter model

The admittance matrix for the transformer’s feeder stations without considering the ATs would look like the admittance matrix mentioned in Section 3.1. The transformer circuit is a 6404 by 6404 matrix.

However, in order to make the ATs effective in the mathematical model, some changes are made to the  $[Y]$  matrix.

The magnitudes of both the positive and negative feed voltages are 25 kV. The number of turns between the OHL and the rails, and the rails and the negative feed are equal, i.e. the ratio for the ATs is 1:1. In order to understand the reasons behind the changes to the admittance matrix, Figure 10 shows a schematic diagram for the AT connections. Each AT is connected to the catenary, the rails and the negative feed. The internal impedance of the ATs is represented by two impedances, one representing the internal impedance of the AT connected between the catenary and the rails, the other impedance representing the internal impedance of the AT connected between the rails and the negative feed. As explained previously, the AT has a 1:1 ratio; consequently, the value of each of these impedances is equal and half the value of the internal impedance of the AT. In order to model them in the system, the equation below is formed. In it, the voltage value associated with the node representing the connection of the AT to the catenary is referred to as  $V_{\text{Positive}}$  while the voltage value associated with the node representing the connection of the AT to the negative feed line is referred to as  $V_{\text{Negative}}$ . The element in the voltage matrix representing the AT voltage is referred to as  $V_{\text{AT}}$ .

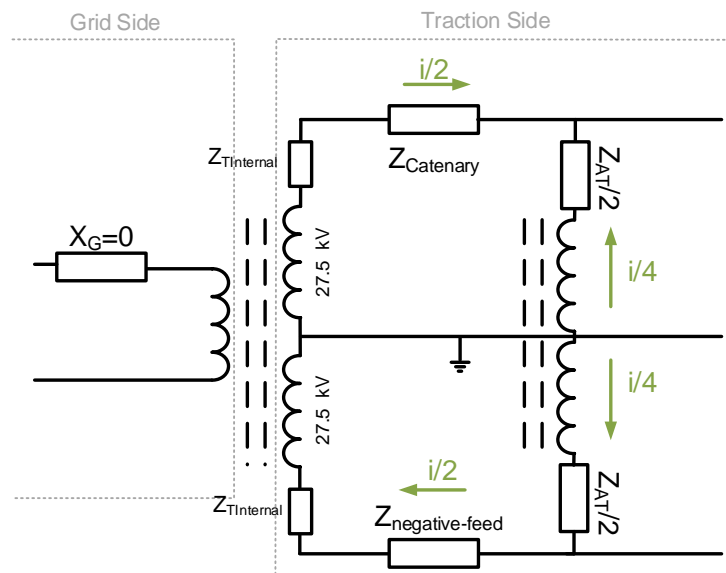


Figure 10 Schematic diagram of AT connections

Knowing that ATs are added to the system to keep the voltage drop to a minimum, or in an ideal case to zero, it is possible to write the equation below for an ideal situation:

$$V_{Positive} + V_{Negative} - 2V_{AT} = 0$$

By applying this equation to the system using the admittance matrix, the effect of the ATs will be taken into account in the power flow calculations.

### 3.1.2.1 EFFECT OF ATs ON THE ADMITTANCE MATRIX

In order to reflect the effect of the ATs on the system, a node for each AT is added to apply changes to the currents and voltages in power flow calculations. If there are  $N_{AT}$  ATs connected to the line and the  $[Y]$  matrix is a square matrix of  $N_{Nodes}$  by  $N_{Nodes}$ , the  $[Y]$  matrix then becomes a square matrix of  $N_{Nodes} + N_{AT}$  by  $N_{Nodes} + N_{AT}$ . Similarly, there are  $N_{AT}$  elements added to the bottom of the voltage and current matrices:

$$[V] = \begin{bmatrix} V_1 \\ \vdots \\ V_{N_{nodes}} \\ V_{AT_1} \\ \vdots \\ V_{N_{ATs}} \end{bmatrix}, [I] = \begin{bmatrix} I_1 \\ \vdots \\ I_{N_{nodes}} \\ I_{AT_1} \\ \vdots \\ I_{N_{ATs}} \end{bmatrix}$$

The admittance matrix for the AT system is then:

$$[Y] = \begin{bmatrix} Y_{11} & \cdots & Y_{1,(N_{nodes}+N_{ATs})} \\ \vdots & & \vdots \\ Y_{N_{nodes},1} & \ddots & Y_{N_{nodes},N_{nodes}} \\ Y_{(N_{nodes}+1),1} & & Y_{(N_{nodes}+1),N_{nodes}} \\ \vdots & & \vdots \\ Y_{(N_{nodes}+N_{ATs}),1} & \cdots & Y_{(N_{nodes}+N_{ATs}), (N_{nodes}+N_{ATs})} \end{bmatrix}$$

In addition to the standard values of the lumped elements in the admittance matrix discussed previously, as shown in Figure 10, a value of  $Z_{AT}/2$  is added to any node which has a connection to an AT.

As an example, for a 160 km line and where ATs are connected to the line every 10 km, there are two lines of catenary and two lines of negative feeder lines (four lines in total). This means that there are  $4 \times 1601$  nodes on each line (6404). The ATs are connected to nodes 1, 101, 201, 301, ..., 1601 on the

catenary side and 3203, 3303, 3403, ... , 4803 on the negative feeder side. In addition to the elements of the admittance matrix which include the line admittance and cross-bond admittances, there are non-zero elements associated with the nodes for ATs(6405, 6406, ... , 6020):

$$Y(1,6405) = \frac{Y_{AT}}{2}, Y(101,6406) = \frac{Y_{AT}}{2}, Y(201,6407) = \frac{Y_{AT}}{2} \dots$$

$$Y(3203,6405) = \frac{Y_{AT}}{2}, Y(3303,6406) = \frac{Y_{AT}}{2}, Y(3403,6407) = \frac{Y_{AT}}{2} \dots$$

This repeats for all AT nodes.

The above equation is achieved by manipulating the AT nodes in the form below:

$$Y(6405, 1) = 1, Y(6406, 101) = 1, Y(6407, 201) = 1 \dots$$

$$Y(6405, 3203) = 1, Y(6406, 3303) = 1, Y(6407, 3403) = 1 \dots$$

$$Y(6405, 6405) = 1, Y(6406, 6406) = 1, Y(6407, 6407) = -2 \dots$$

### 3.1.3 MODELLING OF THE SFC SYSTEM

For the model representing the SFC system, there is no requirement for a neutral section. Consequently, mesh and dual end feeding of the load by more than one SFC is possible, unlike in the transformer cases. It is also possible to use ATs in conjunction with the SFCs and enable these substations to be placed even further apart; however, placing the feeder stations further apart means reducing the security of the supply system and is not desired. As a result, the SFC case is modelled with a simple RR arrangement. There is no RC (previously referred to as ‘negative feed’) in this system and there are two catenary lines, one per direction and of track, there will be correspondingly more catenary lines for multiple track layouts.

The internal arrangement of the SFCs has been discussed extensively in Section 2.2.2. Figure 11 shows the schematic diagram of the SFC system using the lumped parameter model. It must be noted that inside

the SFC feeder stations there is a voltage loop that regulates the output voltage independently from the current. The SFCs are modelled as ideal voltage sources with a small impedance connected in series.

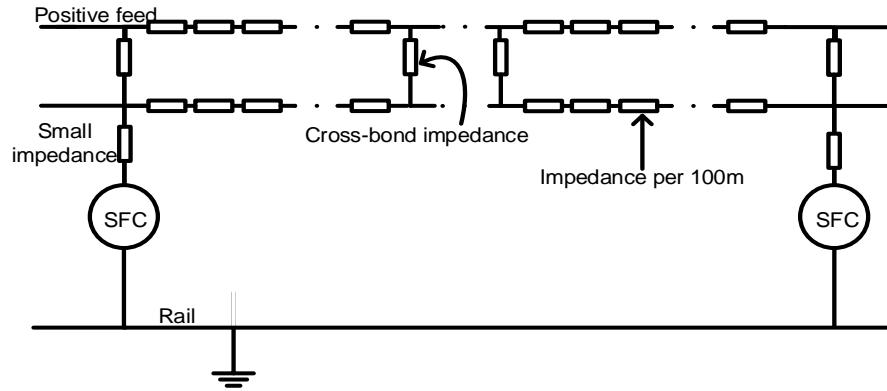


Figure 11 Schematic diagram of the SFC system based on the lumped parameter model

The admittance matrix for this scenario is as described in Section 3.1.1. In this scenario, there are two 160 km catenary lines hence there are two times 1601 nodes which makes the admittance matrix a 3202 by 3202 matrix. This matrix is a sparse matrix with admittance values for the lumped elements of 100 m of line as well as cross-bond admittances every 4 km. The voltage and current matrices are 3202 by 1 matrices.

### 3.1.4 POWER FLOW SOLUTION

The current ( $i_{train}$ ) and voltage ( $v_{train}$ ) at the train are calculated with the Holomorphic Embedding Load-Flow Method (HELM) (Trias, 2018) using the train's complex power ( $S_{train}$ ), the no-load voltage on the OHL ( $V_0$ ), and a matrix derived from the general admittance matrix ( $Y$ ) which represents the voltage drops for each train when an ampere is drawn from every train, one at a time ( $A$ ).

There have been many numerical models used to solve power flow equations since computing developed sufficiently to support them. The Gauss–Seidel model is the earliest method which, due to its slow convergence and the current availability of memory in computational calculations, has been replaced by the faster Newton–Raphson model thanks to its quadratic convergence properties (Tinney and Hart, 1967; Ward and Hale, 1956). The Newton–Raphson method, however, as an iterative method still

requires an initial estimation for the answer. As the power flow problems are multi-valued, iterative methods are highly dependent on the initial guess and can behave unreliably (Mori, 2000). The HELM method can run unattended and produce reliable results, which is vital for modern power systems applications (Trias, 2018). Considering the properties mentioned above, the HELM method has been chosen as the means of solving the power flow problems in this project, using the equations below according to HELM as explained in (Trias, 2018):

$$v_{train} = v_0 - A \times i_{train}$$

$$S_{train} = v_{train} \times i_{train}^*$$

In this method, feeder stations are represented in the no-load voltage condition. Each train is a separate bus in the power flow problem while current is injected to the nodes of the feeder stations in the current matrix. A very small series impedance, equivalent to 1 m of the OHL, has been connected to the SFCs in order that the voltage sources are converted to their equivalent current source representations to solve the power flow in nodal form.

### 3.2 CONTROL OF SFCs

Figure 12 shows an example circuit consisting of two AC voltage sources feeding a load. The first voltage source is referred as  $V_1$ .  $V_1$  has a phase angle of  $0^\circ$  and is considered to be the reference for the phase angles. The second voltage source is referred to as  $V_2$  which has a phase angle of  $\delta_{v_2}$ . There is a complex impedance  $Z$  connected between the voltage sources. There is a current  $i$  flowing through the circuit.

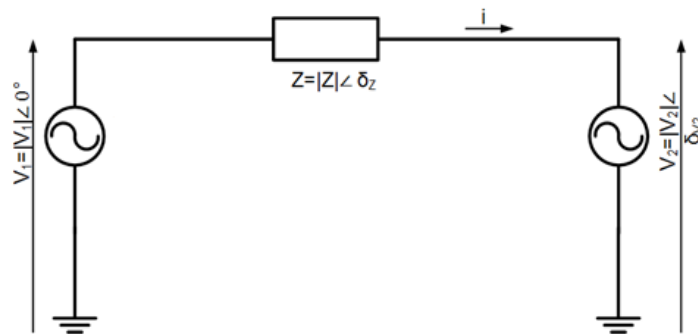


Figure 12 Schematic diagram for two substations feeding a load

Using this basic circuit and writing the active and reactive equations for the primary source, it is mathematically demonstrated that the active power control is dependent on output voltage phase angle, and reactive power control is dependent on the output voltage magnitude.

### 3.2.1 ACTIVE POWER CONTROL

The basic equation for the active power for the first voltage source is shown below:

$$P_1 = \Re \{v_1 i^*\}$$

where  $P_1$  is the active power,  $v_1$  is the complex voltage output and  $i$  is the complex current.

Considering that the phase angle of  $v_1$  is zero degrees, it is possible to write:

$$v_1 = |v_1|$$

Also, the current  $i^*$  can be written as:

$$i^* = \frac{v_1 - v_2}{Z}$$

Therefore, substituting  $|v_1|$  for  $V_1$  gives:

$$i^* = \frac{|v_1| - v_2}{Z}$$

Consequently, it is possible to write:

$$P_1 = \Re \left\{ |v_1| \frac{|v_1| - v_2}{Z} \right\}$$

Expanding the equation above gives:

$$= |v_1|^2 \Re \left\{ \frac{1}{Z} \right\} - \Re \left\{ \frac{|v_1| v_2}{Z} \right\}$$

Assuming the impedance is a purely inductive impedance, consisting of only imaginary parts, i.e.,  $Z = -jX$ , it is possible to rewrite the equation above as:

$$P_1 \cong |v_1|^2 \Re \left\{ \frac{1}{-jX} \right\} - \Re \left\{ \frac{|v_1|v_2}{-jX} \right\}$$

As  $\Re \left\{ \frac{1}{-jX} \right\} = 0$ , it is possible to rewrite the equation above as:

$$P_1 \cong -\Re \left\{ \frac{|v_1|v_2}{-jX} \right\}$$

Substituting  $v_2$  for its trigonometrical polar form i.e.  $v_2 = |v_2|(\cos \delta_{v2} - j \sin \delta_{v2})$  and multiplying the equation by  $\frac{j}{j}$ , it is possible to rewrite the above equation as:

$$P_1 \cong \Re \left\{ \frac{|v_1||v_2|(-j \cos \delta_{v2} + \sin \delta_{v2})}{X} \right\}$$

Using the small-angle approximation, i.e.,  $\sin \delta_{v2} = \delta_{v2}$ , it is possible to write:

$$P_1 \cong \frac{|v_1||v_2|\delta_{v2}}{X}$$

Assuming the magnitudes of the voltage generated by the two substations are approximately equal, i.e.,  $|v_1| \cong |v_2|$ , it is possible to write:

$$P_1 \cong \frac{|v_1|^2}{X} \delta_{v2}$$

And, consequently, it is possible to draw the conclusion:

$$P_1 \propto \delta_{v2} - \delta_{v1}$$

From the equations above, it is possible to conclude that active power is directly proportional to the difference between the phase angles of the output voltages.

### 3.2.2 REACTIVE POWER CONTROL

The basic equation for the reactive power for the first voltage source can be written as:

$$Q_1 = \Im\{v_1 i^*\}$$

where  $Q_1$  is the reactive power output,  $v_1$  is the phasor voltage output, and  $i$  is the phasor current.

Considering that the phase angle of  $v_1$  is zero degrees, it is possible to write:

$$v_1 = |v_1|$$

Also, the current  $i^*$  can be written as:

$$i^* = \frac{v_1 - v_2}{Z}$$

Therefore, substituting  $|v_1|$  for  $v_1$  gives:

$$i^* = \frac{|v_1| - v_2}{Z}$$

Consequently, it is possible to write:

$$Q_1 = \Im\left\{|v_1| \frac{v_1 - v_2}{Z}\right\}$$

Expanding the equation above gives:

$$Q_1 = |v_1|^2 \Im\left\{\frac{1}{Z}\right\} - \Im\left\{\frac{|v_1|v_2}{Z}\right\}$$

Assuming the load is a purely inductive load consisting of only imaginary parts, i.e.  $Z = -jX$ , it is possible to rewrite the equation above as:

$$Q_1 \cong |v_1|^2 \Im\left\{\frac{1}{-jX}\right\} - \Im\left\{\frac{|v_1|v_2}{-jX}\right\}$$

Substituting  $v_2$  for its trigonometrical polar form, i.e.  $v_2 = |v_2|(\cos \delta_{v2} - j \sin \delta_{v2})$ , it is possible to rewrite the above equation as:

$$Q_1 \cong \frac{|v_1|^2}{X} - \frac{|v_1||v_2|}{X} \cos \delta_{v_2}$$

Using the small-angle approximation, i.e.  $\sin \delta_{v_2} = \delta_{v_2}$ , it is possible to write:

$$Q_1 \cong |v_1| \frac{|v_1| - |v_2|}{X}$$

And, consequently, it is possible to draw the conclusion:

$$Q_1 \propto |v_1| - |v_2|$$

From the equations above, it is possible to conclude that reactive power is also directly proportional to the difference between the magnitudes of the output voltages.

### 3.3 CONTROL METHOD

From the mathematical demonstration above, it is possible to see that using a control system which manipulates the phase angle and the magnitude of the substation voltages enables control over the contribution of active and reactive power from each feeder station.

It is important to notice that although a power flow analysis is easily conducted in a scenario where the location of the train is known, and the impedances can be calculated, it is not easy to accurately obtain and communicate this information to the control system. The control system for this project has been designed in a way that it does not require information about the location of the train, as explained later in Section 3.3.1.

A central control system has therefore been designed which communicates with all the feeder stations in the network. This central control could be placed in a cubicle anywhere on the line, including at one of the feeder stations in the event of a commercial implementation or prototyping.

Figure 13 is a high-level schematic diagram showing the required data communications between the feeder stations and the central control system. For the control system designed, the output voltage and current of each feeder station on the network should be measured and converted into complex form. Using these data inputs, it is possible to calculate the complex power for each feeder station and

consequently its active and reactive power. The control centre then calculates and adjusts the values for the phase angle and voltage of each feeder station as further explained in this chapter.

It must be noted that the central control's communication with each SFC as well as the processing time for calculations will result in a delay in the system. The communication platform shall be chosen such that the time required to receive the data in the central control unit, carry out calculations and transmit the data back to the SFC is shorter than the switching period.

For example, assuming a scenario where the longest distance the data needs to travel is 40 km, one-way transmission will take  $134 \mu\text{s}$  and both ways would take  $268 \mu\text{s}$ . Assuming that the PWM generator has a switching frequency of at least 1 kHz, the switching period for the pulses is 1 ms. The delay incurred by transmitting the data is smaller than the switching period and, consequently, the delay would not cause significant disturbance to the accuracy of the system. The error would be 0.842 radians in the calculation of the phase angle for the second substation, as the phase of the first substation changes during transmission. Predictive control techniques can be used to compensate for these issues.

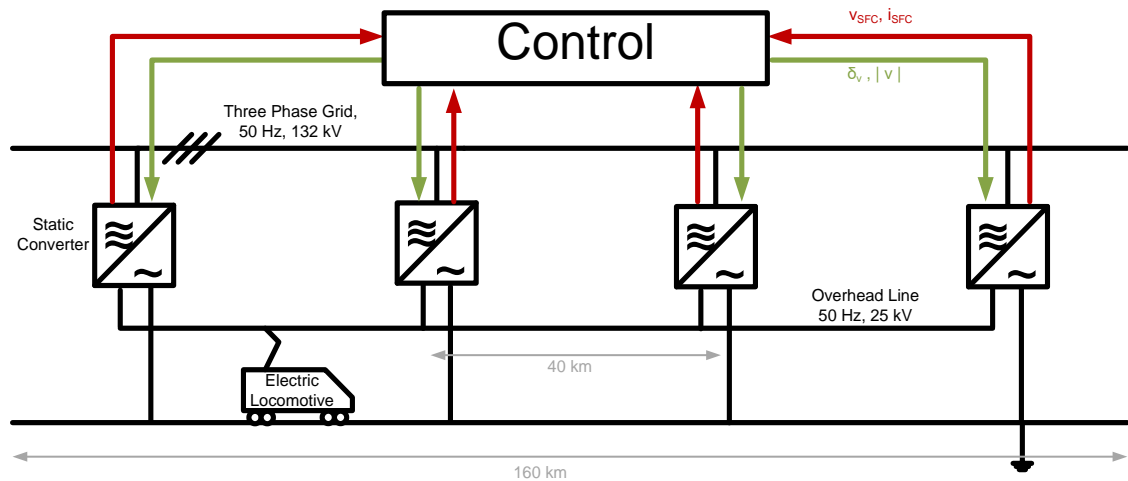


Figure 13 Schematic of the communication system between the feeder stations

Given that both active and reactive powers can be manipulated, and that a distributed control system capable of simultaneously managing a network of SFC feeder stations is realisable, it is therefore conceivable that a control system for the whole SFC network based on management of these outputs could be developed. The author of this thesis proposes a control strategy, where active and reactive

power will be manipulated at each feeder station in order that the network of SFC feeder stations can work together to share the loads on the network equally.

This control strategy has been proposed in order to support the evaluation of the hypothesis that intelligent control of SFC feeder stations would have the potential to reduce costs and increase operational robustness and flexibility within the railway network. Specifically, the control system is used to investigate the potential benefits available through reduction of the power ratings for each SFC feeder station.

### 3.3.1 EQUAL SHARE OF ACTIVE AND REACTIVE POWER

In order to implement the required control system which enables smart control of the contribution of power from each feeder station, PI closed-loop controllers are used in the central control system.

As the aim of the system is to share the active and reactive power equally between the feeder stations, the error signals are calculated by comparing each feeder station's active and reactive power with the average of the active and reactive power generated by all feeder stations on the network, respectively. Using the main principles of PI controllers for a discrete time system, it is possible to write:

$$u_k = k_p e_k + k_i \sum_{n=1}^k e_n \Delta t$$

For active power control:

$$P_{average} = \frac{1}{n} \sum_1^n P_n$$

$$e_n(t) = P_n - P_{average}$$

For reactive power control:

$$Q_{average} = \frac{1}{n} \sum_{1}^n Q_n$$

$$e_n(t) = Q_n - Q_{average}$$

Figure 14 shows a block diagram of the PI controller for active power for an example of four feeder stations and Figure 15 shows a block diagram of the PI controller for reactive power for an example of four feeder stations.

A saturation limit is implemented to avoid exceeding a change of angle of more than a value of  $\pi/2$  as in such a case the active power would change sign and, consequently, make the system unstable.

The coefficients for the PI controller have been found using an iterative approach as, due to the non-linearity of the system, it is not within the scope of the PhD thesis to calculate the coefficients mathematically.

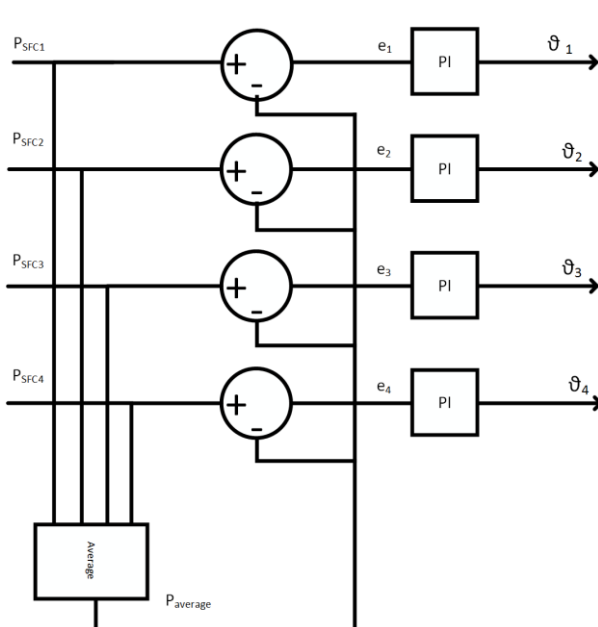


Figure 14 Block diagram of the closed-loop controller for determination of the reference voltages of the feeder stations – active power

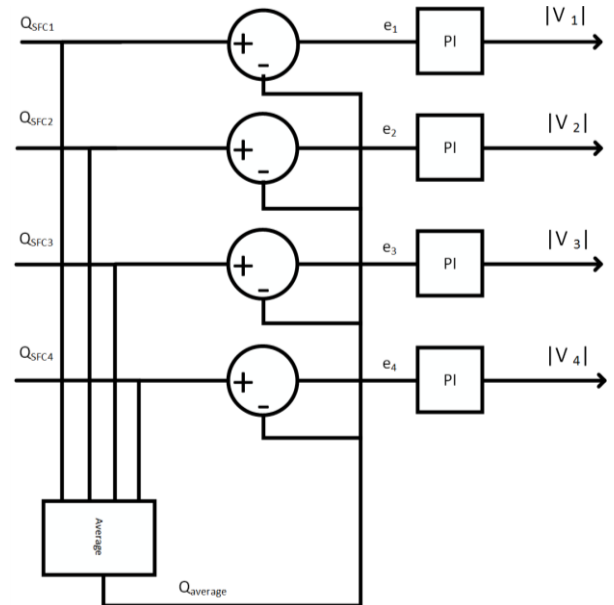


Figure 15 Block diagram of the closed-loop controller for determination of the reference voltages of the feeder stations – reactive power

Control of the SFCs is achieved through 20 iterations of 0.08 s each at every time-step, i.e. the time-step is 1.6 s in total. This, in an ideal situation, transfers the information of phase angle and magnitude of voltage to be implemented through PWM generation of the SFC converters to produce the desired output.

### 3.4 SUMMARY

This chapter has described the principles behind the mathematical modelling of the traction system infrastructure and the use of lumped parameter modelling for both transformer- and SFC-based systems as well as the power flow solutions required to calculate the voltage and current values across the systems. A conventional synchronised phase angle control strategy for SFC-based feeder stations has been described. Additionally, a novel control strategy has been conceptualised that manipulates voltage magnitude and phase angle to output specifically desired reactive and active power levels in order to allow the equal sharing of loads across a network of SFC feeder stations.

While this chapter has defined the mathematical model behind the transformer-based and SFC-based power systems, in order to support the analysis required to validate the hypothesis of this PhD, example scenarios are required where trains run on this mathematically represented infrastructure and, hence, using the output data it is possible to investigate the behaviour of a network of running trains to draw conclusions and address the hypothesis. These scenarios are designed to represent close-to-real-life examples of a high-speed railway line and are then developed into numerical simulations based on the theory described in this chapter. These examples are defined in detail in the following chapter.

# 4 SIMULATIONS OF SFCs FOR AC RAILWAYS AND COMPARISON WITH AT SYSTEMS

## 4.1 INTRODUCTION

In order to be able to facilitate an analysis of the proposed control systems for SFC-based AC railway supply systems and their comparison with the current state-of-the-art transformer-based traction supply systems, a mathematical model of the AC electrification system was developed and described in Chapter 3. Chapter 3 provides the basis of the electrification system which includes a central PI control, however, tuning of the PI controller is dependent on the arrangements in which it is applied. In this chapter, and building on the mathematical models, detailed simulations have been developed to represent scenarios close to real circumstances, thereby allowing analysis of system performance and realistic comparisons between electrification system options.

The simulation scenarios developed for this project have been designed and approximated based on the duration of a full journey on the existing line between Birmingham New Street station and London Euston station, at peak time of weekdays. This line is approximately 160 km long, which has been used as the distance of the journeys investigated in this PhD thesis.

The transformer-based system has also been taken into account and analysed as, in order to make a valid comparison and analysis, it is important to analyse the conventional electrification scenarios in the study as a point of reference and means of comparison. Consequently, both transformer-based and SFC-based line arrangements have been simulated. The detailed basis of the mathematical design of these systems has been described in Section 3.1.

## 4.2 LINE CONFIGURATION: TRANSFORMER-BASED ELECTRIFICATION SYSTEM WITH AUTOTRANSFORMERS

As discussed in Section 2.2.1, the average distance between each pair of transformer feeder stations on a conventional railway is 80 km, and there are neutral sections every 40 km. Consequently, for a line 160 km long there are pairs of transformers located at 40 km and 120 km, as shown in Figure 16. For the detailed mathematical design of such a line, please refer to Section 3.1.2.



Consequently, the effect of increasing the distance between two SFC feeder stations is smaller than increasing the end distance for the same amount.

However, in order to have a fair comparison between the different electrification and control systems, in this chapter a line arrangement has been designed for the SFC-based system which uses four SFC feeder stations, the same number as in the AT case, but not in the same locations.

Assuming a simplified scenario with a single load which draws constant power, if  $x$  metres is added to the distance between two feeder stations, the energy loss over the journey will increase with approximately in proportion to  $\frac{x^2}{4}$  but if the same  $x$  metres is added to the end section (i.e., not between the feeder stations) the energy loss will be greater, increasing approximately in proportion to  $\frac{x^2}{2}$ . Hence, in this configuration, the SFC feeder stations are 40 km apart, and the end sections between the end of the line and the SFCs are 20 km long. The end of the line distances are each half the distance between each SFC feeder station, which makes the impedance around each SFC feeder station symmetrical and identical to one another. The symmetry reduces the effects of too many variations on the analysis of the results. The arrangements are as presented in Figure 17.

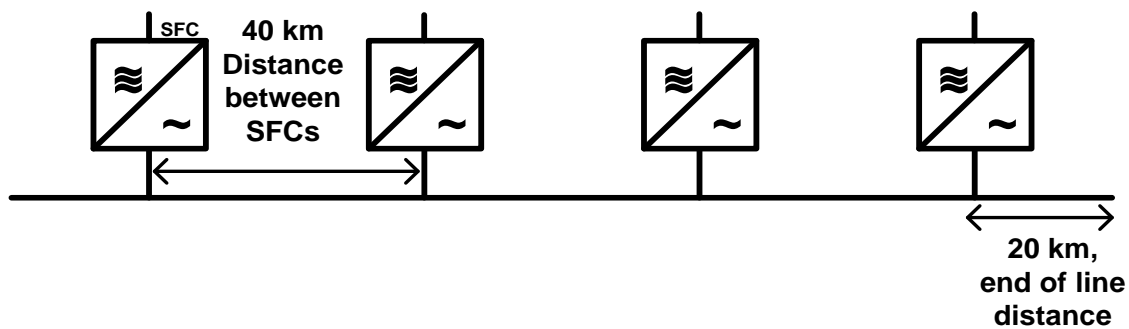


Figure 17 Arrangement of SFC feeder stations

The positions of the SFC feeder stations on the line are summarised in Table 3 below.

Table 3: SFC Positions along the line

SFC	1	2	3	4
Node Number	201	601	1001	1401
Distance [km]	20	60	100	140

The line configuration described above is compatible with both of the control strategies being considered in this thesis. By retaining the same arrangement, it is possible to undertake a direct comparison of the SFC system without and with smart control that shares the active and reactive power load equally between all feeder stations. The basic mathematical models of the electrification system for both these scenarios are identical.

- a- A scenario where SFC feeder stations are synchronised. In this case, the phase angle and magnitude of the voltage are always synchronised (equally) for all SFC feeder stations on the line.
- b- A scenario where the phase angle and magnitude of the output voltage from the SFC feeder stations are manipulated in order to enable equal sharing of active and reactive power outputs.

#### 4.4 TRAIN ACCELERATION, SPEED, POWER AND TIMETABLE

In this PhD thesis, some simulations are conducted using a constant power load in order to provide more easily interpretable and comparable results. However, in general, assuming the trains to be a constant power load does not represent a real-life scenario. Class 390 trains have therefore been used for the train simulations. An estimation of the acceleration and deceleration power profiles has been calculated from measurements obtained for a British Class 390 train.

The maximum train power used or deployed is 5.1 MW while accelerating or braking, this drops to 3.125 MW during cruising where the train moves with constant speed, which has been calculated using the Davis Equation as presented below (Rochard and Schmid, 2000):

$$R = A + Bv + Cv^2$$

Where R is the rail vehicle's resistance, V is the velocity of the vehicle, A is mass resistance coefficient (speed independent), B is the mechanical resistance coefficient and C is the air resistance coefficient.

The Power is then calculated based on the following equation:

$$P = Fv$$

Where P is power, F is force, in this case the rail vehicle's resistance, and v is velocity.

It must be noted that, due to an error in earlier stages of the project, the value used for the train when moving at constant speed in Chapters 5, 6, 7 is lower than the value calculated here using the Davis Equation. The value used for the calculations in these chapters is 675 kW. This does not affect the conclusions drawn in this thesis, however, and has consequently been considered acceptable by both examiners of this thesis.

The values used for the above equations in this thesis are for a Class 390 Pendolino train. The values used are presented in Table 4. Using the coefficients presented in Table 4 for the Davis Equation would result in the following values of train resistance (R) in kN, kN/m/s and kN/m<sup>2</sup>/s<sup>2</sup>.

*Table 4 Class 390 Pendolino Parameter values used for Davis Equation*

Parameter	Value
A	5.421599486
B	0.069031701
C	0.0103098948

The train is not 100% efficient and, consequently, the electrical power requirements are greater than the mechanical power. Coefficients are therefore used to establish the electrical power requirement for acceleration, and the electrical power output during braking. These coefficients are 1.43 and 0.57 respectively and have been obtained from (ABB Traction, 2018). The maximum electrical power required for acceleration is therefore 7.293 MW, cruising is 4.468 MW, and the electrical output of the train when braking is 2.907 MW. The maximum line speed considered for these simulations is 225 km/h.

The acceleration of the train has been calculated using real data for tractive effort, drag, velocity and mass from a British Class 390 train travelling at up to a maximum line speed of 225 km/h. From Newton's second law, it is possible to write the following equation:

$$mf = T(v) - D(v) - B - mg \sin \alpha$$

Where  $m$  is the mass of the train,  $f$  is the acceleration,  $T(v)$  is the tractive effort of the train as a function of velocity,  $D(v)$  is the drag or train resistance as a function of velocity,  $B$  is the braking force and  $\sin \alpha$  is the gradient.

Using the equation above, it is possible to build an acceleration and deceleration profile for the vehicle.

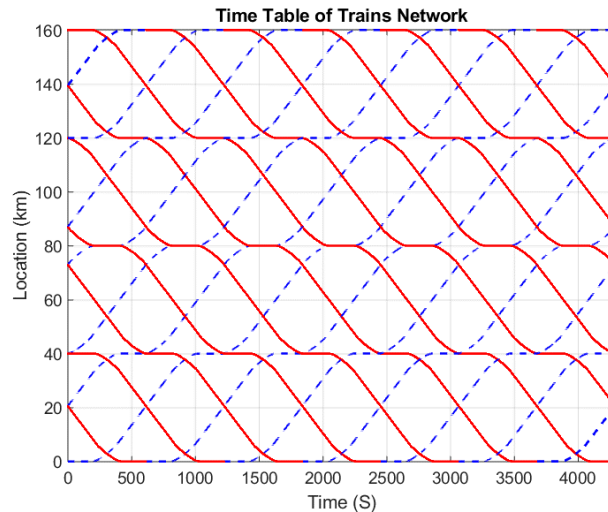


Figure 18 Time-distance graph of train service

In order to implement a scenario that demonstrates the complexities of multiple trains operating within the network, a simple timetable for the route has been designed in which multiple journeys occur simultaneously and trains run in both directions. The trains have a 10-minute headway in each direction according to the timetable shown in Figure 18. There are five train stations on the line, located at nodes 1, 401, 801, 1201 and 1601. These correspond to the start and ends of the line, and at 40 km, 80 km, and 120 km along the line. All trains travelling on this route stop at every station, regardless of their direction of travel. The stations are evenly distributed over the entire route in order to facilitate clear interpretation of the results.

## 4.5 ENERGY LOSS AND SYSTEM EFFICIENCY

This section considers the mechanisms for calculating first the losses incurred during the transmission of power throughout the system, be it between the feeder stations and the trains, or between trains. Once the transmission losses are calculated they are used in the calculation of transmission efficiency, which, combined with the internal efficiency of the feeder stations, provides a metric for overall system efficiency.

### 4.5.1 ENERGY LOSS

The transmission energy loss during the journey has been calculated based on the difference between the total energy generated by the feeder stations and the total energy consumed by the loads on the line, i.e., the trains. The regenerative power fed back into the system is described with a negative sign in the power generation profile of the feeder station as well as for the train power profile; consequently, it is also taken into account when calculating the total energy loss and transmission energy loss of the system.

The total energy supplied and recovered by each feeder station is calculated as shown in the equation below:

$$E_{SFC_i total} = \sum_{1}^{n=N} P_{SFC_N} \times TimeStep$$

where  $E_{SFC_i total}$  is the total energy supplied and recovered by the  $n^{\text{th}}$  SFC over the journey,  $N$  is the total number of time steps taken in the journey,  $P_{SFC_N}$  is the instantaneous active power generated by the SFC at the  $N^{\text{th}}$  time step and  $TimeStep$  is 1.6 s as explained in Section 3.3.1.

The total energy supplied and recovered by all feeder stations is then calculated by summing the individual contributions as described in the equation below.

$$E_{SFCs total} = \sum_{1}^{n=i} E_{SFC_n total}$$

where  $E_{SFCs\ total}$  is the total energy supplied and recovered by all SFCs combined over the completed journey,  $i$  is the total number of SFCs and  $E_{SFC_i\ total}$  is the contribution by the  $n^{\text{th}}$  SFC over the journey.

The total energy consumed, or generated in the case of regenerative braking, by the trains over the journey is calculated in a similar fashion to that for the SFCs where the SFCs are replaced by trains:

$$E_{Train_i\ total} = \sum_1^{n=N} P_{Train_N} \times TimeStep$$

where  $E_{Train_i\ total}$  is the total energy consumed, or generated by the  $i^{\text{th}}$  train over the journey,  $N$  is the total number of time steps taken in the journey,  $P_{Train_N}$  is the instantaneous active power consumed or generated in the case of regenerative braking by the train at the  $N^{\text{th}}$  time step and  $TimeStep$  is 1.6 s.

The total energy consumed or generated in the case of regenerative braking by all trains is then calculated by summing the individual total consumption/generation, as described in the equation below.

$$E_{Trains\ total} = \sum_1^{n=i} E_{Train_n\ total}$$

where  $E_{Trains\ total}$  is the total energy consumed/generated by all trains combined over the completed journey,  $i$  is the total number of trains and  $E_{SFC_i\ total}$  is the total energy generated by the  $n^{\text{th}}$  train over the journey. It must be noted that in the simulations for this project, the trains' journeys are implemented in such a way that when a train finishes a journey, another one starts the journey from the start point. The total number of trains within the simulation remains constant.

The transmission loss over the whole journey is then calculated by subtracting the total energy consumed/generated by the trains from the total energy generated/fed back into the grid by the SFC feeder stations.

$$E_{TransmissionLoss} = E_{SFCs\ total} - E_{Trains\ total}$$

#### 4.5.2 SYSTEM EFFICIENCY

The efficiencies of the transformers and the ATs have been accounted for by the values of the internal impedances used in the impedance matrix used to solve the power flow equations of the system. The AT system efficiency is calculated by deducting the total energy loss of the system from the total energy output from the transformer feeder stations in the system.

While the efficiency of the transformers and ATs has been taken into account as internal impedance, the same approach cannot be applied to the SFC feeder stations as their efficiency does not affect the impedance matrix used to solve the power flow of the system. Consequently, the method in which the efficiency of the system is calculated is different for the SFC system from that for the AT system.

The efficiency of the SFC system is calculated based on the total transmission energy loss described in Section 4.5.1 and the internal efficiency of the feeder stations. The internal power losses of SFCs have been modelled using the efficiency curve shown in Figure 19, which is based on Siemens Sitras plus converters (Burlein and Gruber, 2013).

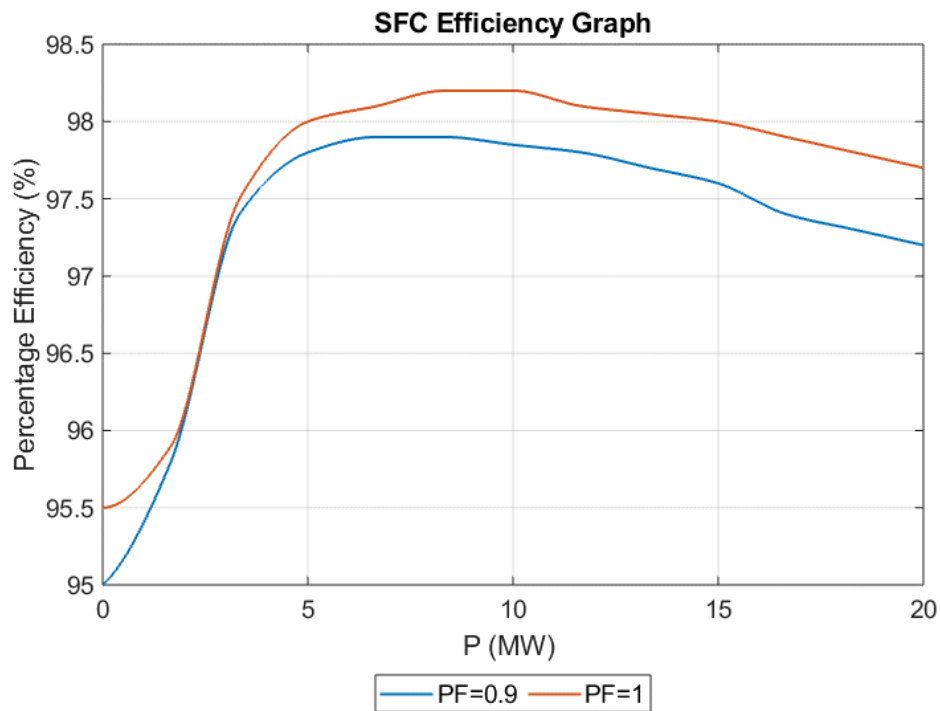


Figure 19 SFC efficiency curves plotted for PF 0.9 and PF 1

As visible from Figure 19, the maximum rated efficiency is not aligned with the maximum rating of the SFC. The SFC should be rated in a way that the average estimated power required to be supplied falls in the most efficient section of the efficiency curve. In order to find the true efficiency curves associated with the SFC feeder stations, the efficiency curve should be refitted for an SFC system supporting the maximum power calculated throughout the journey for each scenario plus a margin.

The overall efficiency of the system is therefore calculated based on this, the inputs to the system, i.e., the regenerated energy and the sum of the output energy from the SFC feeder stations, and the outputs, i.e. the energy that the SFC feeder stations put back into the grid and the energy used by all the trains on the line.

$$\text{System Efficiency} = \frac{\sum E_{Trains} + \sum E_{SFC\ Input}}{\sum E_{SFC\ Output} + \sum E_{Regen}} \times \bar{\eta}_{SFC}$$

where  $\sum E_{Trains}$  is the total energy consumed by the trains throughout the service,  $\sum E_{SFC\ Input}$  is the total energy fed back to the grid due to the energy generated by the deceleration of the trains,  $\sum E_{SFC\ Output}$  is the total energy output from the SFC feeder stations into the system,  $\sum E_{Regen}$  is the total energy generated by the trains throughout the journey and  $\bar{\eta}_{SFC}$  is the average internal efficiency of the SFC feeder stations throughout the journey.

#### 4.6 VOLTAGE LIMITS

Voltage regulation is one of the biggest problems which the railway electrical network is currently facing with conventional AT systems (Celli et al., 2000). The maximum voltage limit defined for the line without creating damage to the equipment, trains or the infrastructure of the rail electrical network is 29 kV and the minimum voltage limit is 16 kV according to Network Rail standard EN 50130 (CENELEC, 2007).

In the simulations, it is possible to observe all nodal voltages and react to reaching the maximum and minimum voltages at any node. It is not possible, however, to use this in any real-life scenario as not all nodal voltages are known. In order to design a regulation mechanism applicable to real scenarios, a voltage estimator could be used to estimate the lowest and highest voltages based on the arrangements

of the transformers or SFC feeder stations on the line. Using the nodal voltages available within the simulations, a voltage regulation system has been implemented for this project in order to ensure that the systems being simulated operate within the permitted voltage limits.

The magnitude of the voltage output from the SFC feeder stations can be increased to compensate for the voltage drop on the line up to the point at which it reaches the limit for the line. Due to the SFC feeder stations' dual-end and mesh-feeding capabilities (Behmann and Rieckhoff, 2011), the voltage drop for scenarios with SFC feeder stations is significantly lower than for BT and AT feeder stations. This is because of the shorter distance a single feeder station covers in the SFC scenario. Where the feeder stations are operating at the maximum possible output and yet the minimum voltage limit has been reached somewhere on the line, the distance is too great and not acceptable. It has to be considered, in the scenarios where there are smart control capabilities, that the magnitude of voltage output from the feeder stations can be tuned dependent on a voltage predictor which can predict the minimum voltage on the line and increase the magnitude of the output voltage from the SFC feeder stations accordingly (Antonio De Souza Ribeiro et al., 2018; Porcarelli et al., 2015).

In the simulation case with equal sharing of active and reactive power between the SFCs, it is possible that while attempting to achieve equal reactive power the maximum voltage is reached at one or more SFCs. In this case, the SFC which has reached the maximum voltage maintains its voltage value regardless of instructions to further increase it from the PI control system. The other SFCs would provide additional power and equal reactive power would not be attained.

#### 4.7 DEMONSTRATION WITH SINGLE-TRAIN EXAMPLES

In order to clarify the concepts described in this chapter and to help understand the power system arrangements in different scenarios, in this section, examples of a single train completing journeys in different scenarios are included.

To show the behaviour of the power system without the complication of the train's acceleration, cruising and regeneration, a set of scenarios is presented showing the feeder station profiles for the journey of a single train drawing a constant maximum (acceleration) power at all times. A scenario with a single

train drawing variable power, as described in Section 4.4, is also presented to show more detailed and realistic behaviour of the system.

These journeys are modelled in the following three power system arrangements:

- 1- AT system, as described in Section 4.2.
- 2- Synchronised SFCs, as described in Section 4.3.
- 3- Equally sharing active and reactive power SFCs, as described in Section 4.3.

#### 4.7.1 SINGLE TRAIN WITH CONSTANT POWER

The active and reactive power profiles of the four transformers on the line for a single train completing a normal journey profile, but drawing a constant power of 7.293 MW, are presented below.

The train starts its journey spending 3 minutes (113 time steps, each time step being 1.6 s) stationary at the first station. Once accelerating, the speed gradually builds up as described in Section 4.4. This means that the train is not travelling a whole node (100 m) with every time step (1.6 s) when stationary, accelerating or decelerating. The train only moves a node with every time step where it is moving with constant maximum speed (225 km/h). This is the reason why the graphs are based on time step as the x axis rather than node number. The train is, however, drawing the 7.293 MW at all times in this case, even when stopping at the stations.

##### 4.7.1.1 ACTIVE POWER PROFILE FOR A SINGLE TRAIN WITH CONSTANT POWER

###### 4.7.1.1.1 AT SYSTEM

Figure 20 shows the active power profile of four transformer feeder stations placed on the line, as described in Section 4.2, for a single train going through a complete journey drawing constant power at all times.

For the first 113 time steps, the train is at its furthest location from the transformer feeder station which is providing its required power, i.e., Transformer 1. Consequently, the losses are greatest at that point and Transformer 1 provides its maximum active power at that point. After the stationary period, the train

moves towards Transformer 1; the losses decrease due to the closer proximity and consequently the active power output of Transformer 1 reduces. The ripples on the curve are due to the presence of ATs in the system, which affect the voltage levels and consequently the active power output from Transformer 1. The train reaches Transformer 1, located on node 400, at time step 630. There is a neutral section between Transformer 1 and Transformer 2. The output active power for both transformers is zero at that point. After passing the neutral section, the train then takes its required power from Transformer 2. At time step 631, the train has reached the second station and stops for 3 minutes. The train is at its closest location to Transformer 2 and hence the least active power output supplied by Transformer 2 is at that location and between time steps 631 and 784 when the train then starts moving again. The second isolation point is located at node 800 which means the furthest location where the train is taking its power from Transformer 2 is time step 1271 and hence the maximum active power output of Transformer 2 is at that point. The train then switches to Transformer 3's feeding zone at the furthest location from it. It then moves towards Transformer 3 located at node 1200 and passes the isolation point between Transformer 3 and Transformer 4.

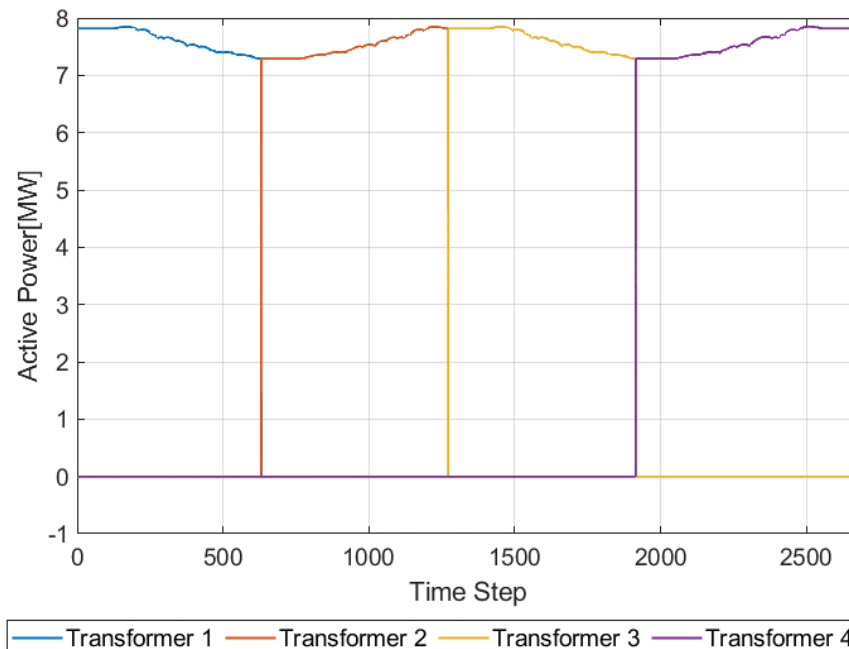


Figure 20 Single-train with constant power, active power profile for the AT system scenario

The train then switches to Transformer 4's feeding zone until the end of its journey. The maximum active power output amongst all transformer feeder stations is 7.849 MW. This occurs when the train is furthest from the feeder station supplying it.

#### *4.7.1.1.2 SYNCHRONISED CONTROL OF SFCs*

Figure 21 presents the active power profiles of four SFC feeder stations located on the line, as described in Section 4.3.

In this case, the feeder stations have a synchronised voltage magnitude and phase angle. This means that dual-end feeding will occur when the train (load) is between two feeder stations. At the end sections of the line, in this case between the start and SFC1 and between SFC4 and the end of the line, only one feeder station is supplying the load.

As described in Section 4.7.1.1.1, the train starts its journey with a 3-minute stopped period at the first station, which is located at the beginning of the line. This location is the furthest from SFC1 and, due to this SFC being the only feeder station directly connected to the load, it is the sole source of power supply to the train. Due to the location being the furthest and only one SFC providing the supply, the losses are largest at node 1 which corresponds to time steps 0 to 113. While the train passes SFC1 at time step 378, located at node 201, then the required load power is provided by both SFC1 and SFC2. As shown in Figure 21, immediately after passing SFC1 most of the power required by the train is still supplied by SFC1. As the train moves away towards SFC2 a bigger share of the power is provided by SFC2. The active power provided by each of SFC1 and SFC2 is inversely proportional to the distance of the train from each SFC. The second station is located at node 401 which is reached by the train at time step 635. This station is equidistant between SFC1 and SFC2 which means the power required for the train is equally shared between these two feeder stations at this point.

It must be noted that, although at this point the train is 20 km away from its nearest feeder station, the outputs of both SFC1 and SFC2 are lower than when the train starts its journey despite it being the same distance between the train and the single feeder station in that case. This is because at the beginning of

the journey the train is taking all its power from SFC1, as it is at the end of the line, whereas at the middle point between SFC1 and SFC2, which is the train's furthest distance from the two feeder stations and consequently has the largest losses, the required power is shared equally between SFC1 and SFC2. Moving on from the station, SFC2 has a bigger share of the active power required by the train compared to SFC1. This is due to the shortening of the distance of the train from SFC2 compared with SFC1. The train then carries on until reaching SFC2 (located at node 601 and reached at time step 1020) where the train takes almost all of its required active power from SFC2 due to being located at this feeder station at that point. This point is where SFC2 has its maximum active power output as it alone is supplying all the train's required power. Passing SFC2, SFC2 and SFC3 both provide a proportion of the train's required power depending on the train's location, as previously described for when the train moves between SFC1 and SFC2.

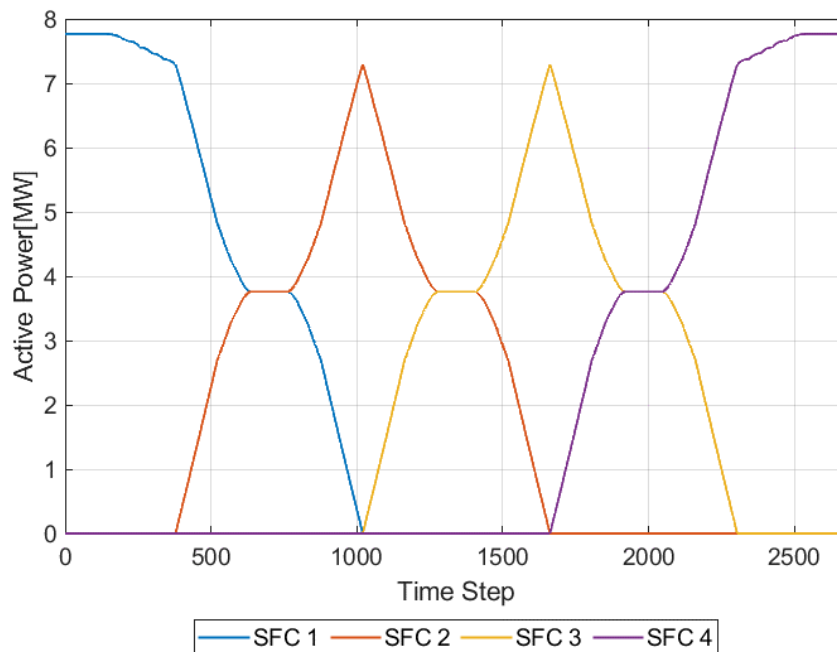


Figure 21 Single-train with constant power, active power profile for the synchronised control SFC system scenario

The same profile repeats when the train travels between SFC3 and SFC4. When the train passes SFC4, this feeder station is the only one providing power for the train for the remaining 20 km, until the end of the journey. This is the same situation as SFC1 at the beginning of the journey before the train reaches

SFC1. Consequently, SFC1 and SFC4 have greater maximum active power outputs compared with SFC2 and SFC3; the value of this maximum active power is 7.769 MW whereas for SFC2 and SFC3 the maximum active power output is 7.292 MW.

The maximum active power output amongst all SFCs in this scenario is 8% less than the maximum active power output amongst all transformer feeder stations described in Section 4.7.1.1.1.

#### *4.7.1.1.3 EQUALLY SHARED POWER CONTROL OF SFCs*

Figure 22 presents the active power profiles of four SFC feeder stations located along the line, as described in Section 4.3 and in the synchronised control case introduced above. In this case, the new ‘equally shared power’ control strategy is applied, such that the active and reactive power requirement of the load is constantly and equally shared between all SFC feeder stations on the line. The sharing is achieved by controlling the phase angle (for active power) and voltage magnitude (for reactive power) of each SFC separately using a PI controller, as described in Section 0 and Section 3.2.2, respectively.

The train starts its journey with its 3-minute stop at the first station located at node 1. When the train is at this location, it is furthest from SFC1, its nearest feeder station, and consequently furthest from all feeder stations on the line. As in this scenario active power is constantly and equally shared between all SFCs, being furthest away from all SFCs results in the highest amount of losses as the current is travelling the longest cumulative distance from all SFCs throughout the train’s journey.

It must be noted that the power required by the load in this scenario is the same at all times and the active power is equally shared between all SFCs at all times so the variation in the active power output of the SFCs is due solely to the losses incurred during transmission of power.

As the train moves on, the distance from the train and the SFCs reduces and, hence, the SFC active power outputs reduce. The flat horizontal lines in Figure 22 are due to the train being stationary when stopping at various stations and the ripples are due to the cross-bonds between the contact wires which occur every 4 km, as described in Section 3.1.1.

The active power outputs decrease as the train moves on, up to the point where they reach the smallest cumulative distance which is at the mid-point between SFC2 and SFC3. Passing that location, the active power outputs start increasing again until reaching the maximum value at the end of the journey, equivalent to that at the start.

The maximum active power output for all SFCs is 2.32 MW, however, this only occurs for one time step while the control system stabilises at the start of the simulation. The realistic maximum active power is actually 2.198 MW which is about 70% less than the maximum active power output from the scenario the voltage magnitude and phase angle outputs of all SFCs are synchronised, as described in Section 4.7.1.1.2, and is about 72% less than the maximum active power output from the AT scenario described in Section 4.7.1.1.1.

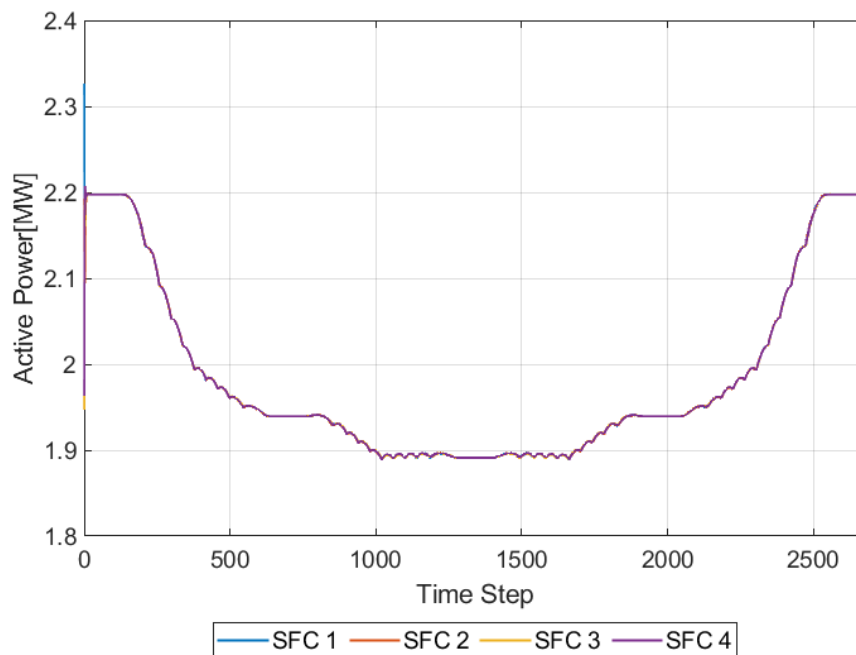


Figure 22 Single-train with constant power, active power profile for the equally shared control SFC system scenario

#### 4.7.1.2 REACTIVE POWER PROFILE FOR A SINGLE TRAIN WITH CONSTANT POWER

##### 4.7.1.2.1 AT SYSTEM

Figure 23 shows the reactive power profile of the single train completing a journey on a line supplied by a conventional transformer system as previously described in Section 4.2.

The ripples in this graph are due to the cross bonds between the contact wires and the ATs connected on the line as described in Sections 3.1.1 and 3.1.2. The reason they are not uniformly spread is the variable speed of the train and hence the non-linear movement through the nodes. The maximum reactive power output from Transformer 1 occurs at the beginning of the train's journey as the train is located furthest from its feeding transformer which is Transformer 1. The train then moves on towards Transformer 1 (located at node 400) and the reactive power output of Transformer 1 reduces as the train gets closer to it. The train crosses the isolation point between nodes 400 and 401, and stops for 3 minutes at the second station which is located at node 401. This occurs between time steps 624 and 767. The train then accelerates away from Transformer 2 which results in the reactive power output from Transformer 2 increasing. The train reaches the second isolation point at time step 1273. This isolation point is located at the midpoint between Transformer 2 and Transformer 3 and the reactive power at this point is zero. The train then moves onto Transformer 3's feeding section in which the third station is also located and hence the train has a 3-minute stop. At this point, the train is furthest from Transformer 3 and hence the reactive power output for Transformer 3 is at its peak. Similarly, as the train moves towards Transformer 3, the reactive power output decreases until the train reaches Transformer 3 and then goes through the isolation point located between Transformer 3 and Transformer 4. At this point, the reactive power output from all transformers is zero as the train is disconnected from all supplies. The train then moves on to the feeding zone of Transformer 4 and stops for 3 minutes as the fourth station is located there. The reactive power outputs remain at zero between time steps 1907 to 2051. The train then accelerates away from Transformer 4 and hence the reactive power outputs increase until the train reaches the end of its journey.

There are drops in the reactive power output when the train is the furthest from a transformer feeder station, for example at time step 1273; this is due to the presence of the ATs connected to the feeding system which regulate the voltage and consequently control the reactive power levels. The maximum reactive power output value from all transformer feeder stations is 2.683 Mvar.

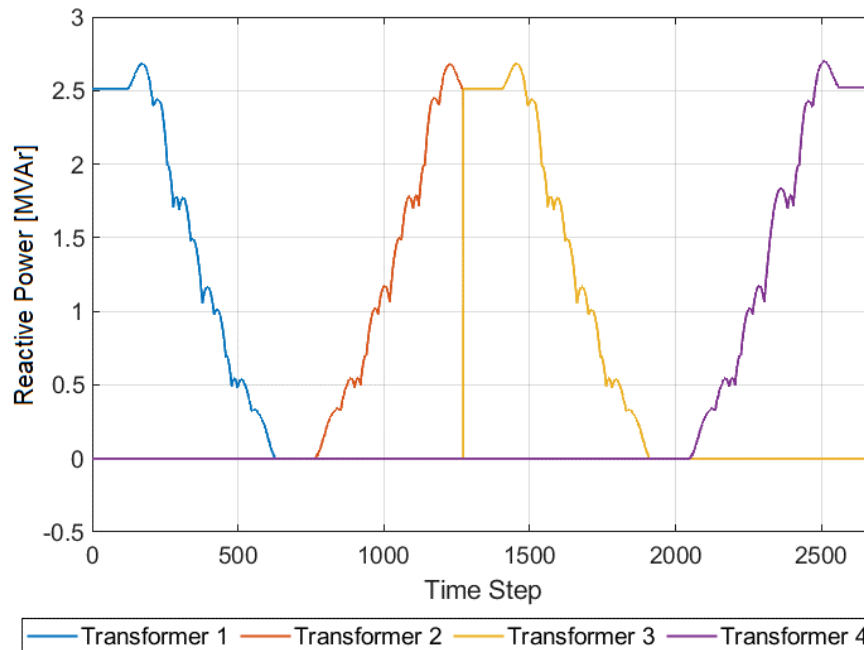


Figure 23 Single-train with constant power, reactive power profile for the AT system scenario

#### 4.7.1.2.2 SYNCHRONISED CONTROL OF SFCs

Figure 24 shows the reactive power output profile of the SFCs located on the line where a single train, drawing a constant acceleration power, completes the journey previously described in Section 4.7.1.1.2.

The train starts its journey at the station that is 20 km away from SFC1, i.e., the furthest point. After stopping for 3 minutes at the station, it moves towards SFC1. The ripples on the graph are due to the cross-bonds between the contact wires. The reactive power output reaches zero when the train reaches SFC1. Moving on from SFC1, the train enters a location where it is directly connected to both SFC1 and SFC2 and, hence, as previously described in Section 4.7.1.1.2, the SFCs output an amount of reactive power which is inversely proportional to the distance of the train from each of the SFCs. The train stops at the second station at time step 633. Until the train reaches SFC4, there are always two SFCs to feed the train simultaneously. After the train passes SFC4, the reactive power output of SFC4 peaks as it is the end section of the line and only one SFC is feeding the train in this synchronised control scenario. The maximum reactive power output by all SFCs is 1.28 Mvar. This is about 52% less than the maximum reactive power of the transformer feeder stations described in Section 4.7.1.2.1.

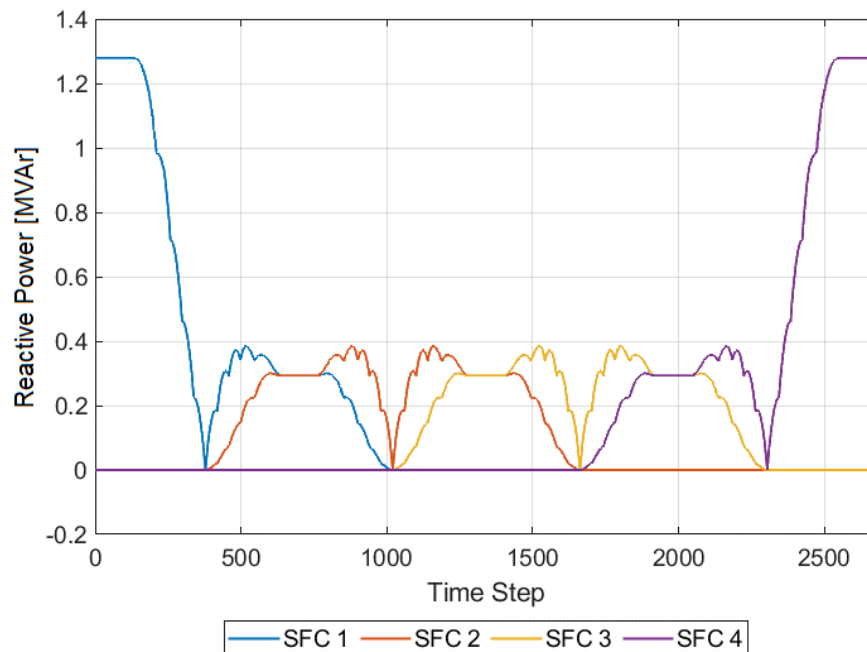


Figure 24 Single-train with constant power, reactive power profile for the synchronised control SFC system scenario

#### 4.7.1.2.3 EQUALLY SHARED POWER CONTROL OF SFCs

Figure 25 shows the reactive power profiles of the four SFCs located on the line while a single train completes a full journey taking constant acceleration power at all times. In this scenario, the active and reactive power is equally shared at all times using the new control strategy introduced in Section 3.3.1.

The train follows the same journey as described in Section 4.7.1.2.3. As presented in Figure 25, it is possible to see that all SFCs output the same amount of reactive power at all times during the trains' journey regardless of the location of the train with respect to the SFCs on the line. The maximum reactive power output by the SFCs observed in this scenario is 1.795 Mvar which drops to 1.007 Mvar after one time step when the control system stabilises the reactive power outputs of all SFCs. This is approximately 20% less than the synchronised SFC case described in Section 4.7.1.2.2 and approximately 62% less than the AT system case described in Section 4.7.1.2.1.

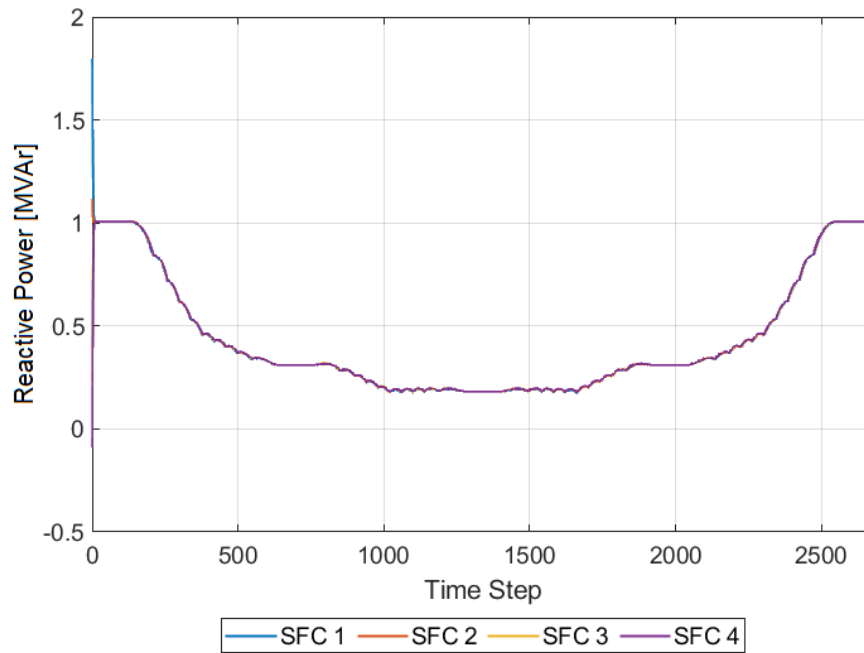


Figure 25 Single-train with constant power, reactive power profile for the equally shared control SFC system scenario

## 4.7.2 SINGLE TRAIN WITH VARIABLE POWER

This section describes active and reactive power profiles of the four feeder stations (transformers for one scenario and SFCs for the two other scenarios) on the line for a single train completing a journey drawing and regenerating variable amounts of power depending on whether it is accelerating, cruising or braking. The journey of the train is described in detail in Section 4.4.

### 4.7.2.1 ACTIVE POWER PROFILE FOR A SINGLE TRAIN WITH VARIABLE POWER

#### 4.7.2.1.1 AT SYSTEM

Figure 26 shows the active power profile of the four transformer feeder stations on the line, as described in Section 4.2, when a train completes a journey such as the one described in Section 4.4.

The journey starts with a 3-minute stop at the first station and hence zero active power from the feeder stations as the train is not drawing any power while stationary. The train then starts accelerating, drawing 7.293 MW of power. As the location of the train at the start of the journey is furthest from its feeder, Transformer 1 has to supply a higher amount of active power to compensate for the losses. After the

period of acceleration and when the train has reached the required speed, it then moves into cruising mode which requires 0.675 MW and, considering the efficiency of the train, it draws approximately 0.965 MW. When the active power drawn is smaller, the current is smaller and hence the losses are smaller. The active power output of Transformer 1 decreases gradually from when the cruising starts at time step 234 as the train moves towards Transformer 1. This is not easily visible on the graph due to the very small changes but the output value of Transformer 1 changes from 0.9724 MW at time step 234 to 0.967 MW at time step 522 when the train starts braking.

Regeneration from the train starts at time step 522. Considering the regeneration efficiency of the train, the active power injected into the power system by the train is 2.907 MW. This is shown as negative active power on the graph. As the train moves towards Transformer 1, the amount of regenerated power lost due to transmission losses decreases and, consequently, the magnitude of the active power injected back to the grid increases from 2.891 to 2.907 MW, as can be seen between time steps 523 and 631. The train then goes through a neutral section where all transformers' output power is zero and switches to Transformer 2. The train then stops at the second station which means there is no power being drawn. The train then accelerates away from Transformer 2; in this instance, as the train is accelerating at a location very close to its feeder station, the losses are smaller, in comparison with the case departing Transformer 1, and hence Transformer 2 has a smaller output while the train is accelerating. Transformer 2's active power output increases as the train moves further from it (time steps 763–875). When the train crosses the neutral section to enter Transformer 3's feeding zone and stops at the third station, i.e., after its final regeneration phase, it is at its furthest location from the transformer and, consequently, when the train starts accelerating away from the third station, greater losses occur. Hence the active power output of Transformer 3 is higher than that of the case when departing from Transformer 2 (7.849 MW). This reduces as the train moves closer to Transformer 3.

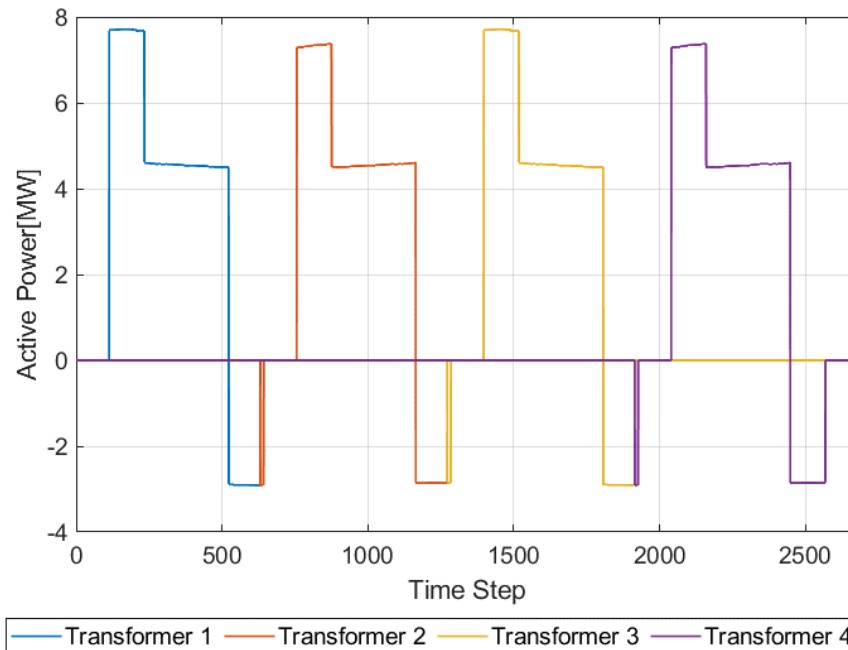


Figure 26 Single-train with variable power, active power profile for the AT system scenario

#### 4.7.2.1.2 SYNCHRONISED CONTROL OF SFCs

Figure 27 presents the active power profiles of four SFC feeder stations located on the line, as described in Section 4.3, when they are supplying active power for a single train completing a journey drawing or regenerating variable power, depending on whether it is accelerating, cruising or regenerating.

When the train starts its journey, only SFC1 is supplying the required load to the train. Because the train is at its furthest point from this SFC, the losses are large and hence the SFC output is larger than the required acceleration active power in order to compensate for the losses. It gradually reduces from 7.769 to 7.644 MW as the train gets closer to SFC1. The train then enters the cruising stage at time step 234 but is still taking all its power from SFC1. At time step 385, the train passes SFC1 and the power required by the train is then shared between SFC1 and SFC2. At time step 523, the train starts braking and hence regenerates power. The regenerated power is fed back to the grid through both SFC1 and SFC2 until the train reaches the second station at time step 644. The second station is located at the midpoint between SFC1 and SFC2 which means that, when the train is accelerating away from the second station, the power it requires is equally shared between SFC1 and SFC2. As it moves towards SFC2, more of its power is supplied by SFC2. While it is not visible in this graph, it must be noted that, despite the lower

value of active power output supplied by SFC1 and SFC2 when the train is accelerating away from the second station, the losses are greatest due to the greater distance the current has to travel. At time step 876, the train enters the cruising stage and at time step 1020 the train passes SFC2 and hence SFC2 and SFC3 share the load from there up to the point where the train crosses SFC3. In the final stage of the journey, the regenerated power, which is going back to the grid through SFC4, is larger than in other cases during the journey, but it must be noted that this is because in those cases it has been shared between two SFCs and in this case is only going back to the grid through SFC4.

The maximum active power output of the SFCs in this case is 7.767 MW. It should be noted that when the active power is shared between two SFCs the maximum at each of them is significantly lower than an equivalent AT system where a single feeder station supplies the load.

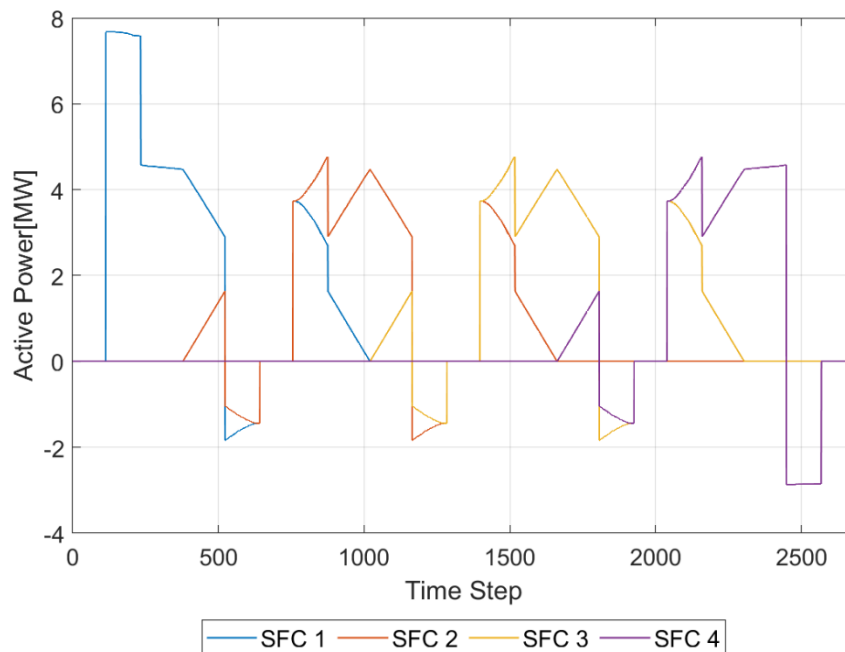


Figure 27 Single-train with variable power, active power profile for the synchronised control SFC system scenario

#### 4.7.2.1.3 EQUALLY SHARED POWER CONTROL OF SFCs

Figure 28 shows the active power profiles for the four feeder stations located on the line where a single train completes a journey drawing or regenerating variable power, depending on whether it is accelerating, cruising or regenerating. In this scenario, the active and reactive power required by the

load is shared equally at all times between all SFCs on the line, using the new control strategy described in Section 3.3.1.

As presented in Figure 28, the active power outputs of all SFCs are equal to one another throughout the whole journey of the single train. All SFC active power outputs are overlapping and, hence, appear as one line on the figure. The highest active power output is when the train is pulling away from the first station as it has the greatest distance from all SFCs. The active power output of the SFCs reduces as the train accelerates towards SFC1. This is because the train is getting closer to all SFCs and hence the current has to travel a shorter distance which means lower active power requirements to supply the train's load, thanks to the lower losses. The initial step reduction at time step 234 corresponds to the train entering a cruising phase. A similar reduction in active power occurs in this phase, although it is difficult to discern from the graph. The second acceleration point has a lower corresponding active power output from the SFCs as it is then between SFC1 and SFC2 and has a shorter cumulated distance from all SFCs compared to the first acceleration instance. In this case, the active power outputs also reduce as the train travels further into its journey as the distances are further reduced while the train travels towards the middle of the line. In the third acceleration instance, as the train draws its required power at the mid-point of the track, the active power required is less than in the other two instances. Pulling away from the third stop which is between the second and third feeder stations, the train has the smallest overall distance for the currents travelling to it from all feeder stations and consequently the peak power corresponding to the acceleration of the train from the third station is the smallest peak power. The active power output increases as the train accelerates away from the third station as it is moving away from the middle point of the line and hence increased the cumulative distance again. The case for the fourth station is a mirror of the second. In the final regeneration case, a smaller amount of active power is injected back to the grid as it incurs losses while travelling back to all SFCs. In the single train case for regenerative power, feeding the regenerative power back equally through all feeder stations is not the best solution as this will incur more transmission losses travelling to other SFC feeder stations further away and hence would make the system less efficient. However, a single-train case is not a

realistic case and, for a set of trains on the line, the regenerative power will get picked up by other loads, i.e., other trains on the line. The same applies to drawing equal power from all feeder stations, however, in this case the increased energy losses may be compensated for by the overall reduction in rating required for each feeder station. This will be explored further in Chapter 5.

The maximum active power output by the SFCs is 2.204 MW which is approximately 72% less than for the synchronised SFC case and the AT system case which had similar levels of performance.

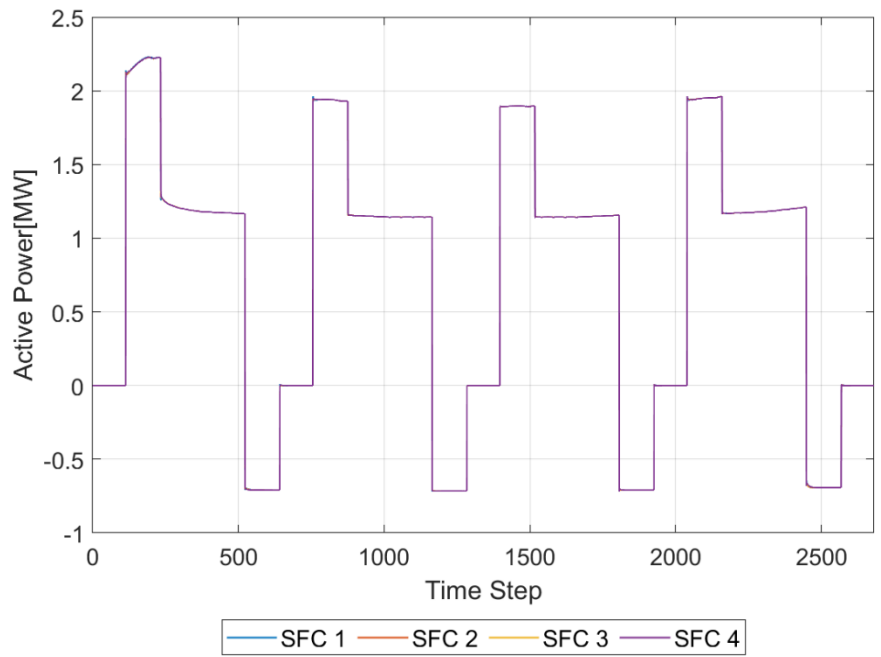


Figure 28 Single-train with variable power, active power profile for the equally shared control SFC system scenario

#### 4.7.2.2 REACTIVE POWER PROFILE

##### 4.7.2.2.1 AT SYSTEM

Figure 29 shows the reactive power profile of four transformers on the line as described in Section 4.2 where a single train completes a journey drawing or regenerating power depending on whether it is accelerating, cruising or braking.

The journey of the train is discussed in detail in Section 4.7.2.1. The peaks of reactive power occur where the train accelerates at the locations furthest from the transformer feeder station providing its power. In this case, the train is accelerating at the beginning of the line from the first station where it is fed by Transformer 1. It also occurs when the train accelerates away from the third station where it is

fed by Transformer 3. The peaks at time steps 873 and 2159 are when the train accelerates away from the second and fourth stations, respectively. At those locations, the stations are close to Transformer 2 and Transformer 4 which feed the train at those points, respectively, and hence the reactive power is small at the beginning and peaks as the train gets further away from the transformers. At time steps 524 and 1807, the train is regenerating towards stations that are located near transformer feeder stations 1 and 3. Consequently, the value of the reactive power output on these occasions of regeneration is smaller than for time steps 1165 and 2453 where the train regenerates at a location approximately 20 km away from its feeding transformer (Transformers 2 and 4).

The maximum transformer reactive power output during this journey is 2.183 Mvar.

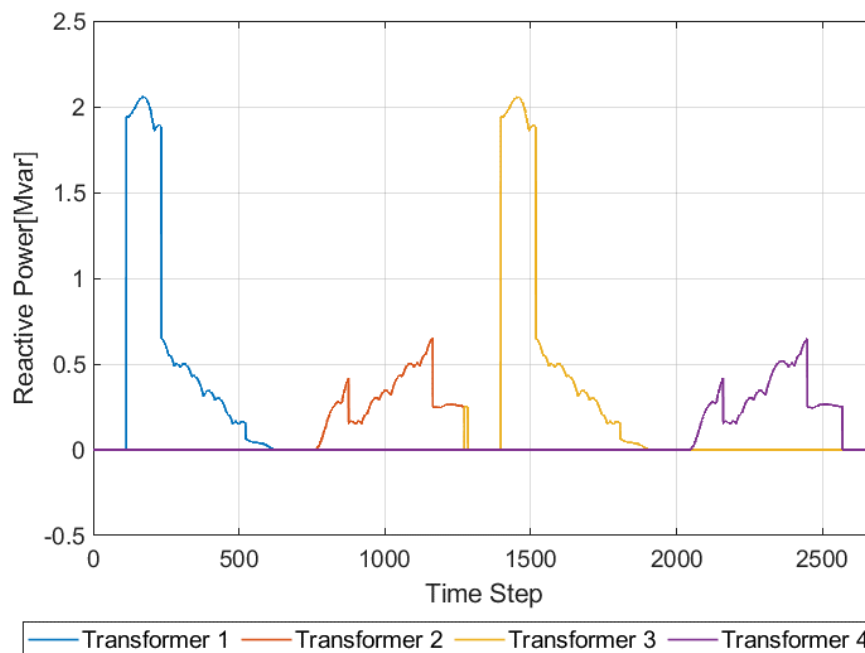


Figure 29 Single-train with variable power, reactive power profile for the AT system scenario

#### 4.7.2.2.2 SYNCHRONISED CONTROL OF SFCS

Figure 30 shows the reactive power profile where a single train completes a journey with variable power. The details of the journey are described in Sections 4.3 and 4.7.2.1.2.

The peak of the reactive power occurs at time step 114, at the beginning of the journey, when the train is accelerating a great distance away from SFC1 and is solely fed by that SFC. The train is equally far

from the closest SFCs when accelerating away from the second, third and fourth stations but as the load is shared between two SFCs at those points, the peak of an individual SFC is not higher than the one at the beginning; however, the sum of the reactive power at those points is greater. For the same reasons at regeneration points, the peak at the end of the journey is greater than for the other three occasions of braking.

The maximum reactive power output of the SFCs during this journey is 1.28 Mvar. This is 52% less than the value for the AT system described in Section 4.7.2.2.1.

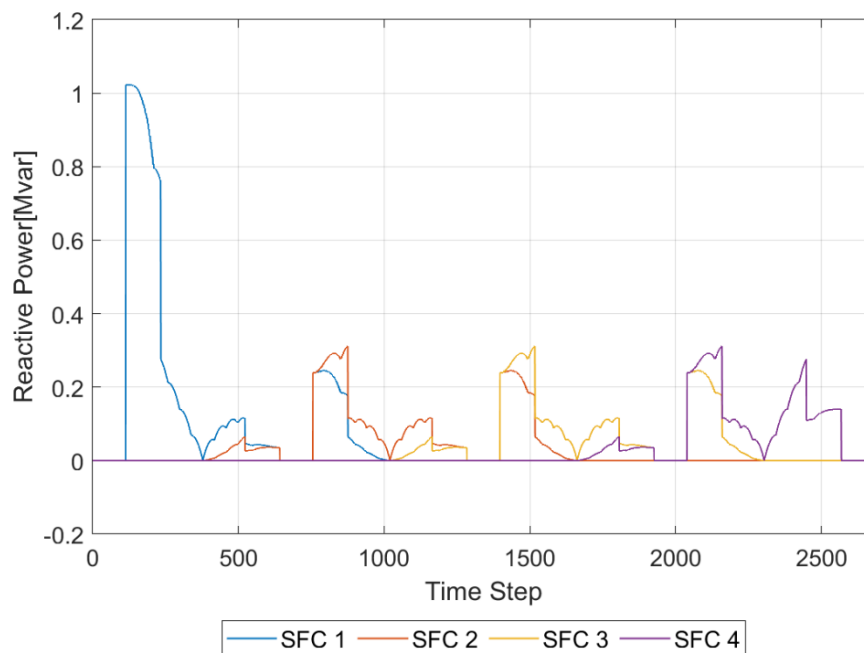


Figure 30 SFC single-train with variable power, reactive power profile for synchronised control SFC system scenario

#### 4.7.2.2.3 EQUALLY SHARED POWER CONTROL OF SFCs

Figure 31 presents the reactive power profiles of the four SFCs on the line when a single train completes a journey where all SFCs share the required active and reactive power of the load equally and at all times. The arrangements and details of the journey are described in Sections 4.3 and 4.7.2.1.2.

In this case, the reactive power is equally shared between all SFCs at all times and peaks occur where the control system is stabilising significant changes. Due to the limitation on the maximum voltage on

the line, it is not possible to tune the system to reduce these peaks further. The increases and drops in the reactive power follow the same patterns as the active power and for the same reasons.

The maximum reactive power output amongst all SFCs during this journey is 0.752 Mvar which occurs for one time step as the train initially draws power, and the control system stabilising reduces this to 0.301 Mvar. This is 76% less than the equivalent value for the synchronised control SFC scenario described in Section 4.7.2.2.2 and 86% less than the equivalent value for the AT system case described in Section 4.7.2.2.1.

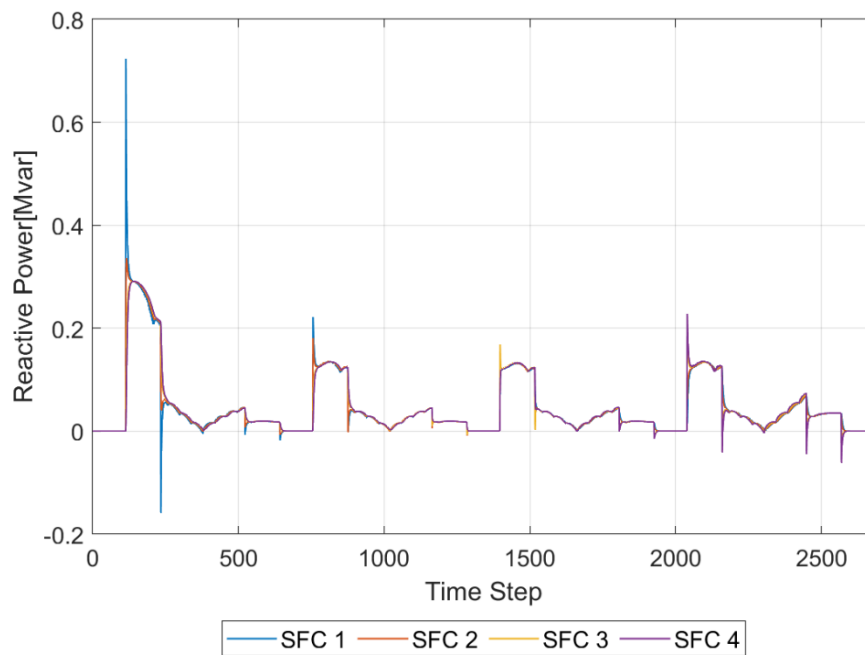


Figure 31 Single-train with variable power, reactive power profile for the equally shared control SFC system scenario

## 4.8 CONCLUSIONS

In this chapter, the mathematical model defined in Chapter 3 is applied in order to develop a simulation system suitable for exploring the performance of SFC systems. An example using a single train with a constant power demand is provided in order to understand and verify the operation of the simulator. This is extended to include a realistic power profile for the single train to further confirm the operation of the simulator.

This initial application includes many aspects of the final cases for simulations which will be undertaken in the remainder of this thesis. These include the train's power consumption profile, the arrangement of

the power system components on the line, the assembled timetable for the set of trains and the limits within which the voltage levels must be maintained.

The results obtained using the single train example indicate that, in general, the power rating requirements for SFC feeder stations are smaller than their transformer equivalents. The new control system further reduces these requirements. However, while a single train provides a good understanding of how the model works, it is not representative of real-life scenarios. Consequently, Chapter 5 explores the performance of the AT and both control methods for SFC systems for a full timetable of trains drawing both constant and variable power.

# 5 A STUDY OF THE COMPARATIVE PERFORMANCE OF SFC AND AT SYSTEMS FOR A HEAVILY USED HIGH-SPEED RAILWAY

## 5.1 INTRODUCTION

The previous chapters have demonstrated how a mathematical model of a railway electrical supply network based on SFCs can be developed to produce simulations which can be configured to be representative of specific real-world scenarios. This chapter now uses this configured simulator to undertake a novel exploration of the performance of the SFC network. Specifically, a control strategy for the network of SFCs will be introduced for a fully operational line, and the performance of the system evaluated in comparison to the basic, synchronised, operation. The investigation will consider the potential to reduce the size of individual SFCs, while maintaining operational performance, through the inclusion of an appropriate control strategy. This study addresses a gap in the literature, as a comparative study putting SFC-based and transformer-based systems side by side, using examples of real-life situations, has not been previously done. This study also addresses the gap in the literature concerning deliberate distribution of loads across the SFC feeder stations on the line set against the traditional synchronised control.

This comparison study is carried out using simulation results from the three scenarios described below:

- 1- Transformer-based feeder stations feeding isolated sections with autotransformers on the line every 10 km;
- 2- SFC-based feeder stations with constant output voltage magnitude and synchronised phase angle;
- 3- SFC-based feeder stations actively sharing active and reactive power.

The detailed design and configuration of these scenarios is discussed in Sections 4.2 to 4.6.

These scenarios are investigated addressing two load profile configurations; the first mode uses variable power with trains following a realistic scenario, i.e., acceleration, cruising and braking. The second mode considers the worst-case scenario and assumes all trains draw a constant maximum acceleration power throughout their journeys. The objective of this section is not to assume that a scenario can exist where all the trains on the line would draw high power during their whole journeys, but to analyse the

behaviour of the system should an event like this happen. By running the entire simulation with these conditions, it is possible to see the behaviour of the system at any time during the journey and with any possible arrangement of the trains on the line.

Evaluation of the system will consider five distinct aspects of electrical performance. These have been calculated every 1.6 seconds which is equivalent to a time step through the journey, as previously described in Chapter 4.

- (i) **Active Power:** The active power graphs show the magnitude of the active power fed into the railway network from the grid, as well as fed into the grid as an input for, each feeder station.
- (ii) **Reactive Power:** The reactive power graphs show the magnitude of the reactive power output from each feeder station. Analysing reactive power outputs of the feeder stations helps to understand the differences between the behaviour of the systems and, particularly, clearly demonstrates the differences and functionality of the synchronised and equally shared active and reactive power control strategies.
- (iii) **Apparent Power:** The apparent power graphs show the value of the apparent power output from each feeder station. This is the prime indicator for the required size of the feeder stations and helps to understand the effect of each scenario on the rating required for the feeder stations on the line. This is used in later in Chapter 7 where an economic assessment of both the capital and operational costs of the solutions is presented.
- (iv) **Voltage Profiles:** The voltage profile graphs present a 3D representation of the voltage magnitude at each node of the route over the course of the journeys. This is presented to demonstrate that the systems operate within the voltage limits permitted by the railway.
- (v) **Power Loss:** The magnitude of the power losses within the system will be presented. This helps with the comparison of operational differences between different scenarios. These data, obtained from analysing the power losses, are also used to calculate the energy losses which are used in the economic assessment presented in Chapter 7.

It must be noted that the results presented in this chapter have been produced using 675 kW as the cruising power which is lower than the value calculated using Davis Equation and presented in Section 4.4. This error however is easily amendable and does not affect the conclusions drawn in this chapter, and the rest of the thesis.

## 5.2 VARIABLE POWER / FULL TIMETABLE CASE

In this section, a full timetable of trains is run through their designed journey profiles, drawing or regenerating variable power depending on whether they are accelerating, cruising or braking. The arrangements of the feeder stations along the line, the train timetable and a detailed description of the power profiles are included in Sections 4.2 to 4.6.

This study has been designed to achieve a realistic comparison between the three state-of-the-art power system arrangements which can be used to feed the operational power load of the railway.

There are a number of factors that must be considered when evaluating the rated capacity of a feeder station. The train timetable has a significant role in sizing the feeder stations. The further the trains are from a feeder station when they accelerate, the greater the losses incurred in the system, as higher currents will have to travel further to reach the load. Also, the number of trains running on the track would have a direct influence on the load as the greater the number of the trains, the greater the load and consequently the bigger the feeder stations would need to be.

The seven cyclic repetitions visible in the timetable graph shown in Figure 18 are equivalent to 383 time steps or 10 minutes each. This is due to the 10-minute gap between the trains and where the trains at end sections finish their journeys and other trains start their journeys at those points.

## 5.2.1 ACTIVE POWER

### 5.2.1.1 AT SYSTEM

Figure 32 shows the active power profiles of the four transformers located on the line. In the transformer case, due to the isolation sections located on the line, each transformer has its own feeding zone which means any number of trains located in any transformer's feeding zone are fed solely by that transformer. The ATs located on the line improve the transformer systems' voltage quality and efficiency.

In this case, the maximum active power output amongst all transformers is 17.23 MW.

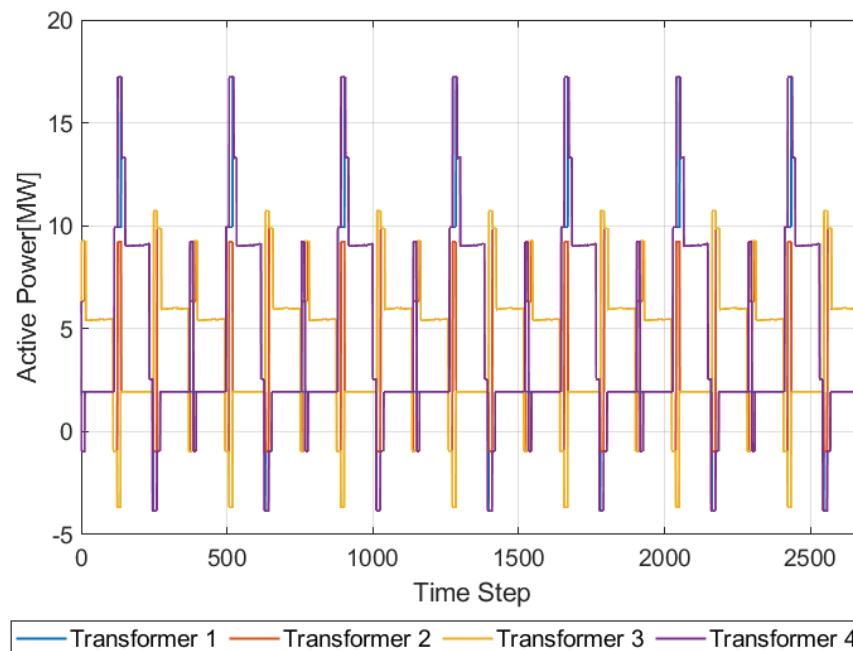


Figure 32 Active power for the AT system with full timetable and variable power

### 5.2.1.2 SYNCHRONISED CONTROL OF SFCs

Figure 33 shows the active power profile of the four SFCs located on the line. The outer SFCs (SFC1 and SFC4) have identical profiles for active power due to the timetable of trains running in both directions, the stations, and the SFCs all being mirrored. Having a symmetrical system simplifies the performance of the system which helps with analysing the outputs from the simulator. For the same reasons, the inner SFCs (SFC2 and SFC3) have identical active power profiles. The load on each SFC depends on the trains that fall into the SFC's feeding zone; it also depends on whether the trains within

the feeding zone are accelerating, cruising or regenerating. The distances that these events occur from the SFCs also makes a significant difference, especially in the event of acceleration when the trains draw their maximum required power.

In this scenario, the maximum active power output for the outer SFCs is 13.58 MW which is approximately 21% less than for the AT system; for the inner SFCs it is 9.706 MW, approximately 44%.

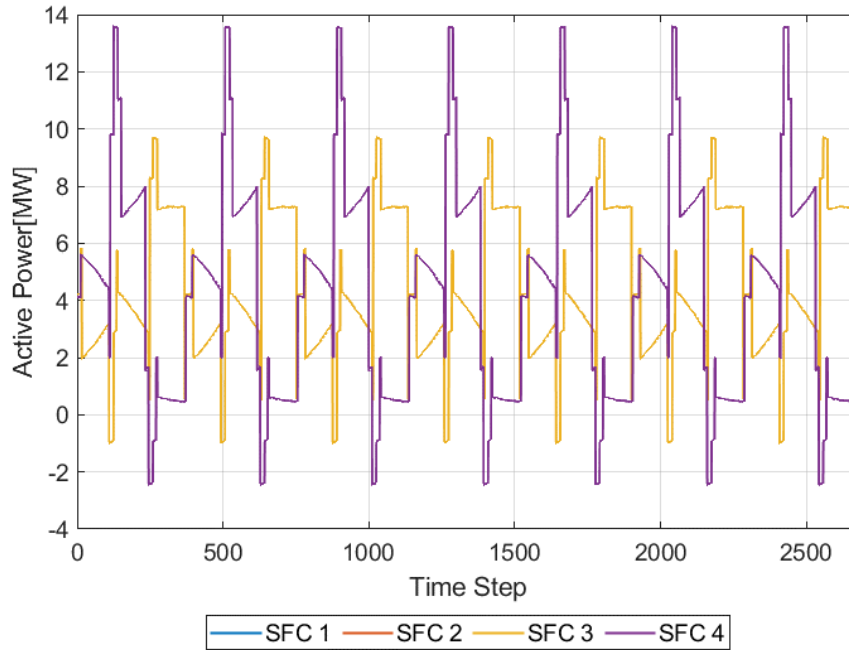


Figure 33 Active power for the synchronised control SFC system with full timetable and variable power

### 5.2.1.3 SHARED POWER CONTROL OF SFCs

Figure 34 shows the active power profiles for the scenario where a full timetable of trains runs and the active and reactive power is shared equally between all SFCs at all times using the novel control strategy. Similar to the previous examples of the equally shared active and reactive power control system presented in Chapter 4, the cumulative distance from the loads to the SFCs has a significant effect on the transmission losses. In this case, due to multiple trains running on the track, it is not possible to identify the locations of the trains on the line by looking at the active power profile. However, the active power output from the SFCs depends on the same parameters: the location of the loads (trains) and their distance from the SFCs, and the location of the stations with respect to the location of the SFCs as the

trains accelerate away from the stations. The acceleration phase has the largest power requirement of the trains.

The maximum active power output of all SFCs is 9.791 MW. The maximum active power output from the SFCs in this case is approximately 43% less than for the AT system and approximately 28% less than for the outer SFCs in the synchronised SFC control case. This reduction is less than the difference that the control system makes to a single train. This is due to the fact that in the synchronised case with a single train some SFCs may not be contributing, but in the equally shared power case they would be active. In a multiple train scenario, all feeder stations will be active for both control strategies.

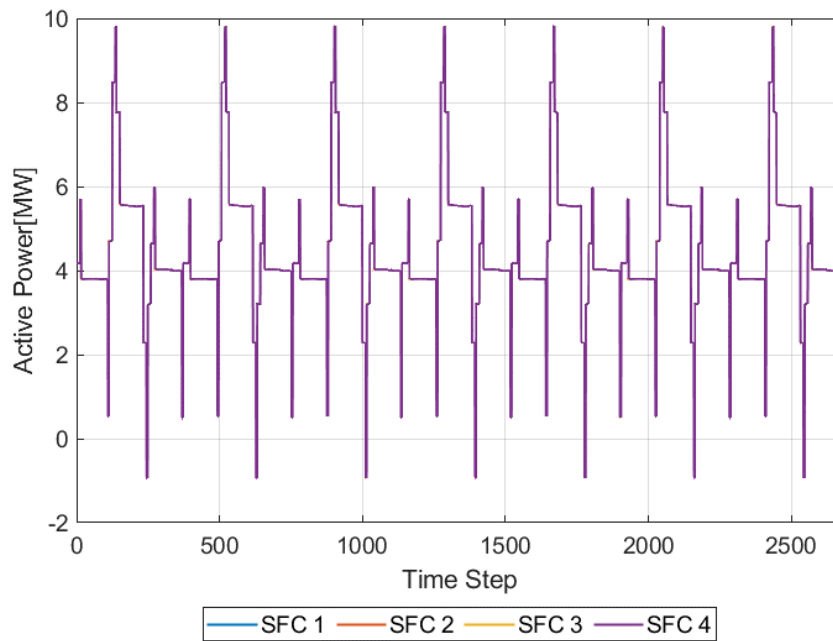


Figure 34 Active power for the equally shared power SFC system with full timetable and variable power

## 5.2.2 REACTIVE POWER

### 5.2.2.1 AT SYSTEM

Figure 35 shows the reactive power profile for the outputs of the four transformers located on the line in the AT system case. The greater the distance of the load from its feeding transformer and the larger the size of the load, the larger the reactive power output.

The maximum reactive power output of the transformers in this scenario is 3.818 Mvar.

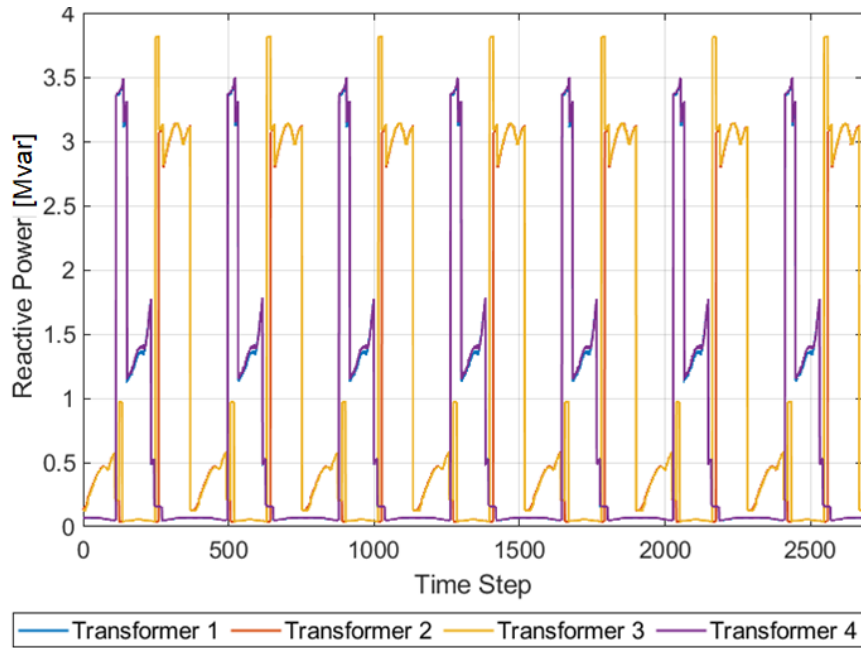


Figure 35 Reactive power for the AT system with full timetable and variable power

#### 5.2.2.2 SYNCHRONISED CONTROL OF SFCs

Figure 36 shows the reactive power profiles of the four SFCs on the line where there are 14 trains running at all times across both directions (7 in each). In this case, the SFC output voltages have synchronised magnitude and phase angle.

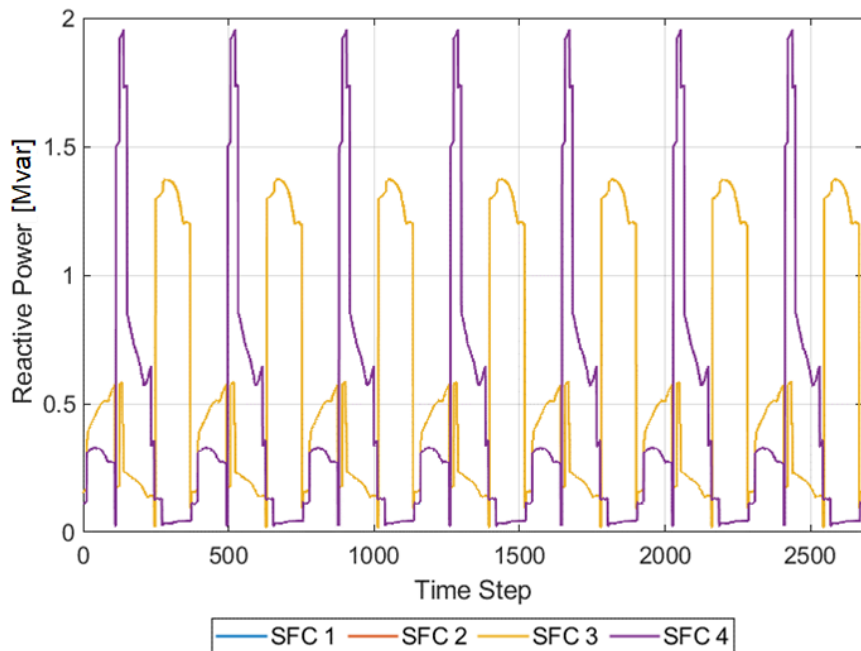


Figure 36 Reactive power for the synchronised SFC system with full timetable and variable power

Similar to the previous cases, the outer and inner SFCs have identical profiles respectively. The lowest reactive power values occur on the occasions where the cumulative distances of the trains from their feeding SFCs are at a minimum.

The maximum reactive power of the outer SFCs in this case is 1.954 Mvar which is approximately 48% less than for the AT system. The maximum reactive power output for the inner SFCs is 1.374 Mvar, which corresponds to 64%.

### 5.2.2.3 SHARED POWER CONTROL OF SFCs

Figure 37 shows the reactive power profiles of the four SFCs located on the line when 7 trains travel in each direction, drawing or regenerating power. In this case, the reactive power is shared equally between all SFCs at all times by using the novel control system to manipulate the magnitude of the voltage. Due to the need to stay within the constraint of the maximum voltage allowed on the system, there is a limitation on the control of the peaks possible using the PI controller. These peaks, however, have no effect on the maximum reactive power which means they would not affect the sizing of the SFCs.

The maximum reactive power output of the SFCs in this scenario is 1.934 Mvar. This value is approximately 49% less than for the AT system but only 1% less than for the synchronised SFC case.

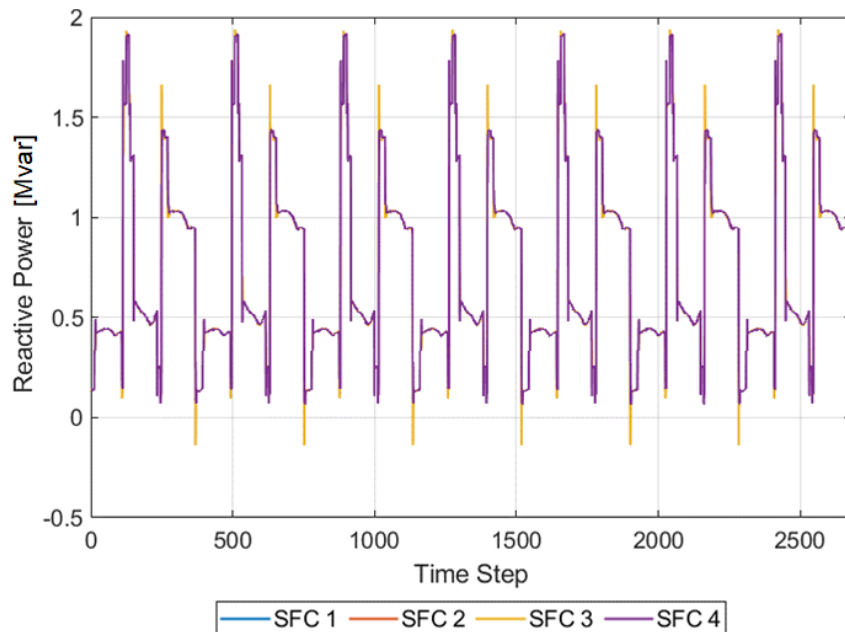


Figure 37 Reactive power for the equally shared power SFC system with full timetable and variable power

### 5.2.3 APPARENT POWER

Figure 38, Figure 39 and Figure 40 show the apparent power profiles of the AT system, synchronised SFC system and the equally shared active and reactive power SFC system, respectively. These figures have been included to demonstrate the variation in the apparent power outputs from different power systems arising from simulations of the same route and timetable of trains.

The maximum apparent power for the AT system's profile is 17.67 MVA. The value for the synchronised control SFC system is 13.71 MVA which is approximately 22.4% less than the AT system value. The maximum apparent power output for the equally shared active and reactive power control SFC system is 9.953 MVA which is approximately 43.7% less than for the AT system and approximately 27.4% less than the synchronised control SFC system's value.

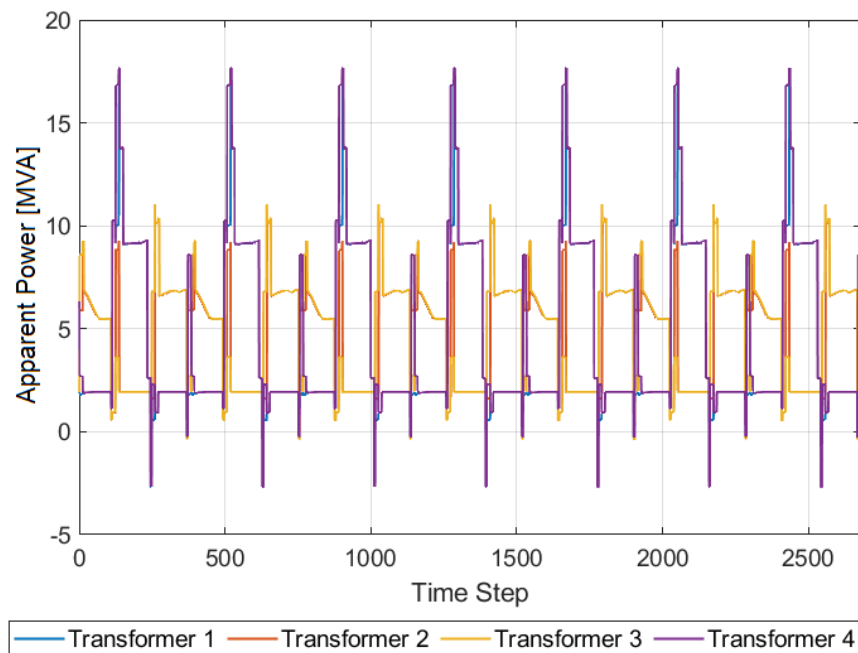


Figure 38 Apparent power for the AT system with full timetable and variable power

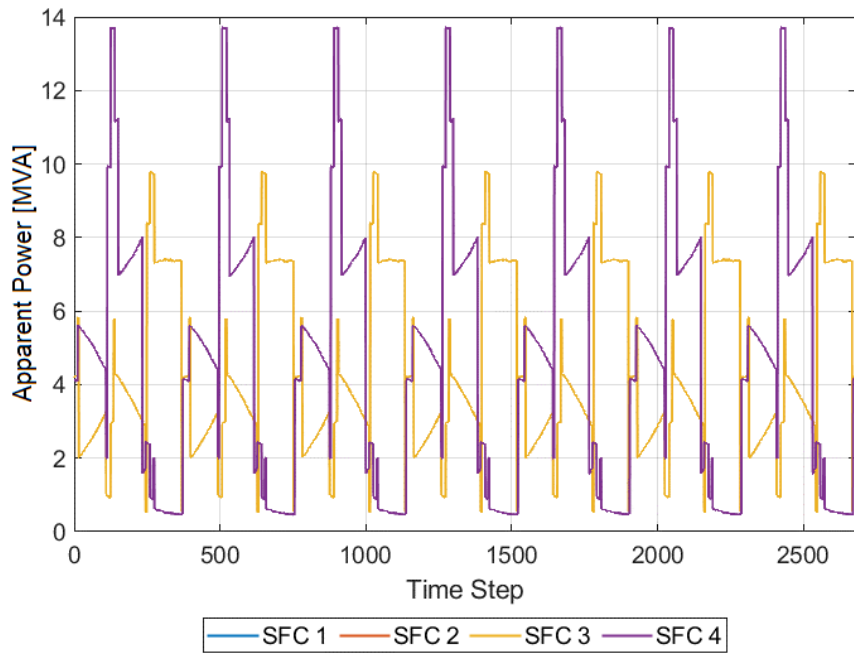


Figure 39 Apparent power for the synchronised SFC system with full timetable and variable power

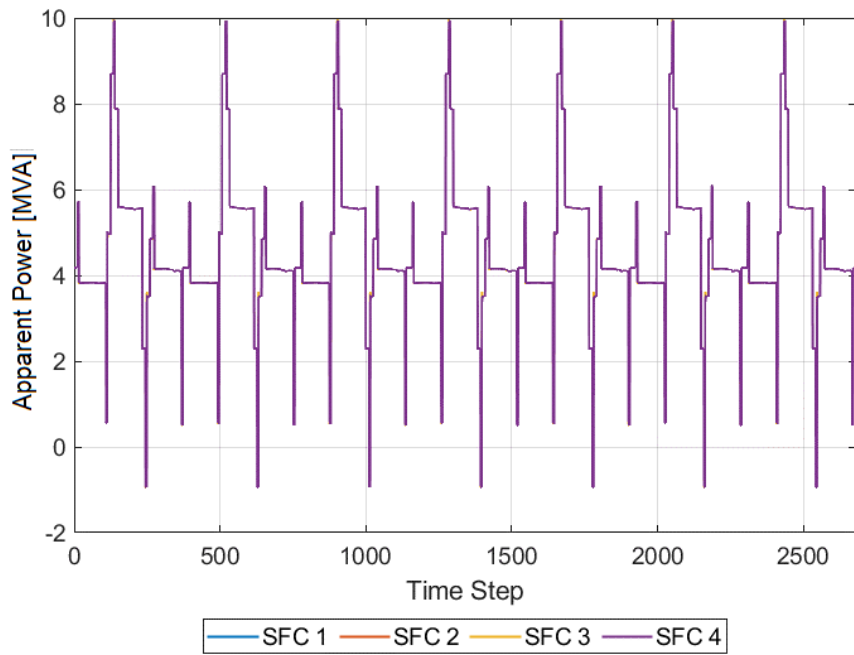
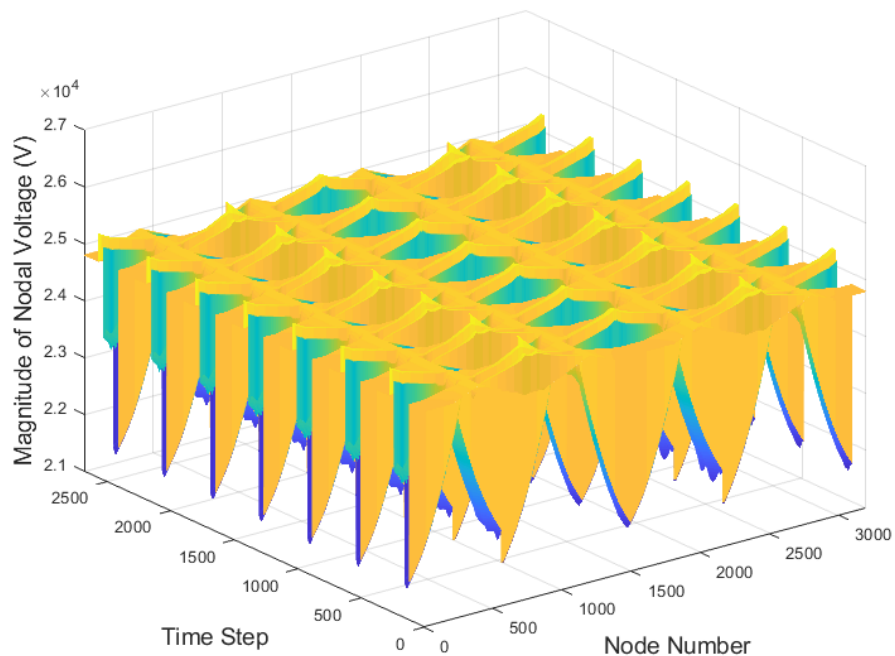


Figure 40 Apparent power for the equally shared power SFC system with full timetable and variable power

## 5.2.4 VOLTAGE PROFILES

Figure 41, Figure 42 and Figure 43 show the nodal voltage profiles of the AT system, the synchronised SFC system and the equally shared active and reactive power SFC system, respectively. These results show the voltage level of each node through all time steps occurring throughout the simulation. These graphs indicate maximum voltage levels of 25.40 kV, 25.50 kV, and 26.87 kV for the three systems considered. These are all in accordance with EN 50130 (CENELEC, 2007) which specifies a maximum voltage of 29 kV, as previously discussed in Section 4.6. Likewise, the minimum voltages are 21.34 kV, 22.96 kV, and 21.40 kV which are all well in excess of the minimum 16 kV mandated by the standard.



*Figure 41 Nodal voltage profile for the AT system with full timetable and variable power*

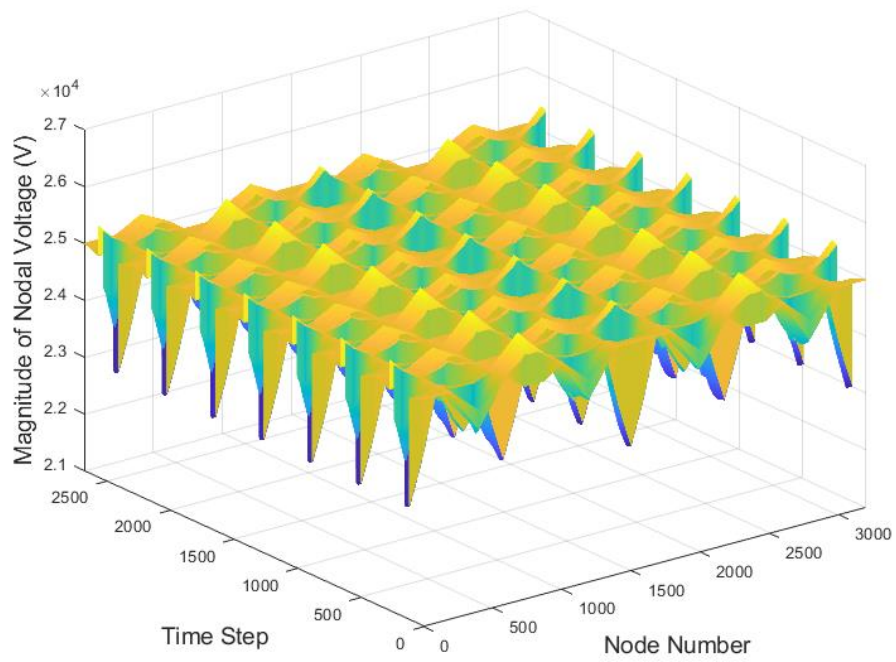


Figure 42 Nodal voltage profile for the synchronised SFC system with full timetable and variable power

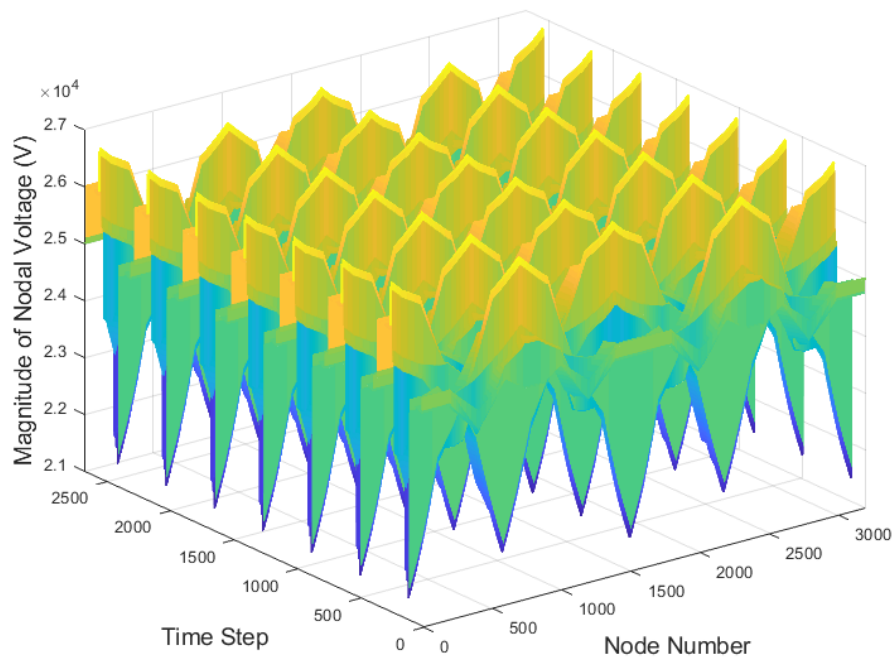


Figure 43 Nodal voltage profile for the equally shared power control SFC system with full timetable and variable power

### 5.2.5 POWER LOSSES

The graphs presented in this section show the transmission loss profiles, across the whole network, which are calculated at each time step. The transmission losses are calculated for acceleration and cruising in a different way compared with regeneration. The acceleration and cruising losses are calculated by deducting the overall power drawn by the trains from the overall power injected into the system by the feeder stations. For regeneration, the transmission losses are calculated by deducting the power fed back to the grid from the overall power regenerated by the trains. These powers are easily separable as the acceleration and cruising power is indicated as positive, and regeneration power is indicated by a negative sign.

Figure 44, Figure 45 and Figure 46 show the power loss profiles for the AT system, synchronised control SFC system, and the equally shared active and reactive power control SFC system, respectively. These power losses are shown in MW and have been calculated at each time step. It must be noted that this profile is not for cumulative power losses and is just for the instance of time for which it is presented.

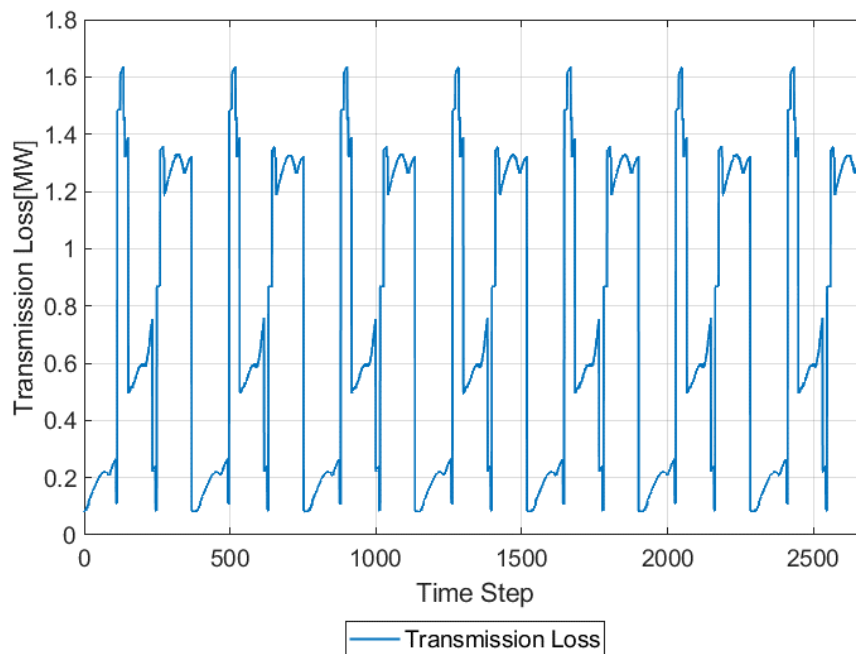


Figure 44 Transmission power loss for the AT system with full timetable and variable power

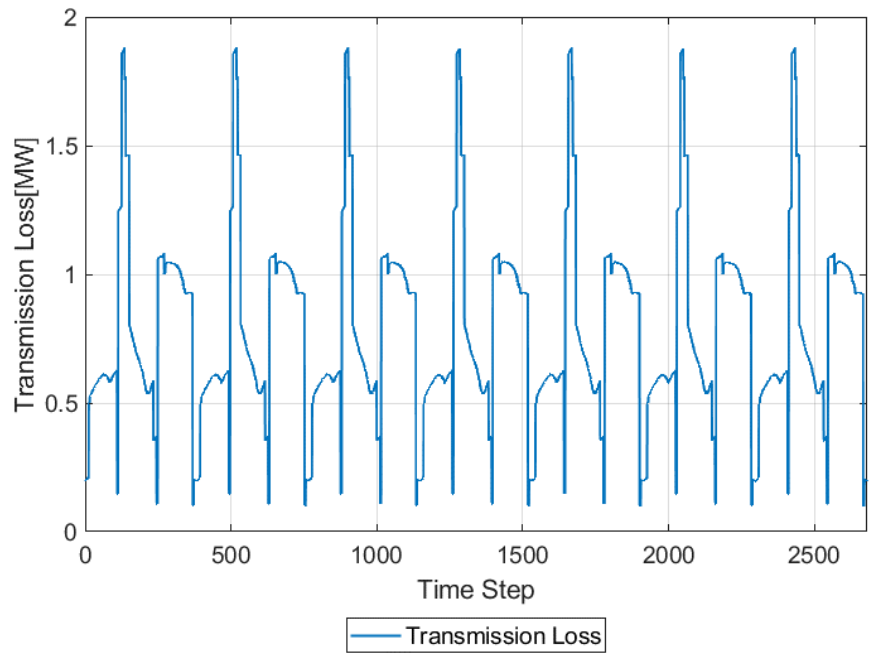


Figure 45 Transmission power loss for the synchronised SFC system with full timetable and variable power

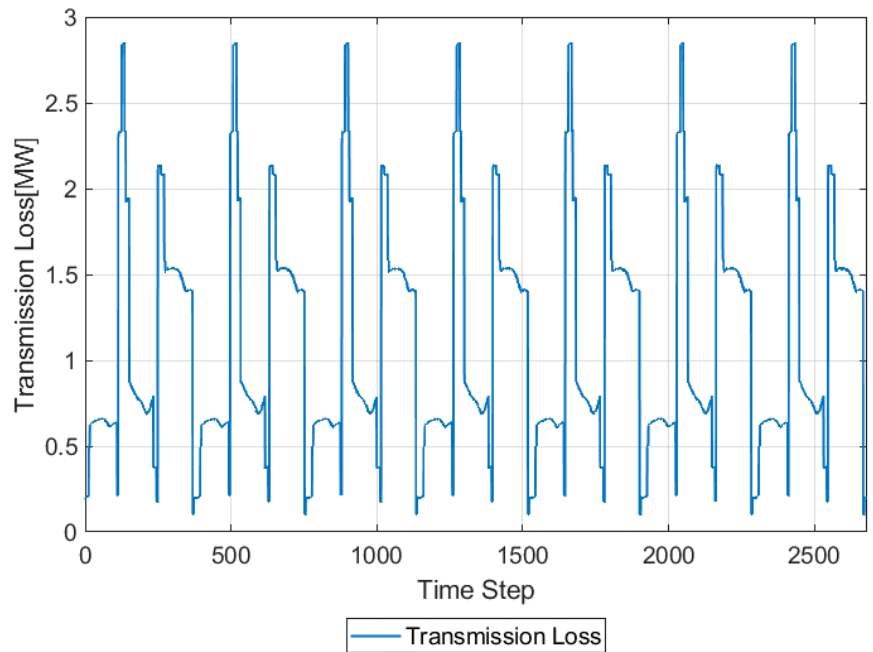


Figure 46 Transmission power loss for the equally shared power SFC system with full timetable and variable power

## 5.2.6 DISCUSSION

Throughout Section 5.2, a study is presented which simulates a realistic timetable of trains running for a period of time as long as a full journey. From this simulation, it is possible to observe a great number of variables for the three different infrastructure and control system configurations being considered, and to analyse the results.

The voltages are kept within the mandated limits by the control systems of the SFC-based feeder stations. There is no danger of over-voltage in the transformer systems as the transformers' base voltage is set to prevent this. This is particularly important in the equally shared active and reactive power control SFC case, as the reactive power output from the feeder stations is controlled using the magnitude of voltage output. The maximum voltage values are limited in accordance with British Standard EN 50130 (CENELEC, 2007).

A set of results that help to draw conclusions from this study has been included in Table 5. This table includes information about the maximum active power output, maximum reactive power output and maximum apparent power output across all feeder stations through the specified period of time. It also includes information on the maximum and minimum voltage across all nodes in the system. The transmission efficiency during this period of time, as well as the overall efficiency considering the efficiency of the transformers, has been included, based on the mechanism for efficiency calculations presented in Section 4.5.

As explained at the start of this chapter, and similarly to the work presented in Chapter 4, the number of SFCs on the line and their locations have been chosen to be most compatible and hence comparable with the AT system. However, the locations of the SFCs are not exactly where the transformer feeder stations for the AT system are located as the SFC system does not require neutral sections and hence there is no need to put two SFCs next to one another. The locations of the stations at which the trains stop are the same, as is the timetable and number of trains. Having the same timetable and station locations but differently located feeder stations means that the distance over which the trains accelerate and hence draw their maximum required power from the feeder stations varies between the AT system and the SFC

cases. A comparison, however, has been made as this is as close to a real comparison between these systems as is sensible, given the operational mechanisms of the technologies.

*Table 5 Summary of results from the study on transformer-based and SFC-based systems*

	Max Active Power [MW]	Max Reactive Power [Mvar]	Max Apparent Power [MVA]	Transmission Efficiency [%]	Max Voltage [kV]	Min Voltage [kV]	System Efficiency [%]
AT System	17.24	3.82	17.67	98.81	25.40	21.34	95.81
Synchronised Control SFC	13.58	1.95	13.72	96.86	25.50	22.96	95.00
Shared Active and Reactive Power Control SFC	9.82	1.93	9.95	95.60	26.87	21.40	93.96

In this case and with this timetable, the AT system is the most efficient system for electrical transmission. It must be noted that in the AT case, two of the stations are located very close to their associated feeder stations and three are located at the end sections of the transformers' feeding zones. The synchronised control SFC case has the second-best transmission efficiency and overall efficiency of the system which makes the equally shared active and reactive power SFC case the least efficient. This result is expected as the equal sharing means that the currents will have to travel greater distances to share the load between all SFCs on the line equally. There is, however, a trade-off. Although the equally shared active and reactive power control SFC case is the least efficient in terms of electrical transmission, it has the lowest requirement for the overall size of the feeder stations in all three cases. The required rating of the feeder stations is smaller than in the synchronised SFC case by 27.4% and the AT system by an even larger percentage of 43.7%. With respect to the sizing, the shared active and reactive power SFC case is optimum; the synchronised SFC case comes second and the AT system requires the highest rated feeder stations for the same timetable of trains and hence the same load.

It must be noted that this study has tried to compare three power supply solutions using a similar infrastructure. Where these systems would be implemented in the real world a thorough optimisation of the system, both in terms of the number of feeder stations and their distribution along the line, and considering the timetable for the trains running, should be carried out. This would further improve the efficiency of the SFC-based systems. One advantage of SFC systems is that, where an optimum solution is found, unlike transformers which have great limitations on cost and availability of high-voltage connections, they can be connected to a more readily available lower-voltage network and, hence, are less expensive and have more flexibility in their range of locations.

What has been discussed above is applied in cases where the trains are running as expected. Fault cases can also occur. While not all fault scenarios have been discussed in this PhD thesis, a fault example is included in Section 5.3 which considers the behaviour of the system when all trains draw the maximum required power regardless of their estimated requirements, based on the power profile and their location. The behaviour for the three infrastructure cases is investigated and compared in the following section.

### 5.3 WORST-CASE SCENARIO

In the previous section, a study was presented in which 14 trains travel along the track at 10-minute intervals. The trains follow a power profile of acceleration, cruising and regeneration. It provided a reasonable comparison between the behaviour of the three different systems, the size of the feeder stations required and the impact of the underlying power system and control strategies on the losses and efficiency of the entire system.

In this section, the behaviour of the three systems under the condition of a worst case for the four feeder stations on the line has been included for the three scenarios of AT system, synchronised control SFC system and shared active and reactive power SFC system. The profiles presented in this section are produced by the simulator where 14 trains run through the timetable described in Section 4.4, as used in the previous study. In this section, however, all the trains draw a constant power equal to the acceleration power at all times. This scenario has been included to show the behaviour of the system in a worst-case situation.

As this is a worst-case scenario and not representative of the normal operation of the railway, only the active, reactive, and apparent power results are presented here.

### 5.3.1 ACTIVE POWER

#### 5.3.1.1 AT SYSTEM

Figure 47 shows the active power profile of the four transformer feeder stations on the line while the trains travel through their journeys according to the timetable, but drawing a constant maximum power.

It is not possible to locate where trains go through the neutral sections on this graph as there is more than one train in each transformer's feeding zone at any given time. The train timetable affects this profile significantly as it determines the location of the trains with respect to the feeder stations and hence the load each transformer has to respond to at all times.

As can be seen in the graph, the transformers are unable to support parts of these journeys. Where there is no possible solution to the power flow analysis, the holomorphic solver returns the currents as zero.

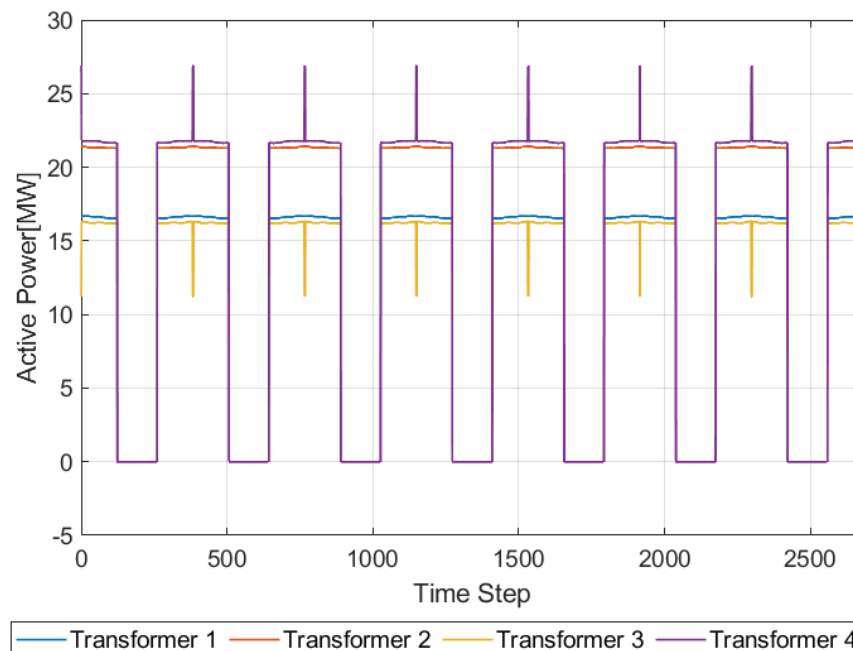


Figure 47 Active power for the AT system scenario with full timetable and constant maximum power

The zero active power sections of the graph show that, considering the structure of the impedances of the OLE and return systems, the arrangements of the loads on the line, the value of the loads and their distances from the feeder stations, the transformers fail to supply the required power in some sections of the line. This shows one limitation of a transformer-based feeding arrangement for the railways. The conditions in which the infrastructure cannot cope with the load occur where two trains travelling in different directions stop at the central station along the line. The central (third) station is located at node 801 which is the furthest location from Transformer 3. The error due to the incapability of the transformers to supply the load lasts for as long as the two trains are stopped at station 3.

#### 5.3.1.2 SYNCHRONISED CONTROL OF SFCs

Figure 48 shows the active power profile of the four SFCs on the line where 14 trains are on the line and drawing a constant acceleration power at all times. The simulation results presented in the figure are for the synchronised control SFC system.

Due to the symmetry of the train timetable, location of stations and location of the feeder stations, the first and fourth SFC feeder stations have the same power profile, as do the second and third SFC feeder stations. The maximum active power amongst all feeder stations is from the first and fourth SFCs as they cover an end section of the line where, in synchronised control, the closest SFC supplies the power required solely for that section of the line. SFC1 and SFC4 also contribute to the sections of the line shared with SFC2 and SFC3, respectively.

In order to account for such a worst-case scenario, and due to the fact that the SFCs cannot be overloaded like transformers, the outer SFCs on the line should be sized to be able to provide the maximum load required from each SFC. It must be noted that this would vary depending on different timetables as the number of trains on the track and the distance they run from one another would affect the active power profile.

In this case, the maximum active power output of SFC1 and SFC4 is 29.8 MW whereas the maximum active power output of SFC2 and SFC3 is 20.64 MW.

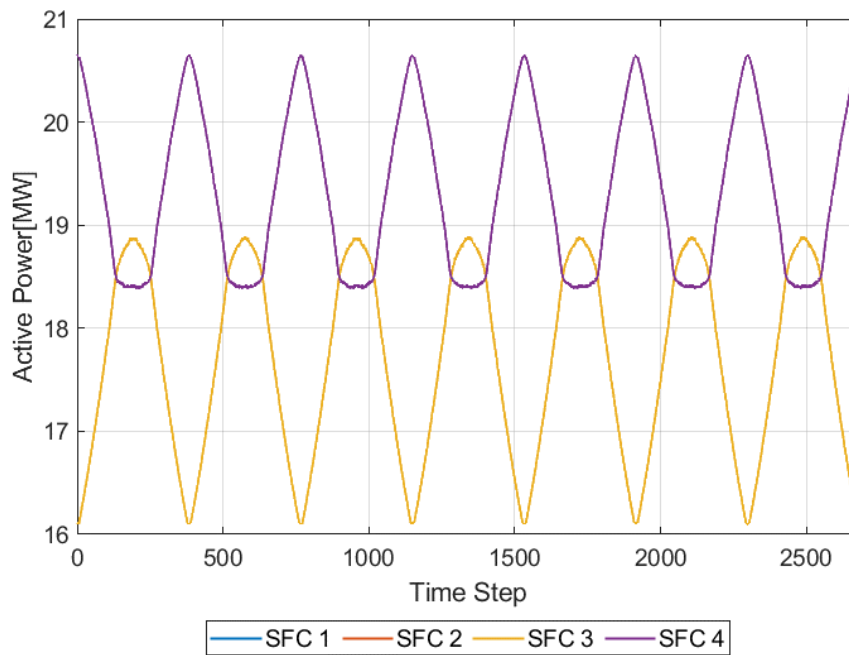


Figure 48 Active power for the synchronised SFC system with full timetable and constant maximum power

### 5.3.1.3 EQUALLY SHARED POWER CONTROL OF SFCs

Figure 49 shows the active power profile of the four SFCs located on the line running through the worst-case scenario using the shared active and reactive power control SFC system.

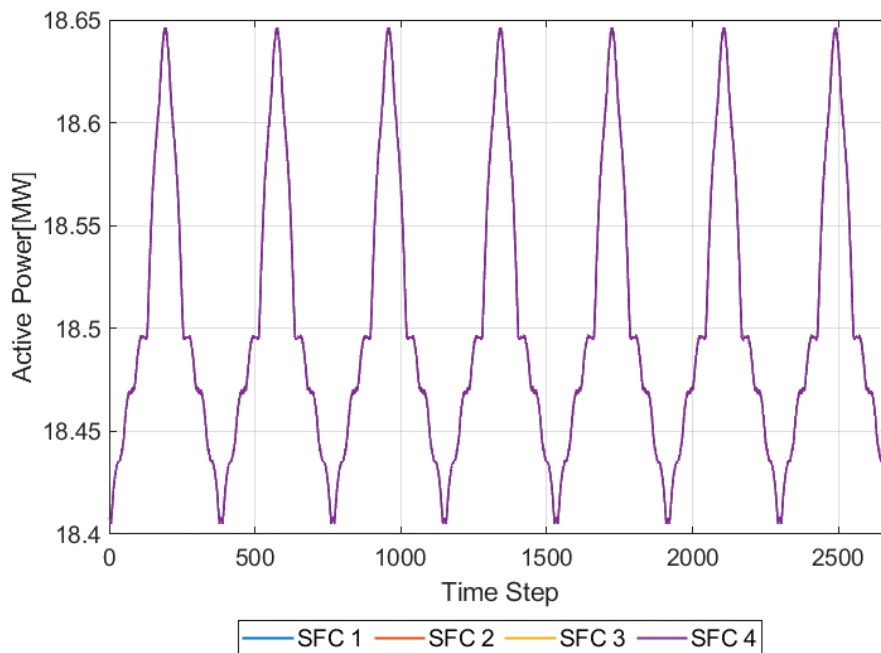


Figure 49 Active power for the shared SFC system with full timetable and constant maximum power

As expected, the maximum active power values in this case are lower than the ones where the SFC output voltages' magnitude and phase angles are synchronised. As the active power is equally shared at all times, the requirements occurring at the ends of the line can be supported by all of the feeder stations whereas when synchronised control SFCs are used, the outer SFCs alone supply the power required for the loads located at the end-of-line sections.

The maximum active power output amongst all SFCs in this case is 18.65 MW. As anticipated, this is significantly lower than for the case where the synchronised control system is used.

### 5.3.2 REACTIVE POWER

Figure 50, Figure 51 and Figure 52 show the reactive power profile of the four feeder stations on the line for the AT system, synchronised control SFC system and equally shared power control SFC system, respectively. The results were obtained for the full timetable of 14 trains (7 in each direction) each operating at a constant maximum power demand. The maximum reactive power output amongst all feeder stations is 6.77 Mvar for the AT system, 2.58 Mvar for the outer SFCs and 1.772 Mvar for the inner SFCs in the synchronised control SFC case and, finally, 2.14 Mvar for the equally shared control SFC case. As expected, the AT system has the highest reactive power output, but interestingly the inner SFCs from the synchronised case have a lower reactive power output than the equally shared power control case. This is because the reactive power component is more affected by the increased transmission distance in the equally shared power case.

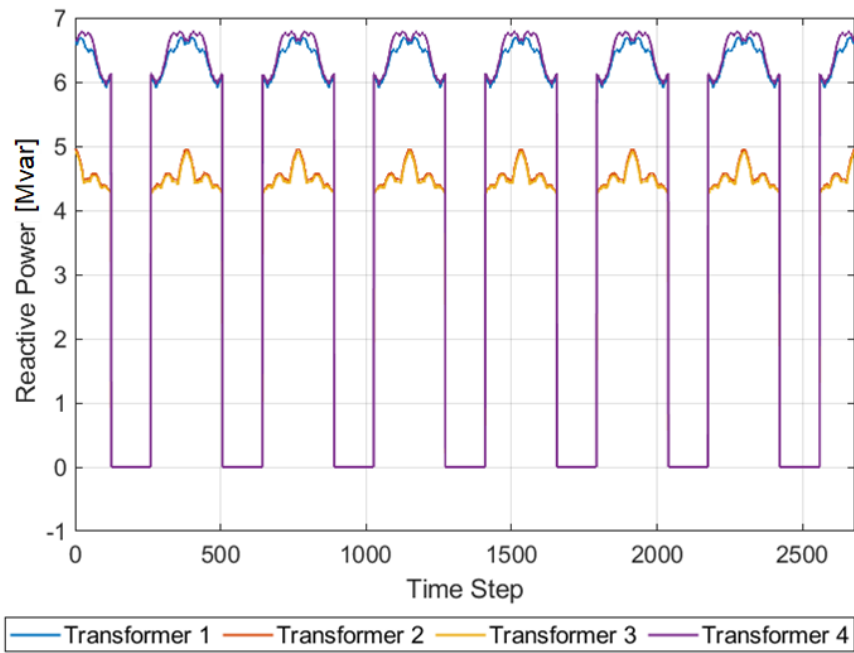


Figure 50 Reactive power for the AT system with full timetable and constant maximum power

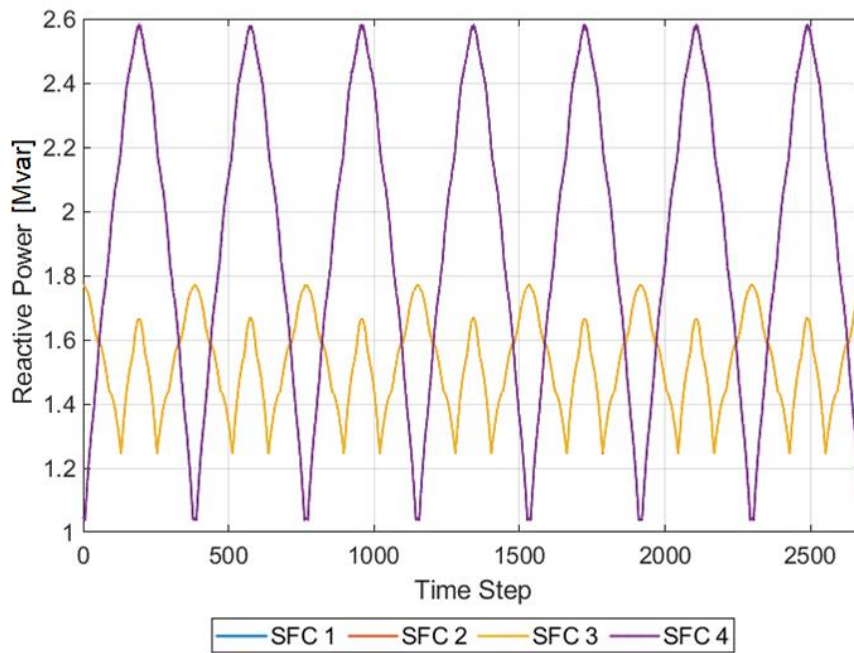


Figure 51 Reactive power for the synchronised SFC system with full timetable and constant maximum power

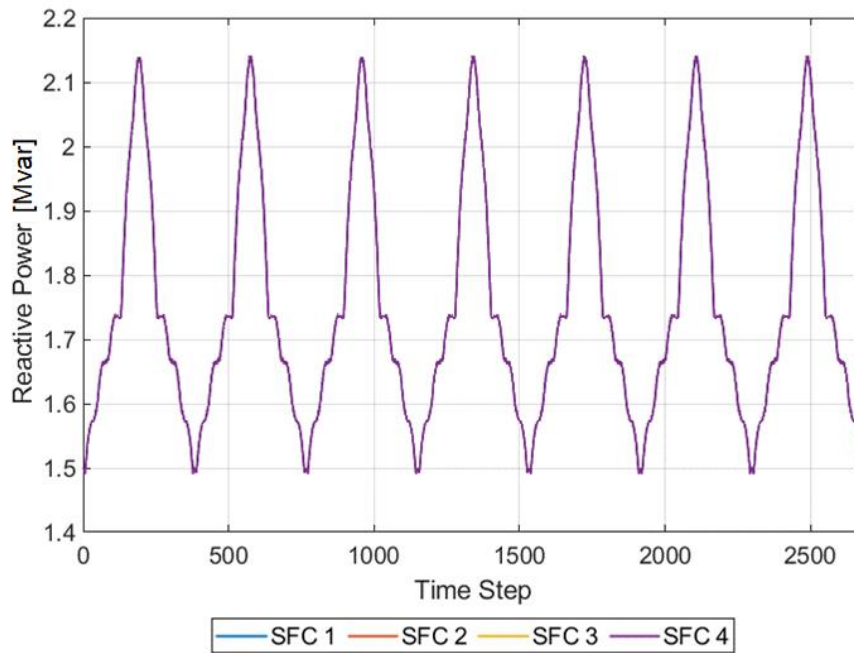


Figure 52 Reactive power for the shared SFC system with full timetable and constant maximum power

### 5.3.3 APPARENT POWER

Figure 53, Figure 54 and Figure 55 show the profiles of the apparent power in the worst-case scenario study for the AT system, synchronised control SFC system, and equally shared control SFC system, respectively. Although an unlikely scenario, these results are significant because sizing of the feeder stations is based on the apparent power. It must be noted that the transformers have capacity for over-loading whereas SFCs do not have this capability. However, the sharing of power in the synchronised control SFC case and the equally shared active and reactive power control SFC case requires a smaller feeder station capacity. In this case, the AT system is unable to support the load and would not be capable of supplying the railway load at all times during this worst-case scenario. Excluding the occurrences for which the AT system has no power flow solution for the required load, the AT system has a maximum apparent value of 28.83 MVA. For the synchronised control SFC case it is 29.66 MVA, and for the equally shared control SFC system the maximum apparent power requirement is 18.77 MVA.

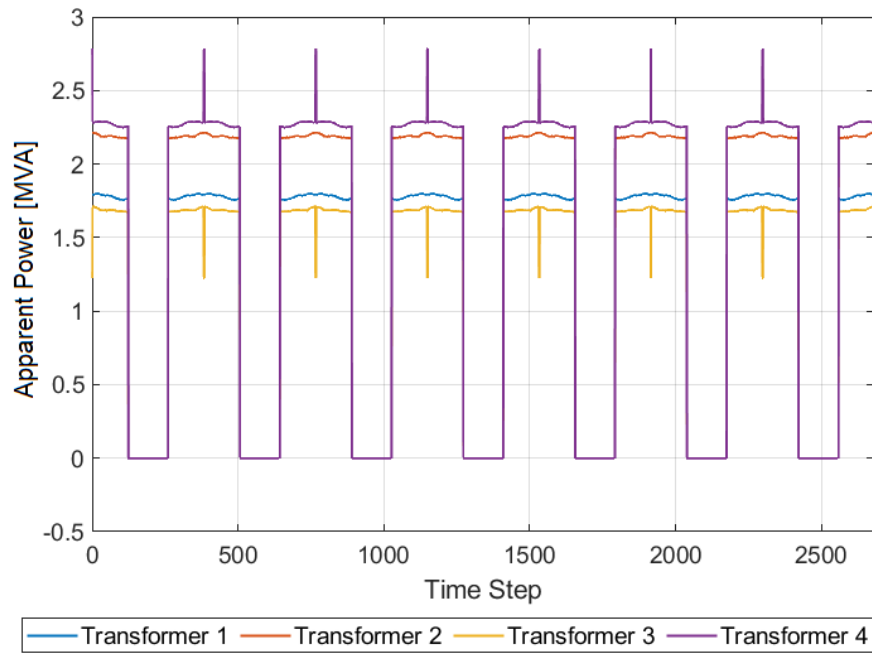


Figure 53 Apparent power for the AT system with full timetable and constant maximum power

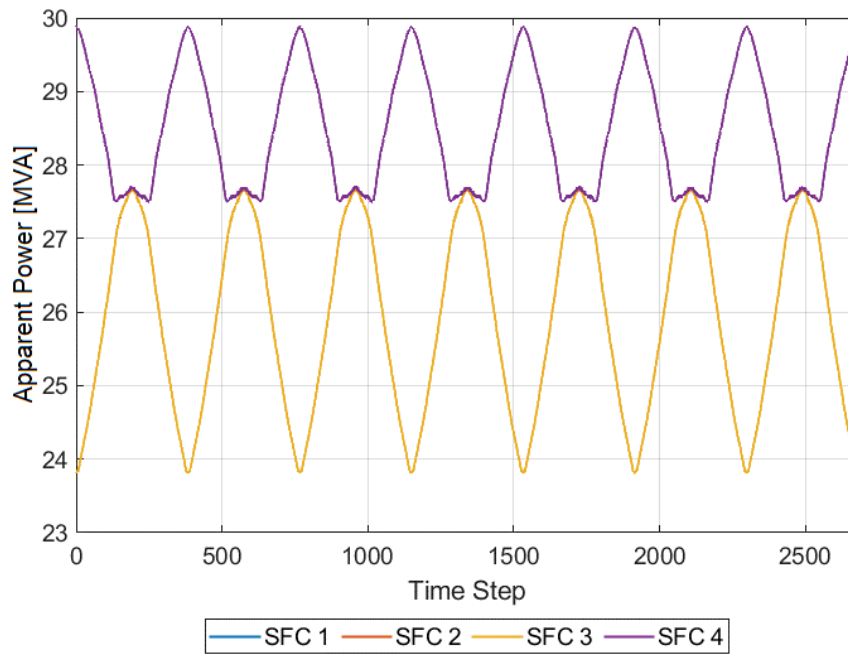


Figure 54 Apparent power for the synchronised SFC system with full timetable and constant maximum power

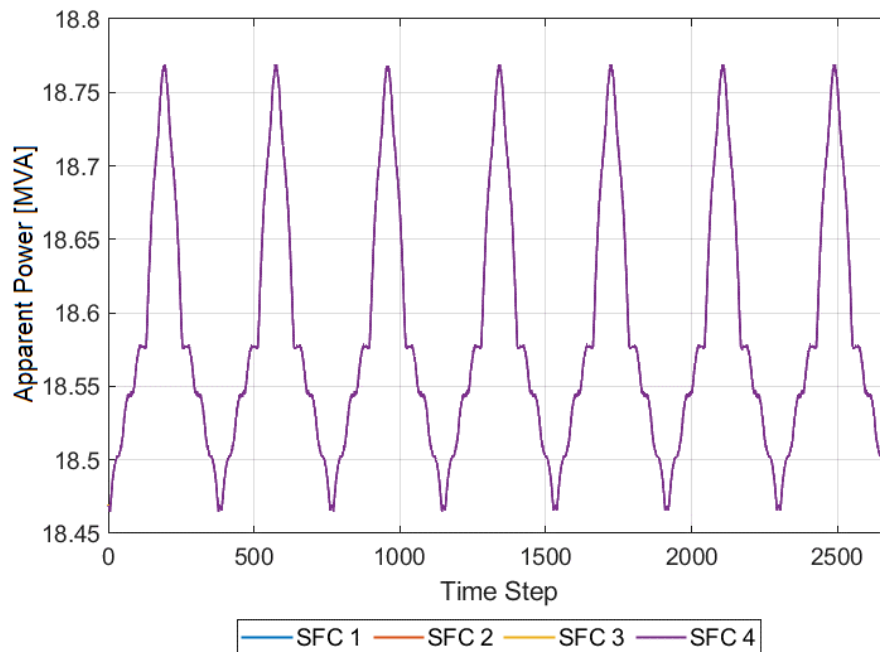


Figure 55 Apparent power for the shared SFC system with full timetable and constant maximum power

### 5.3.4 DISCUSSION

In this case study, a scenario is presented where all trains on the line draw maximum acceleration power throughout their journeys; this is not a scenario that is likely to happen, but has been designed in order to observe the worst case behaviour of the system for any possibly combination of train positions within the timetable.

Active power, reactive power and apparent power profiles have been observed. The losses in this case are not of concern as, in fault scenarios, designing a system that copes through the fault period without disrupting the service is key.

As summarised in Table 6, the AT system case does not work for all combinations of the locations of trains in this case study. This is potentially due to the impedance of the line between the transformer feeder station and the loads. This has resulted in no possible solutions for some parts of the study for the AT system. These results suggest that while the synchronised and equal sharing control systems can

cope with such a fault case with a higher-rated feeder station, the AT system would potentially provide under-rated power to the loads on the line.

*Table 6 Summary of results from the worst-case scenario study on transformer-based and SFC-based systems*

	Max Active Power	Max Reactive Power	Max Apparent Power
AT System (where a solution is possible)	28.02 MW	6.77 Mvar	28.83 MVA
Synchronised Control SFC	29.80 MW	2.58 Mvar	29.66 MVA
Shared Active and Reactive Power Control SFC	18.65 MW	2.14 Mvar	18.77 MVA

## 5.4 CONCLUSIONS

This chapter considered a case where a realistic timetable of trains is run through the infrastructure previously discussed in Chapters 3 and 4. The study investigated the behaviour of the system in three cases: a transformer-based system with ATs, an SFC-based system with synchronised control and an SFC-based system with smart control enabling equal sharing of active and reactive power at all times between the SFC feeder stations located along the line. In this chapter, elements of significant importance have been presented using graphs and data: active, reactive and apparent power as well as nodal voltages and energy loss profiles. The chapter also discussed a fault scenario where all trains on the line are at their highest power demand and analyses the behaviour of the systems in such scenarios.

This study finds that for both cases, the SFC system with equally shared active and reactive power copes with the load on the system with the smallest-rated feeder stations; however, this increases the transmission losses throughout the network. Synchronised control of SFCs requires a smaller rating for the feeder stations than the AT system; however, it incurs more transmission losses as well.

The key results are presented in Section 5.2, however comparing these to the worst-case scenario presented in Section 5.3 indicates that, in order to support a worst case scenario, the increase in the rated capacity of SFC feeder stations required can be minimised through the use of the equally shared power control strategy. The apparent power levels required to support the worst-case scenario are an increase

of 116% of the normal operating scenario for the synchronised case, and 89% for the equally shared powers case. The equally shared powers control strategy is therefore more resilient to extreme fault conditions.

This chapter only includes arrangements of SFC feeder stations where it showcases a scenario most comparable with an AT system. It is essential to understand the effect of the arrangements and number of SFC feeder stations on the line to maximise the benefits of an SFC-based railway power network. Chapter 6 explores the effect of the number and arrangement of SFC feeder stations on the transmission loss, overall efficiency of the system and the required rated power for feeder stations.

# 6 ANALYSIS OF THE EFFECT OF THE NUMBER OF, AND DISTANCE BETWEEN, SFC FEEDER STATIONS ON SYSTEM PERFORMANCE

## 6.1 INTRODUCTION

There are several benefits associated with the use of SFC feeder stations for railway applications, as previously described in Section 2.2.4. Principally, the ability to place feeder stations further away from each other gives the system a degree of flexibility which is augmented by the dual-end and mesh-feeding ability of an SFC system. Given this flexibility, though, one of the most important considerations when using these systems is the arrangement of feeder stations along the line. The locations have an impact on different critical factors of the system such as voltage drops and the transmission efficiency.

There are limitations associated with using the furthest distance possible and feasible between SFCs. These limitations are caused by the voltage limits, transmission losses and maximum apparent power output required from each feeder station, which determines sizing.

In this chapter, an analysis has been carried out to investigate the impact of having different numbers and arrangements of SFC feeder stations. The analysis has been carried out by modelling and simulating three to seven SFCs on a 160 km line which is otherwise as previously described in Chapter 4. For each overall number of SFCs, five arrangements on the line, primarily considering different spacing and end section lengths, have been studied. In all of these arrangements the SFCs themselves are equally distributed, but the end section lengths are varied, thereby leaving a different length of line over which to distribute the SFCs. Although SFCs can be arranged without equal spacing, it is outside the scope of this PhD to investigate those scenarios.

The arrangements studied include a range of distances between SFCs varying between:

- 1- Where the outer SFCs are located at the two ends of the line, i.e.

$$gap = \frac{\textit{The length of the line}}{\textit{number of SFCs} - 1}$$

- 2- Where the end-section distances are as big as the distance between two SFCs, i.e.

$$gap = \frac{\textit{The length of the line}}{\textit{number of SFCs} + 1}$$

The effect of changing the number and distribution of the feeder stations is explored using a number of key simulation outputs: maximum apparent power, transmission energy loss, and system efficiency. These results have been selected to give both a clear understanding of the required scale of the feeder stations themselves, and to allow comparisons of the performance of different control strategies.

- (i) **Maximum Apparent Power:** This output from the simulations has a vital impact on sizing the SFCs for the specified load.

The number of SFC feeder stations as well as the distance between them affects the maximum apparent power output required for a given load. This parameter has been analysed as it is the primary indicator for determining the required rating of the SFCs on the line.

With synchronised SFC control, where the magnitude and phase angle of all SFCs are synchronised, as previously described in Chapters 3 and 4, the timetable of the trains on the line can affect the maximum apparent power greatly, due to the possibility of having periods of time where the number of the trains in a single SFC feeding zone increases. For the reasons described, the spacing of the SFCs combined with the timetable of the trains moving on the line greatly affects the value of the maximum apparent power output an SFC feeder station must provide and, consequently, the required rating of the SFC.

- (ii) **Transmission Losses:** This simulation output determines the cost impact of each arrangement caused by transmission of the power from the feeder station to the load.

The distance between the SFC feeder stations affects the transmission losses of the system as the further the distance between them, the further the current travels from the feeder stations to the loads. It must also be noted that the larger the transmission losses are, the bigger the output from the SFC feeder stations must be to compensate for the losses and to provide the loads with the required power.

As discussed, the train timetable has a significant impact on this study: it determines the location of the trains relative to the SFC feeder stations at each given point in time. Reducing the number of feeder stations increases the impact of the location of the load. This is due to larger

transmission losses due to the greater distances between the SFCs where there are fewer of them on the line.

- (iii) **System Efficiency:** The system efficiency is the percentage efficiency of the system considering both the SFC feeder stations' internal efficiency and the transmission efficiency, as previously described in Section 4.5.2.

It must be noted that the results presented in this chapter have been produced using 675 kW as the cruising power, which is significantly lower than the value calculated using the Davis Equation and presented in Section 4.4. This error is easily amendable though and does not affect the conclusions drawn in this chapter, and the rest of the thesis.

## 6.2 NUMBER OF FEEDER STATIONS AND THEIR ARRANGEMENT

The arrangement, number and spacing of the feeder stations are as summarised in the tables below; all distances in these tables are in km, with the distances for each SFC being from the start of the 160 km line and the gap being the distance between each pair of SFCs.

### Three Feeder Stations

*Table 7 Location and separation of SFCs for three-SFC arrangements*

	Gap	SFC 1	SFC 2	SFC 3
Arrangement A	80	0	80	160
Arrangement B	70	10	80	150
Arrangement C	60	20	80	140
Arrangement D	50	30	80	130
Arrangement E	40	40	80	120

### Four Feeder Stations

*Table 8 Location and separation of SFCs for four-SFC arrangements*

	Gap	SFC 1	SFC 2	SFC 3	SFC 4
Arrangement A	53.3	0	53.3	106.6	160
Arrangement B	46	11	57	103	149
Arrangement C	40	20	60	100	140
Arrangement D	36	26	62	98	134
Arrangement E	32	32	64	96	128

## Five Feeder Stations

Table 9 Location and separation of SFCs for five-SFC arrangements

	Gap	SFC 1	SFC 2	SFC 3	SFC 4	SFC 5
Arrangement A	40	0	40	80	120	160
Arrangement B	36.5	7	43.5	80	116.5	153.1
Arrangement C	33	14	17	80	113	146
Arrangement D	29.5	21	50.5	80	109.5	131
Arrangement E	26.6	26.8	53.4	80	106.6	132.2

## Six Feeder Stations

Table 10 Location and separation of SFCs for six-SFC arrangements

	Gap	SFC 1	SFC 2	SFC 3	SFC 4	SFC 5	SFC 6
Arrangement A	32	0	32	64	96	128	160
Arrangement B	29.7	5.6	35.4	65.1	94.8	124.5	154.2
Arrangement C	27.4	11.5	38.9	66.3	93.7	121.1	148.5
Arrangement D	25.1	17.2	42.3	67.4	92.5	117.6	142.7
Arrangement E	22.9	22.8	45.7	68.6	91.5	114.4	137.3

## Seven Feeder Stations

Table 11 Location and separation of SFCs for seven-SFC arrangements

	Gap	SFC 1	SFC 2	SFC 3	SFC 4	SFC 5	SFC 6	SFC 7
Arrangement A	26.6	0	26.8	53.4	80	106.8	133.4	160
Arrangement B	25	5	30	55	80	105	130	155
Arrangement C	23.5	9.5	33	56.5	80	103.5	127	150.5
Arrangement D	22	14	36	58	80	102	124	145.9
Arrangement E	20	20	40	60	80	100	120	140

### 6.3 LOAD AND CONTROL CONFIGURATIONS

In this chapter, two load configurations are studied. The first of these sees the timetabled trains draw a constant power equivalent to the value of the average power they draw through their acceleration and cruising cycle. Based on the standard traction profile described in Section 4.4, this gives a constant power requirement per train of 2.097 MW. This load configuration is included because it negates the impact of the distance between the feeder station and traction zones and as such allows the results to be interpreted as independently of the timetable as possible. The second load configuration is for the full traction profile described in Section 4.4 which includes acceleration, cruising, braking, and stopping at stations. This is a more involved simulation which produces more representative results, albeit they are more difficult to interpret.

The two load configurations are considered for both of the SFC feeder station control strategies discussed so far in this thesis. That is, the synchronised control case where loads draw from feeder stations immediately adjacent to them, and the novel equally shared active and reactive power control strategy where all feeder stations contribute to all loads equally.

The four load and control configurations are therefore:

- 1- Synchronised control with a train timetable where all trains draw a constant power of 2.0974 MW throughout their journey;
- 2- Shared active and reactive power with a train timetable where all trains draw a constant power of 2.0974 MW throughout their journey;
- 3- Synchronised control with a timetable of trains running with variable power considering acceleration, deceleration, regenerative power and stopping at stations;
- 4- Shared active and reactive power with a timetable of trains running with variable power taking into account acceleration, deceleration, regenerative power and stopping at stations.

## 6.4 RESULTS

The results in this chapter are presented in graphs in which results for the number of SFCs are shown using a standard colour coding as described in Table 12, below.

*Table 12 Colour coding for number of SFC feeder stations*

Number of SFC Feeder Stations	Colour
3	Green
4	Purple
5	Yellow
6	Red
7	Blue

The 25 data points presented in the graphs (five distributions for each of the five numbers of SFC feeder stations) are shown on the graphs as ‘●’. A MATLAB interpolation has been used to estimate the curvature of other possible arrangements in between the five simulated.

For each of the parameters defined in Section 6.1, the results relating to constant power are presented first, followed by variable power – both for the synchronised and equally shared active and reactive power cases.

### 6.4.1 MAXIMUM APPARENT POWER

#### 6.4.1.1 CONSTANT POWER

In this section, all trains are assumed to draw constant power throughout their journeys. The constant power is equal to 2.0974 MWs which is the average of the active power each train draws throughout its journey. With trains drawing constant power throughout their journeys, the effect of the distance from a feeder station between where a train accelerates and decelerates is eliminated and, consequently, it is possible to read the results without the dominating factor of timetables.

#### 6.4.1.1.1 CONSTANT POWER – SYNCHRONISED CONTROL SFC SYSTEM

Figure 56 shows the values of maximum apparent power amongst all SFC feeder stations on the line corresponding to the distance between them as described in Section 6.2. These numbers have been drawn from simulations where the phase and magnitude of the voltages at the SFC feeder stations on the line are synchronised in accordance with the synchronised control strategy.

As expected, having fewer SFCs on the line requires a greater power output per SFC. For each combination of SFCs, there is a pattern which indicates a minimum apparent power required from the SFC feeder stations. However, it is worth mentioning that despite the fact that the application of constant power for trains minimises the effect of acceleration and deceleration, the timetable of the trains on the line can still have an effect on this pattern. This is particularly noticeable when there are more feeder stations, and as such the feeder stations are inherently closer together. In this case the results are more affected by the trains entering and exiting the feeding zones of each SFC.

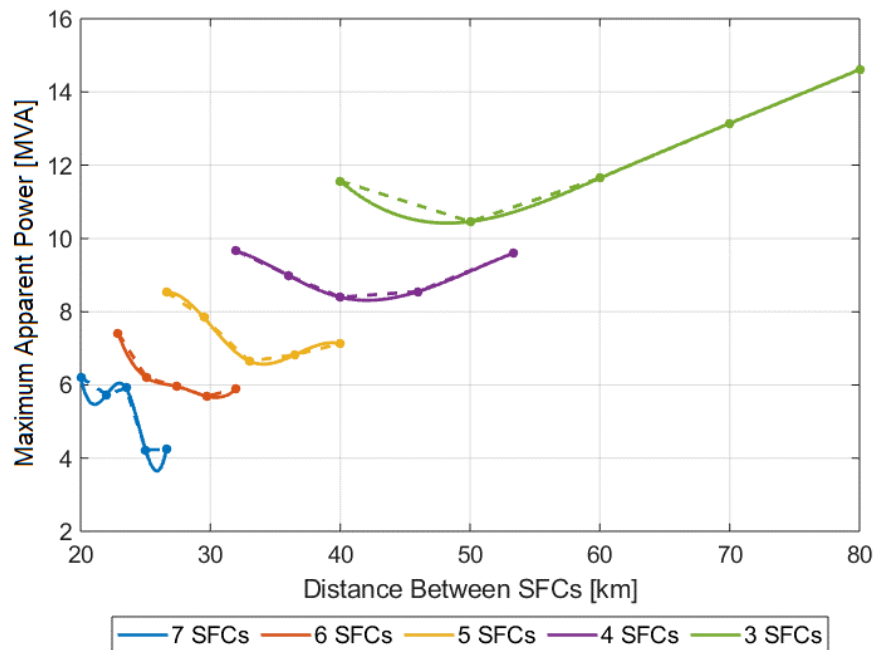


Figure 56 Maximum apparent power for constant power loads using the synchronised control SFC system

#### 6.4.1.1.2 CONSTANT POWER – EQUALLY SHARED ACTIVE AND REACTIVE POWERS

Figure 57 shows the values of maximum apparent power amongst all SFC feeder stations on the line corresponding to the distance between, them as described in Section 6.2. These numbers have been drawn from simulations where the active and reactive power outputs from SFC feeder stations on the line are always equally shared as per the equally shared active and reactive control strategy. Figure 57 shows that the variation in maximum apparent power required from the SFCs in each group is very subtle. The same pattern of power requirement increasing with the number of SFC feeder stations (and thus increased spacing) is still present however the power requirement varies less with spacing. This suggests that this control strategy would be more robust to variations in the positioning of SFC feeder stations against the ideal design, which may be beneficial in practical deployments.

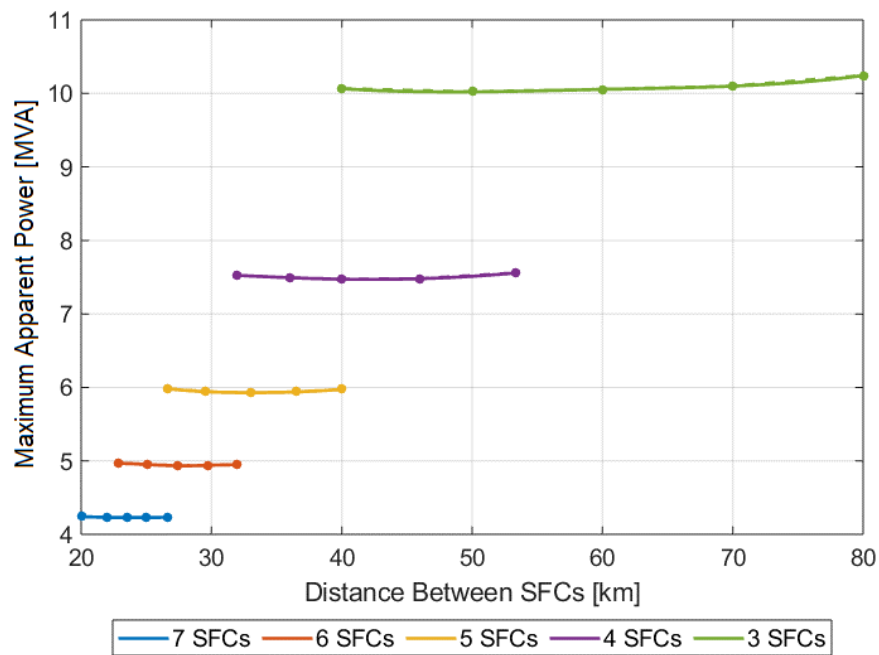


Figure 57 Maximum apparent power for constant power loads using the equally shared control SFC system

#### 6.4.1.1.3 CONSTANT POWER – COMPARISON OF SYNCHRONISED AND EQUALLY SHARED ACTIVE AND REACTIVE POWERS

Figure 58 shows the maximum apparent power data points for both synchronised and shared active and reactive power control systems. As presented, for all arrangements of the SFC feeder stations, the scenario with shared active and reactive power control, graphically symbolised with ‘X’s, has a lower

value for the maximum apparent power. In some cases, for example the 40 km gap for the three-SFC case and the 20 km gap for the seven-SFC case, the maximum apparent power is 49% less than the equivalent cases for synchronised control. This would allow for fewer SFCs to be installed per line and consequent cost, installation and maintenance savings. This will be discussed further in Chapter 7.

Another point to consider is that the variation of the maximum apparent power output requirements from the SFC feeder stations, amongst each SFC number group, in the shared active and reactive power scenarios is as small as 0.3% to 2% whereas for synchronised control it is 15% to 46%. The variation is calculated based on the percentage difference between the smallest and largest maximum apparent power amongst the same SFC number group.

In real-life applications, it would not be possible to build a feeder station in any desirable location; consequently, a smaller impact of the arrangement of the SFCs along the line on the rating of the SFC feeder stations helps to keep the ratings down even though the SFCs cannot be put in the most efficient locations.

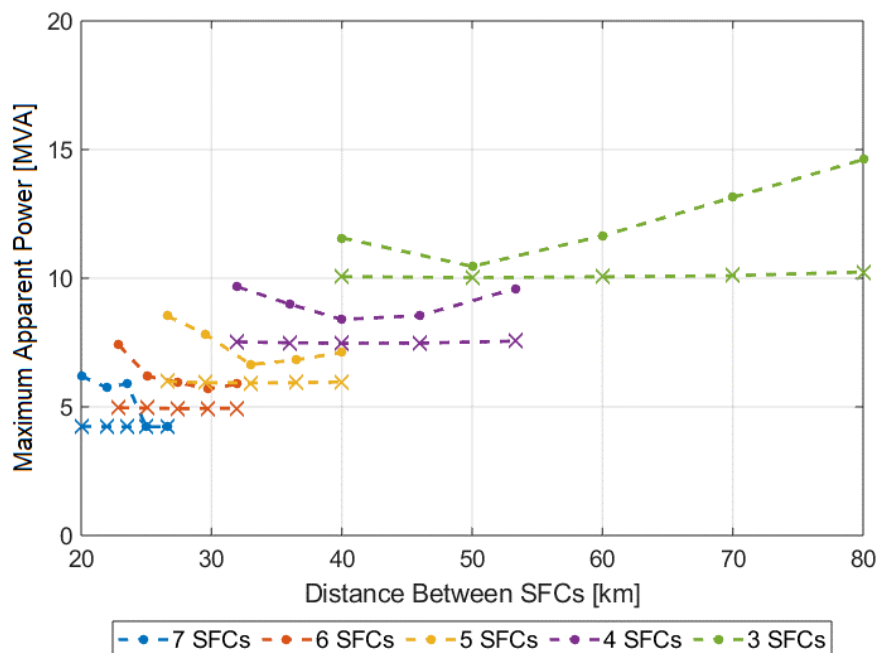


Figure 58 Maximum apparent power for constant power loads using both SFC control strategies ('•' synchronised, '×' equally shared)

#### 6.4.1.2 VARIABLE POWER

In this section, all trains draw variable power according to the timetable and train power profile described in Section 4.4. With trains drawing variable power throughout their journeys, the effect of the distance from the feeder stations between where the train accelerates and decelerates is considered.

##### *6.4.1.2.1 VARIABLE POWER – SYNCHRONISED CONTROL SFC SYSTEM*

Figure 59 shows the values of maximum apparent power amongst all SFC feeder stations on the line, corresponding to the distance between them as described in Section 6.2. These numbers have been drawn from simulations where the phase and magnitude of the voltage of SFC feeder stations on the line are synchronised.

As is evident from Figure 59, the values of maximum apparent power in this case do not follow an intuitive or repetitive pattern. In some cases, a greater number of feeder stations on the line does not result in a lower value of apparent power required from the SFC feeder stations. The smallest number of SFC feeder stations on the line is three; this predictably corresponds to the largest values for maximum apparent power. Having seven SFC feeder stations on the line, however, results in a greater value of maximum apparent power than the scenario with six SFC feeder stations. This is due to the pattern of the location of the trains on the line and where the trains accelerate and regenerate with respect to the SFC feeder stations. A number of scenarios might have caused this effect compared with six SFC feeder stations:

- There are a greater number of trains in an SFC feeder station's zone to feed, which would cause a need for a greater value of apparent power;
- The position in which the trains accelerate falls in a different pattern, closer to one SFC feeder station for multiple trains.

These scenarios may also have caused the significant change in the values in the four-SFC feeder station arrangements. There may be scope for further investigation into the optimisation of train timetables vs SFC placement, but this is outside the scope of this PhD.

In comparison with the constant power cases shown above, there is not enough of a pattern in this case from which to draw definitive conclusions.

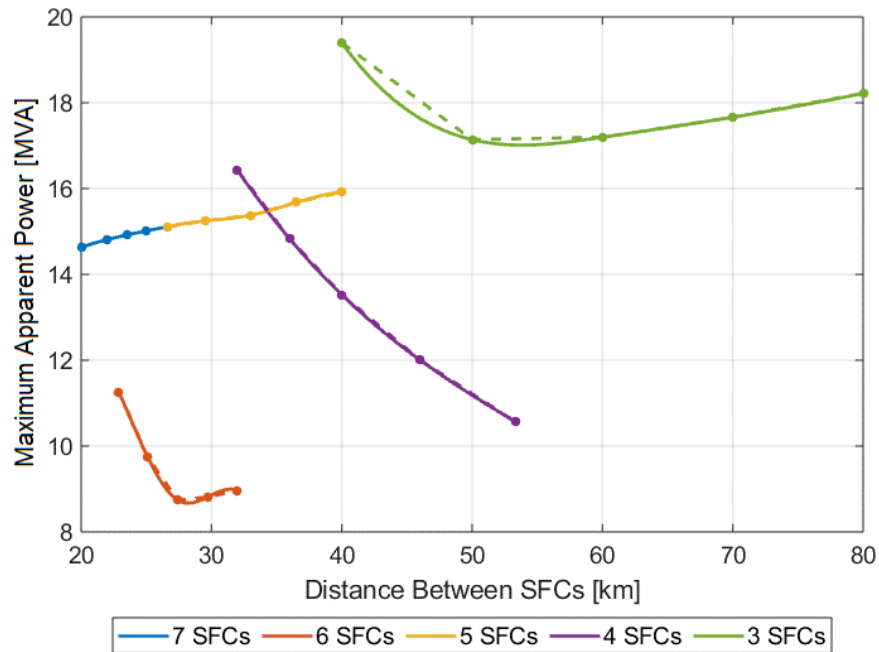


Figure 59 Maximum apparent power for variable power loads using the synchronised control SFC system

#### 6.4.1.2.2 VARIABLE POWER – EQUALLY SHARED ACTIVE AND REACTIVE POWERS

Figure 60 shows the values of maximum apparent power amongst all SFC feeder stations on the line corresponding to the distance between them as described in Section 6.2. These numbers have been drawn from simulations where the active and reactive power outputs from SFC feeder stations on the line are always equally shared as directed by the new equally shared active and reactive control strategy.

The values of maximum apparent power in this scenario follow a clear intuitive pattern where increasing the number of SFCs decreases the maximum apparent power. It must, however, be noted that although the pattern of the location of the trains with respect to SFC feeder stations and acceleration and regeneration positions does not cause a dramatic deviation from the intuitive results due to the continuous sharing of active and reactive powers, they have a noticeable effect on the final values for maximum apparent power required.

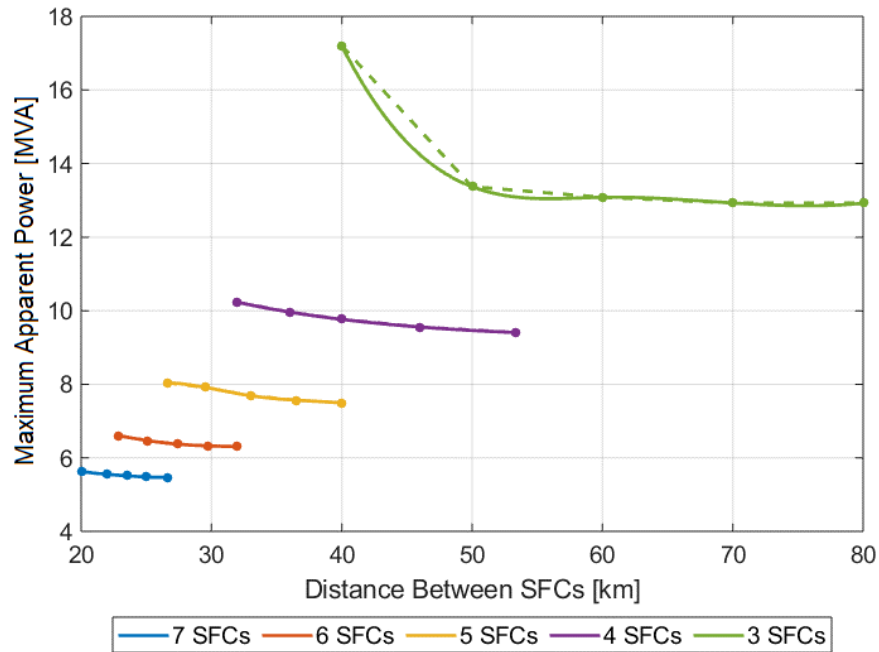


Figure 60 Maximum apparent power for variable power loads using the equally shared control SFC system

#### 6.4.1.2.3 VARIABLE POWER – COMPARISON OF SYNCHRONISED AND EQUALLY SHARED ACTIVE AND REACTIVE POWERS

Figure 61 shows the results from both Sections 6.4.1.2.1 and 6.4.1.2.2 in the same graph. The lines with nodes graphically symbolised by ‘●’ represent the results from Section 6.4.1.2.1 (synchronised control) while the lines with nodes graphically symbolised by ‘X’ represent the results from Section 6.4.1.2.2 (equally shared active and reactive powers control).

Comparison of the results from synchronised output and equally shared active and reactive power output from the SFC feeder stations shows that the system which utilises the smart control capability of SFC feeder stations offers predictability and stability where the gap between the maximum apparent power levels from closest to furthest distances between feeder stations is not large. This would provide flexibility when these systems are implemented in the real world, as any system greatly affected by a change in timetable or the accurate location of feeder stations imposes significant limitations on the applicability of the system. With an equally shared active and reactive power scenario, it is possible to rely on the system regardless of the details of arrangements that are potentially outside of the designer’s control. This result shows that having smartly controlled feeding arrangements reduces the effects of

feeder station locations on the sizing of the feeder stations. This is important as feeder stations cannot always be built and connected in the optimum theoretical locations.

The other significant point in this comparison is, as presented in Figure 61, the significantly higher values of the maximum apparent power in each of these arrangements demonstrated for the synchronised control strategy. In all arrangements, the value of the maximum apparent power for the synchronised scenario is larger than for the equally shared active and the reactive power scenario. It is, however, not possible to draw a definitive conclusion about this with numbers in the scenarios presented in this section due to the complications relating to train location described earlier in this chapter.

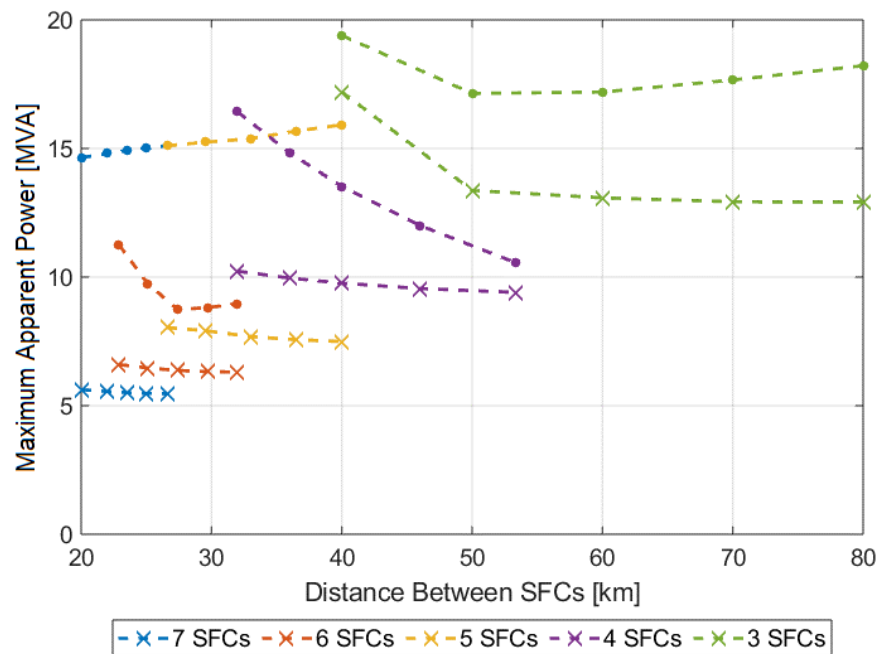


Figure 61 Maximum apparent power for variable power loads using both SFC control strategies ('•' synchronised, '×' equally shared)

## 6.4.2 TRANSMISSION LOSSES

In this section, the transmission loss results have been analysed using the method described in Section 4.5.1. The following sections present the results from this analysis.

### 6.4.2.1 CONSTANT POWER

#### 6.4.2.1.1 CONSTANT POWER – SYNCHRONISED CONTROL SFC SYSTEM

In order to obtain a set of results which is more reliably analysable, the effect of acceleration and deceleration has been minimised through the application of a timetable of trains drawing a constant power.

Figure 62 shows the values of total transmission energy loss throughout the journey corresponding to the distance between SFC feeder stations on the line as described in the introduction to this chapter. In this section, these numbers have been drawn from simulations where the phase and magnitude of the voltage of SFC feeder stations on the line are synchronised.

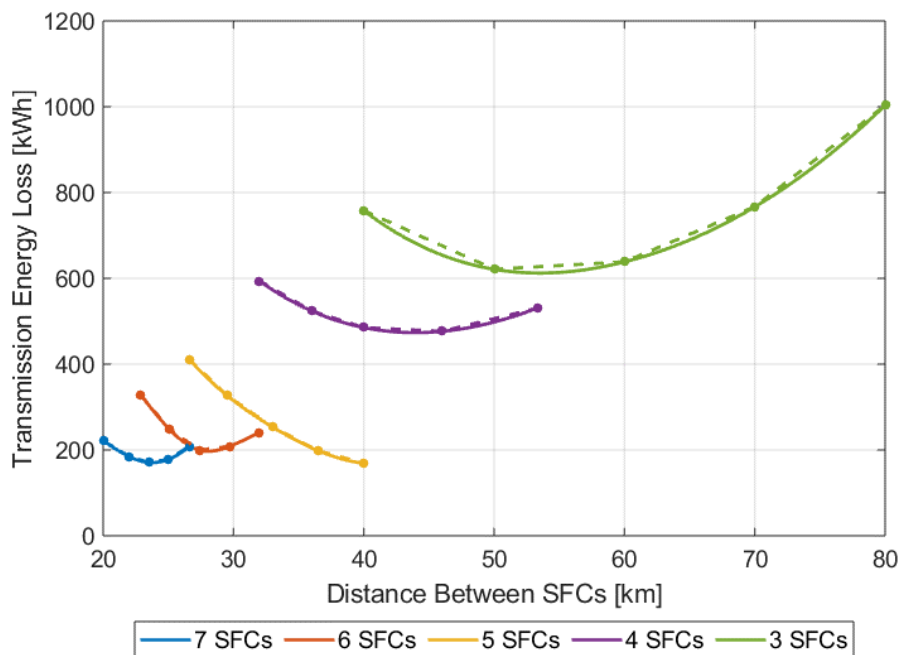


Figure 62 Total transmission energy loss for constant power loads using the synchronised control SFC system

As presented in Figure 62, the different values of energy lost due to transmission through a complete journey follow a reasonably intuitive pattern. With a larger number of SFCs on the line, the overall

transmission energy losses are reduced. This is due to the shorter distances between sources which leads to shorter travel distances for high currents and consequently reduces the transmission loss. The number and spacing of trains in the system, according to the timetable, would also play a notable role, even with the constant power vehicle model.

#### 6.4.2.1.2 CONSTANT POWER – EQUALLY SHARED ACTIVE AND REACTIVE POWER

Figure 63 shows the values of total transmission loss corresponding to the distance between SFC feeder stations on the line as described in Section 6.2. These numbers have been drawn from simulations where the active and reactive power outputs from SFC feeder stations on the line are always equally shared as per the smart control strategy.

The results presented in Figure 63 show that the graph follows an intuitive pattern. The reason that in some cases a smaller number of SFCs on the line have lower transmission energy losses than a larger number of SFC feeder stations is due to the effect of arrangements of SFCs on the line.

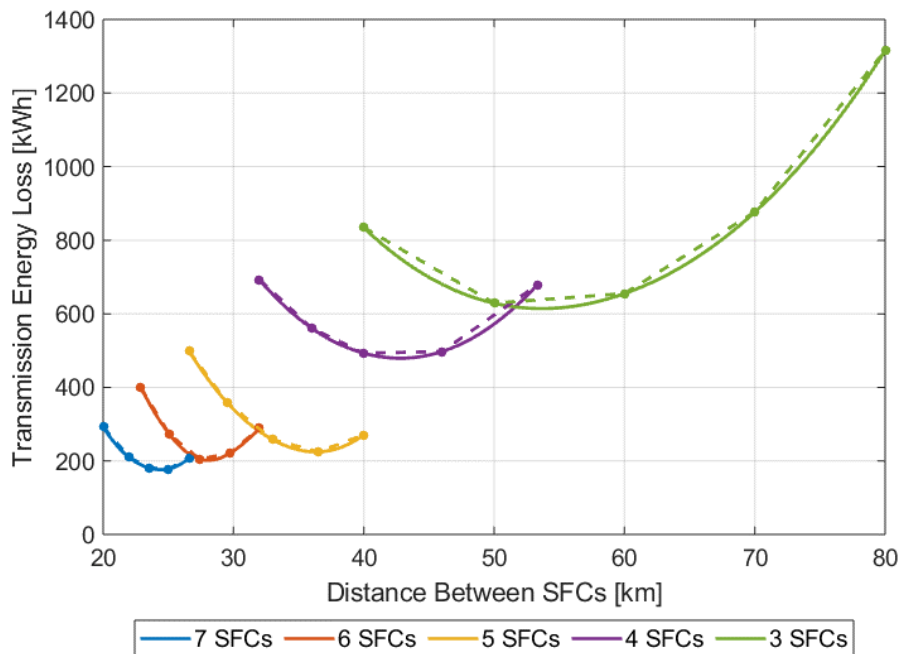


Figure 63 Total transmission energy loss for constant power loads using the equally shared control SFC system

6.4.2.1.3 CONSTANT POWER – COMPARISON OF SYNCHRONISED AND EQUALLY SHARED ACTIVE AND REACTIVE POWERS

Figure 64 shows the data points representing the transmission energy loss throughout the whole journey for both synchronised and equally shared active and reactive power control strategies.

As illustrated below, in all cases, the transmission energy loss for the equally shared active and reactive power cases is higher than for the synchronised cases. This is due to the greater distance travelled by the currents when the required load throughout the journey is equally shared between all SFCs, resulting in higher impedance along the line, leading to further transmission losses. However, in cases where the arrangement of the SFCs is such that they are at the most efficient points, these values are of negligible difference. The figure shows a division between three and four SFC feeder stations, and five, six, and seven SFC feeder stations. This suggests that between four and five SFC feeder stations adding only a small amount of further infrastructure can have a significant impact on losses. It must be noted that despite higher transmission losses, the apparent power value and hence the size of the SFC feeder stations in the case for equally shared active and reactive power is significantly lower.

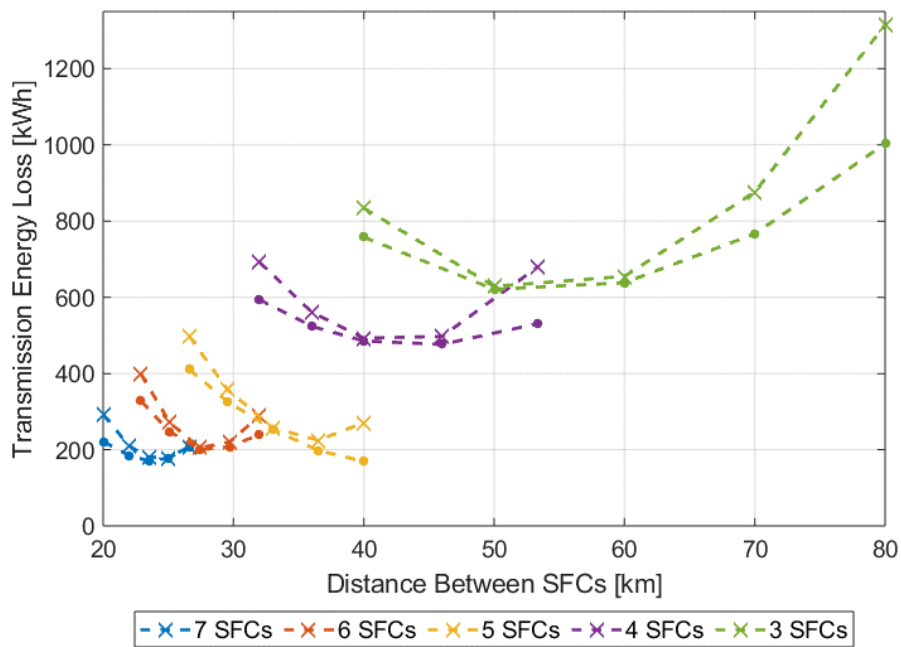


Figure 64 Total transmission energy loss for constant power loads using both SFC control strategies ('•' synchronised, 'x' equally shared)

Where the difference in maximum apparent power values for the synchronised case varies between being 4% to 49% higher than for the equally shared active and reactive power cases (Section 6.4.1.1.3), the transmission losses are 2% to 60% higher. This is further analysed in Chapter 7 where an economic evaluation for SFC systems is presented.

## 6.4.2.2 VARIABLE POWER

### 6.4.2.2.1 VARIABLE POWER – SYNCHRONISED CONTROL SFC SYSTEM

Figure 65 shows the data output from analysis of the total transmission energy loss as described in Section 4.5.1. The effect of the train timetable on transmission losses can be clearly seen from the lack of a clear relationship within the diagram. Contrary to expectation, in some cases the arrangements with a smaller number of SFCs on the line have a smaller total associated transmission energy loss. This is due to the location of the accelerating and decelerating trains with respect to the SFC feeder stations.

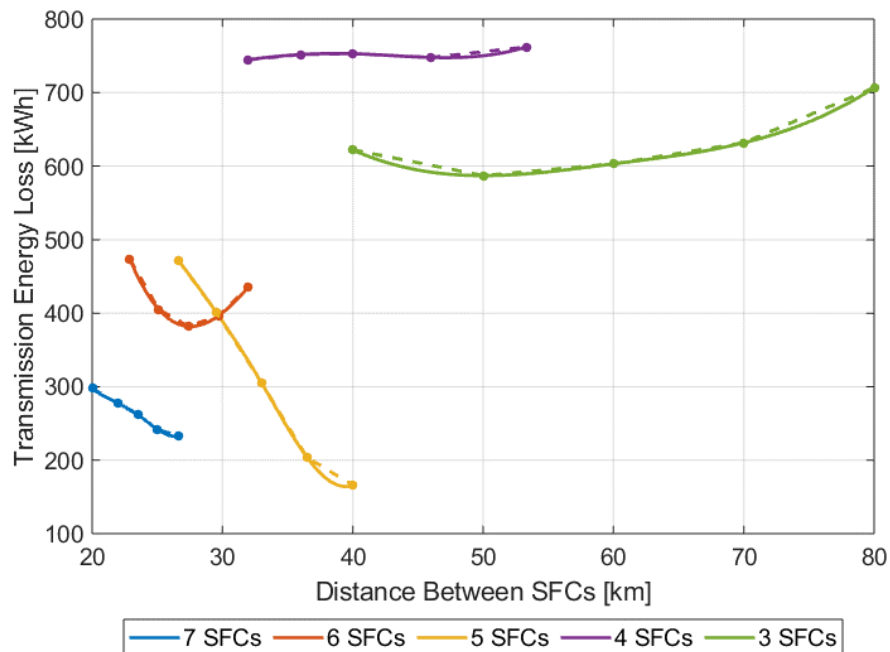


Figure 65 Total transmission energy loss for variable power loads using the synchronised control SFC system

With the train timetable being fixed and the arrangement and location of the SFCs changing, the number of trains within one SFC's feeding zone varies as well as the current they require when accelerating. When a train is accelerating, the current required is larger, which results in greater losses. The further

an accelerating train is from its feeding SFCs, the greater the impedance of the line and hence the transmission losses.

#### 6.4.2.2.2 VARIABLE POWER – EQUALLY SHARED ACTIVE AND REACTIVE POWER

Figure 66 shows the values of total transmission loss during the journey analysed using the method described in Section 4.5.1 and for the arrangements described in Section 6.2. The results have been drawn from simulations where the active and reactive power outputs from SFC feeder stations on the line are always equally shared, as per the smart control strategy.

In the figure, it is visible that, unlike in the synchronised case, in the case where active and reactive power is equally shared, the results follow an intuitive pattern. This makes the behaviour of the system more predictable.

The results corresponding to different arrangements of any number group of SFCs on the line follow a similar curve which has a minimum. This suggests that there is a balance point where the losses are at a minimum depending on the distance between the SFCs.

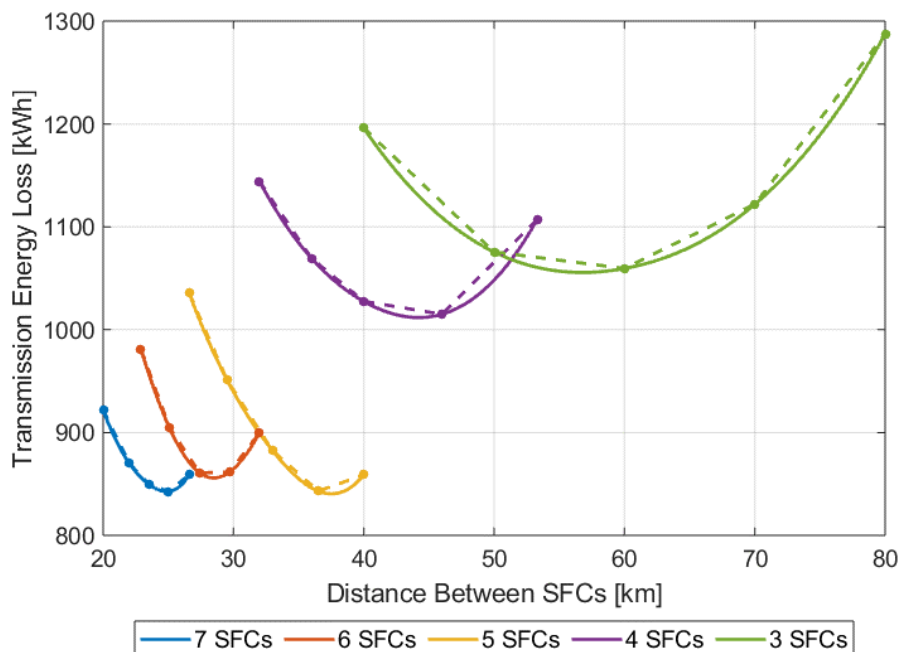


Figure 66 Total transmission energy loss for variable power loads using the equally shared control SFC system

6.4.2.2.3 VARIABLE POWER – COMPARISON OF SYNCHRONISED AND EQUALLY SHARED ACTIVE AND REACTIVE POWERS

Figure 67 presents the transmission losses for the combined simulation results for both control strategies in the case where the trains have a variable tractive load. As observed when considering the results individually, the synchronised control strategy produces unpredictable values with generally lower values. The figure also suggests that for a particular timetable of trains, it is possible to determine an optimum arrangement of SFCs where the transmission losses would be minimal. This strategy, however, would not necessarily work accurately in real life for SFC feeder stations operating synchronised control as the SFC feeder stations cannot necessarily be located in a particular desirable location along the line. However, with equal sharing of active and reactive powers, the effect of moving any one SFC does not give a significant loss of efficiency, retaining the majority of the benefits of this approach.

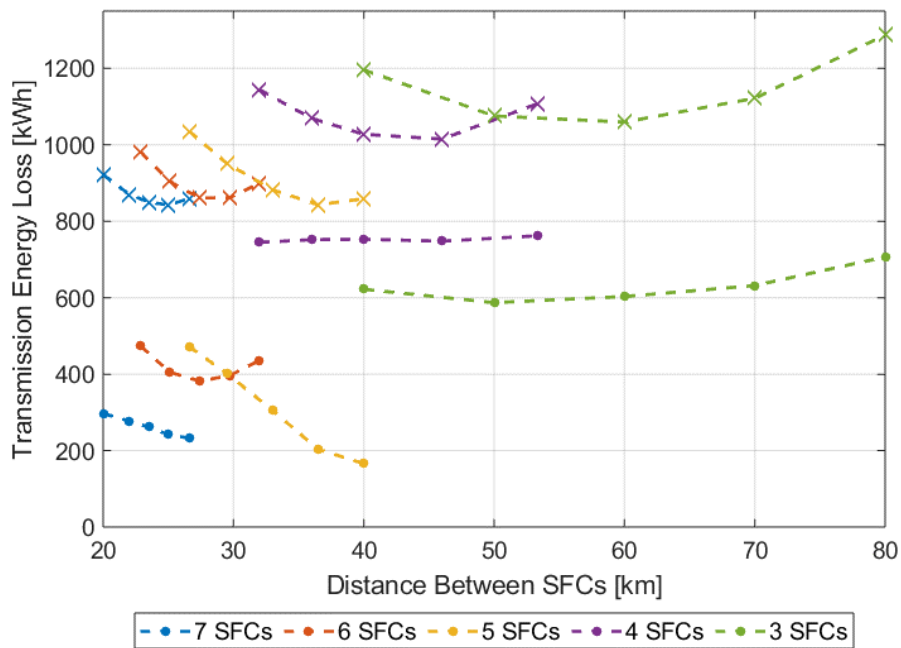


Figure 67 Total transmission energy loss for variable power loads using both SFC control strategies ('•' synchronised, 'x' equally shared)

### 6.4.3 SYSTEM EFFICIENCY

This section presents the comparative figures of the overall system efficiencies of both synchronised and equally shared active and reactive power control with different numbers and arrangements of SFCs, as previously described in Section 6.2. The details of the calculation of system efficiency are described in Section 4.5.2.

#### 6.4.3.1 CONSTANT POWER

Figure 68 shows the system efficiency for the case where all trains consume a constant power throughout their journeys as described in Section 0. The figure shows results for both synchronised and equally shared active and reactive power control. Comparing the respective arrangements between the synchronised and shared active and reactive power scenarios, in the best comparative case for the equally shared strategy, the system efficiency is equal to the respective synchronised case. The worst case for the equally shared strategy shows it to be 0.8% less than the corresponding system efficiency for the synchronised control strategy. Overall, the efficiency results for both control strategies under constant power loads are generally very similar.

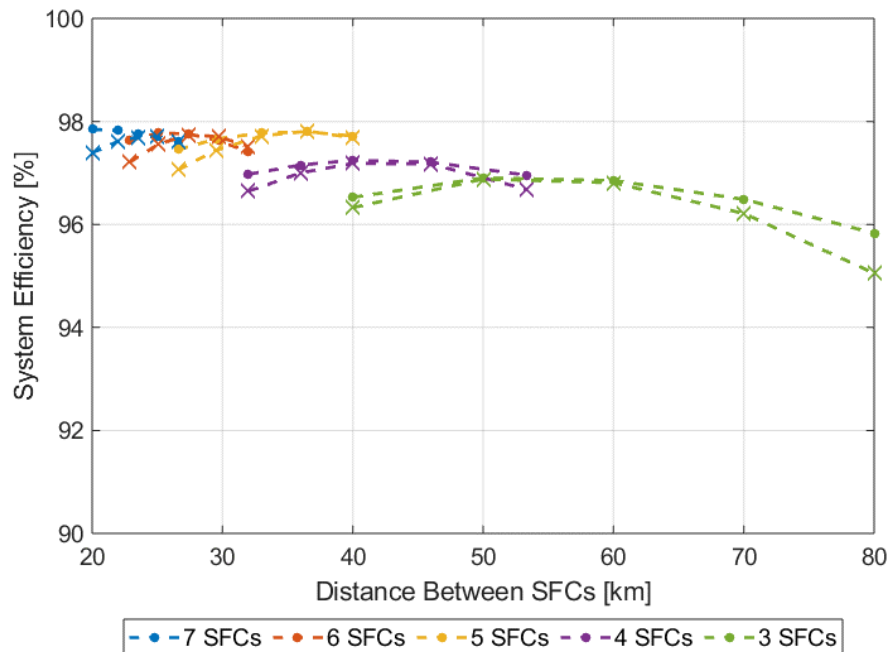


Figure 68 System efficiency for constant power loads using both SFC control strategies ('•' synchronised, 'x' equally shared)

### 6.4.3.2 VARIABLE POWER

Figure 69 shows the data points for the overall efficiency of the system for both cases of synchronised control and shared active and reactive power control. As previously explained in Section 4.5.2, the system efficiency is calculated taking into account both transmission losses and the internal losses of SFCs on the line. Consequently, the results presented in Figure 69 reflect the results from Figure 67 where the total energy loss in transmission with variable power for both synchronised control and shared active and reactive power is presented.

As shown in Figure 69, the system efficiency for all arrangements and SFC numbers for synchronised control systems is higher than the respective system efficiency for the equally shared active and reactive power control. Comparing the respective arrangements between the synchronised and shared active and reactive power scenarios, the shared power scenario is 0.68% to 2% less efficient than the corresponding synchronised case.

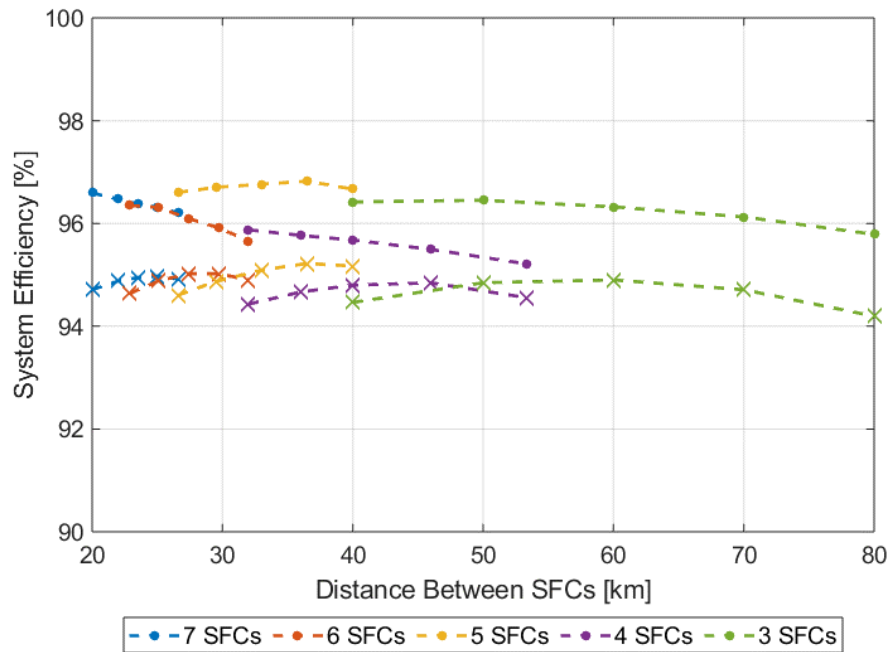


Figure 69 System efficiency for variable power loads using both SFC control strategies ('•' synchronised, '×' equally shared)

As both control scenarios are feeding the same level of load with the same arrangements of stations and SFCs on the line, it is possible to say that the overall energy input into the system is larger for the shared active and reactive power case compared with the synchronised case. This makes the shared active and

reactive power case less desirable in this respect; however, the increased losses may be compensated by a reduced maximum power rating requirement. This will be considered in an economic evaluation to be presented in Chapter 7.

## 6.5 CONCLUSIONS

This chapter considers the effect of the number and arrangement of the SFC feeder stations along the line specified in Chapters 3 and 4 on the maximum apparent power output of the feeder stations, the transmission losses incurred, and the overall efficiency of the system. Both the synchronised control and smart control (equally shared active and reactive powers) strategies have been considered. This chapter analysed these effects when the trains draw variable power (a real case), as well as when they draw constant power equal to 2.0974 MW, in order to minimise the effects of the timetable on the results.

The variable power case shows specific results for the timetable designed for this project; however, as a result of different load values during the journey for the trains, the analysis is heavily influenced by the location of acceleration and deceleration events with respect to the location of the feeder stations. It is not reliable to design a system based on specific timetables and station locations due to the ever-changing nature of timetables and specific stops; consequently, the constant load scenario helps to understand the overall behaviour of the system with these aspects minimised.

The results show that while for the synchronised case the behaviour of the system for the variable and constant power loads is considerably different and unpredictable, the SFC-based case with smart control has a predictable behaviour in both cases. The synchronised SFC case is the more efficient system overall and has a more efficient transmission of power in all comparative arrangements. However, the rated power required for each SFC feeder station is greater in this case than with the equally shared power control strategy.

The results presented in this chapter show that for each possible number of SFC feeder stations on the line, there is a distribution that maximises energy efficiency and minimises the rating required for the feeder stations. The effect is more pronounced in the constant power cases than in the variable power cases. The results suggest that there is a balance between additional infrastructure and savings in energy

caused by reductions in energy loss. The results are clustered in two groups, suggesting that for the line and timetable being considered five SFC feeder stations may be the optimum configuration as more units would incur additional costs without significant improvements in performance.

The design of the SFC feeder stations is done according to the apparent power rating required as discussed in Section 6.4.1. While the results presented in Section 6.4.1 show that there is a clear optimal arrangement of SFC feeder stations on the line to minimise the rated power (maximum apparent power) required, the equally shared power case provides a smaller variation of the maximum apparent power with respect to the SFC arrangements. Considering the limitations of the locations available to connect a feeder station onto the railway power supply network, this feature provides flexibility of arrangements with the least impact on the rating of SFC feeder stations. Additionally, the results suggest that the spacing of feeder stations is not as significant as the size of the end-sections when evaluating the optimum distribution of the feeder stations.

There are clearly then several factors that feature in the design process for a railway electrification strategy. These will be considered and discussed in detail in the following chapter.

# 7 ECONOMIC ANALYSIS

## 7.1 INTRODUCTION

When a potential new technology is to be introduced to the railway, its benefits should be measured against the cost it will incur. Putting a price on some benefits that may not have a specific monetary value is not straightforward. For the SFCs considered in this project, the benefits consist of the environmental improvements, flexibility, availability and the potential for advances in the future. This chapter provides cost data regarding the capital and operational costs to run both AT and SFC systems as well as insight into the potential benefits of SFC technologies in a rail application. As many of the benefits identified for SFCs are not directly monetarily calculable, this section of the chapter will be constrained to a discussion of the benefits.

Although every instance of arrangements and applications for these technologies is unique and would require a different approach, it is possible to draw an outline of steps to achieve a comprehensive analysis.

In this project, the economic evaluation is established for three technologies:

- 1- Conventional transformer-based network with ATs;
- 2- SFC-based network with synchronised control;
- 3- SFC-based network with smart control where the active and reactive powers are equally shared at all times.

To determine the whole life-cycle cost, the initial investment for the installation cost (Capital Expenditure (CAPEX)) is determined as well as the costs of running the system over its life cycle (Operating Expenses (OPEX)), including maintenance and energy costs.

Determination of CAPEX is relatively straightforward for the AT system case, with civils and installation costs being readily available and cabling and mechanical structures being commodity items on the railway. However, the cost of power electronics is currently undergoing significant fluctuation due to variations between exchange rates and supply issues. It is less straightforward for the SFC cases as SFC-based power systems for railway traction at 50 Hz are not currently widely commercialised and

hence there is no significant amount of data available. In this case, industry experts have been engaged to provide estimates for the cost, installation, and maintenance activities.

Calculation of OPEX costs, however, are more convoluted. Mid- to long-term costs of power cannot be predicted with any degree of certainty. Government policy on energy supply could provide either significant excess power capacity within the next 10–15 years, or conversely lead to power cuts, brownouts or rolling blackouts like those seen in Central and Southern American countries. The price of electricity used for the calculations in this project is 10.106 pence per kWh as specified in the ‘Notification of the overall EC4T tariffs applicable to charter operators in 2018/19’ published by Network Rail in March 2018 (Healy, 2018).

As described, the prices of electricity, power electronic equipment, and other factors influencing operational costs are prone to significant change and, consequently, there is a far greater margin of error in calculating OPEX than CAPEX. Due to these uncertainties, the timing of the installation is critical in determining OPEX costs. It is incredibly difficult to predict what the future will bring and while some scenarios can work for the SFC cases, some may work against them. For example, with the relevant power electronics becoming more mainstream and used in a greater number of applications on a daily basis, an oversupply of these components may result in the costs dropping for the overall system and for the spare parts. On the other hand, it is also possible that there will be another energy crisis, pushing the cost of energy up. This would work against the SFC cases as they have a lower overall system efficiency compared to AT systems.

In order to determine the cost of energy for the overall system over its life cycle, a key parameter to consider is the losses, as the load for each scenario is the same. Consequently, the parameter that would differentiate between costs is the amount of losses, which would add to the overall power transmitted and consequently the overall cost of energy. Measuring, comparing, and costing the usage of energy would reveal one of the most considerable differences in running costs between the three scenarios. The cost of electricity consequently has a big role in the comparative cost analysis between the different technologies investigated in this project.

This chapter focuses on an economic analysis of the AT system where there are transformer feeder stations on the line with ATs located every 10 km, the synchronised control SFC case and the shared active and reactive power control SFC case.

There are several measurable parameters as well as some differences between the AT system and the SFC systems which are next to impossible to measure and which would affect the analysis in this chapter. Chapter 7 provides an overview of the key economic aspects of each technology, and the differences between the various scenarios being considered.

## 7.2 EVALUATION OF BENEFITS

The economic analysis in this chapter aims to analyse and compare a conventional AT system with ATs located every 10 km on the line against the SFC cases with a conventional RR arrangement. There are significant differences between these two systems from both an infrastructure and an electrification point of view.

Considering a scenario where a single feeder station can feed a section of the line, it is possible to say that the AT system has the advantage of being able to accommodate a longer section due to the stability in the voltage provided by the ATs on the line. This, however, is overshadowed by the flexibility offered by SFC systems which enables them to use dual-end or mesh-feeding techniques and hence provide an opportunity to be spaced further apart. While the AT system still has the advantage of being capable of supporting a bigger section of the line compared with SFCs, it must be noted that SFCs use a simple RR system. In a case where the SFCs use a system with ATs on the line, they would be able to support a longer section than the AT system with transformers. Supplying a very large section of the line is, however, not desirable as, although it would reduce the costs because fewer feeder stations are needed, supply security would be reduced, and the transmission losses increased. Another great advantage of the AT system over SFC systems is the lower transmission losses and hence saving on energy costs.

The benefits associated with the use of SFC-based traction systems in comparison with the AT system are, however, numerous. These advantages save money on capital costs for the infrastructure required in the SFC cases:

- SFC systems do not require a very high-voltage connection to the grid. High-voltage connections have a significantly higher cost as well as limited availability in comparison with lower-voltage connections. For the AT system case, the transformers require 275 or 400 kV connections whereas the SFCs can be connected to voltages as low as 132 kV or even 33 kV. The difference in the connections required adds to the AT system's capital cost in comparison with that for SFCs (Ufert, 2016).
- As presented in Chapter 5, due to the dual-end and mesh-feeding capability of SFCs, even though the transmission losses are greater, the overall size of the feeder stations can be significantly smaller which saves on capital costs.
- SFC systems can run with a simple RR system and do not need ATs to be located every 10 km. This consequently eliminates the capital cost of ATs, the capital cost of housing the ATs and the capital cost of the AT connections onto the OLE system. It must also be noted that this saves the maintenance costs incurred by the existence of this equipment. The maintenance and refurbishment of power electronic devices used in SFCs are, however, an expensive maintenance requirement for SFCs (Behmann and Schütte, 2012a).
- As an SFC system does not require ATs, it also has no need for the Autotransformer Feeders (ATFs) required for a transformer-based AT system case. These feeders also require 25 kV clearances (Baxter, 2015) which add to the capital cost of the AT system.
- Due to the controllability of SFC feeder stations, there is no requirement for neutral sections. The neutral sections are located at every transformer feeder station as well as every midpoint. The capital cost and maintenance of the neutral sections can be saved with an SFC system.
- Due to the modular nature of SFC feeder stations and the lack of high-voltage connection requirements, the masts and structures required to build a transformer feeder station are not essential and hence less land is required for building an SFC feeder station than an equivalent transformer feeder station.

- Due to the elimination of power quality problems when using SFC systems, the capital costs of using special transformers, large filters, and other preventive and protective measures may be saved.

As well as measurable savings on capital costs, there are benefits associated with SFCs that are not easily measurable. The most important elements of designing a system fed by SFCs are the number and location of the SFCs. Studies similar to the case presented in Chapter 6 can be carried out to find the optimum number and location of the SFC feeder stations for different arrangements, loads and scenarios. While it is possible to carry out studies that would find optimised locations for transformer feeder stations, their location is more often than not imposed by the points where a high-voltage connection to the grid can be made. This makes any optimisation study for the location of transformer feeder stations unreliable. On the other hand, due to the possibility of lower-voltage connections for SFCs, there is a greater degree of flexibility in the places available where SFCs can be located and hence optimisation studies can have a vital role in finding the best solution for a specific railway line. As previously mentioned in the conclusion to Chapter 6, it is possible to improve the efficiency of a system by increasing the number of SFCs to some extent. A greater number of SFCs also means less distance between them and consequently better reliability of the system and smaller voltage drops. Increasing the number of SFC feeder stations, however, adds to the capital and maintenance costs and consequently, for every case, an optimised number of SFCs balancing the benefits and costs of the number of SFCs on the line must be determined. It also must be noted that due to the cost of construction of the foundation and housing of the feeder stations, reducing their size can have a limited effect on cost. This means that lower-rated SFCs do not necessarily reduce overall costs linearly.

It should also be noted that it is not enough to consider the distance between the SFCs in these cases. As demonstrated in Chapter 6, the effect of the end-of-the-line distances is not equal to that for the gap between the SFCs. Even with the same number of SFCs on the line, the specific location of the SFCs on the line would make a great difference (see Figure 66).

### 7.3 SCENARIOS CONSIDERED

In order to carry out a cost evaluation and provide grounds for comparison between different technologies and arrangements of feeder stations for this study, the results from Chapters 5 and 6 have been used. The numbers used in this section should be considered as indicative due to the difficulties imposed by project-specific dependencies of costs and lack of existing deployment of SFC technology on 50 Hz railways as explained earlier in Sections 7.1 and 7.2. The cost of SFC feeder-stations has been estimated based on the known costs for other SFC systems of different scales in the UK.

This study is carried out considering five cases.

- 1- An AT system with four transformers using the results from Chapter 5.
- 2- A synchronised control SFC arrangement with the closest equivalent structure to the AT system, with four SFCs on the line using the results from Chapter 5 (four feeder stations with 40 km between them).
- 3- An equally shared active and reactive power control SFC arrangement with the closest equivalent structure to the AT system, with four SFCs on the line using the results from Chapter 5 (four feeder stations with 40 km between them).
- 4- An optimum synchronised control SFC case using the results from Chapter 6 (five feeder stations with 36.5 km between them).
- 5- An optimum equally shared active and reactive power control SFC case using the results from Chapter 6 (five feeder stations with 36.5 km between them).

### 7.4 COST ANALYSIS

In order to achieve the cost analysis required for the economic evaluation, capital and operational costs have been compared for the scenarios mentioned in Section 7.3. Capital costs for the feeder stations and operational maintenance costs have been obtained through consultation with a number of leading experts from across the industry (Private Communications with Ross MacFarlane, 2019; Chris Wilson, 2019; Garry Keenor, 2019; Alan Hodge, n.d.). The Railway Industry Association's report on the Electrification Cost Challenge has also been considered for this study (RIA, 2019). Energy costs have

been obtained using the data output from the simulations carried out for Chapters 5 and 6. Table 13 presents the capital cost data for all scenarios.

Table 13 shows that although there would be four feeder stations for the SFCs where there would be two structures for the AT system, the effects of several elements result in the initial cost being lower in the SFC case than the AT case. This is partly because SFCs do not need neutral sections, ATFs, 400 kV connections to the grid, ATs or power quality control equipment. Additionally, they can be of lower capacity and require less land and fewer masts and structures (Behmann and Schütte, 2012a). This applies for both the four and five SFC feeder station cases.

The operational costs are the main drawback for SFCs in the cost comparison between the AT and SFC systems. It must be noted that the savings on capital cost have a bigger impact where a line is built from scratch.

To convert a transformer-based line to an SFC line, some elements that incur significant capital costs have already been implemented such as isolation sections, connections to high voltages and ATs. Consequently, upgrading an existing AT system to an SFC system does not have the financial benefits (compared to using an AT solution) of building an SFC line or electrifying a non-electrified railway using SFC feeder stations.

Table 14 shows the operational costs for all the scenarios being considered. The biggest operational cost is the cost of energy. Transformer-based systems with ATs provide a more efficient system which would save on the operational energy costs. However, it should be mentioned that power electronics technology and SFC feeder station equipment are constantly improving and, consequently, the efficiency of these feeder stations is on a path of constant improvement. At this point in time, however, the AT system is a more efficient system than the simple RR SFC system.

The case with smart control which shares the power equally between all feeder stations at all times is, as expected, the least efficient of all systems. This is due to the constant sharing of power and hence the greater distances travelled by currents from the feeder stations to the loads during transmission. It must,

however, be noted that this control system could be put in place in order to become operational in the event of fault scenarios, as analysed in Section 5.3, and the SFC system could operate using a synchronised control system in the majority of cases. Using smart control in fault scenarios provides system robustness helps to reduce the margins required to be implemented for SFC feeder stations. Other operational costs are the maintenance of the switchgear as well as the power electronics elements of the SFC feeder stations which require renewals more frequently than their AT-based transformer system equivalents.

Table 13 Capital costs for installation of AT and SFC systems

Description of Cost Element	Unit Cost [£k]					Total Cost [£k]				
	AT	SFC 4 × 40 km Synch'd  (15 MVA)	SFC 4 × 40 km Equally Shared  (10 MVA)	SFC 5 × 36.5 km Synch'd  (16 MVA)	SFC 5 × 36.5 km Equally Shared  (8 MVA)	AT	SFC 4 × 40 km Synch'd  (15 MVA)	SFC 4 × 40 km Equally Shared  (10 MVA)	SFC 5 × 36.5 km Synch'd  (16 MVA)	SFC 5 × 36.5 km Equally Shared  (8 MVA)
ATs (12 MVA)	175	-	-	-	-	2,100	-	-	-	-
AT Site and Construction, AT Connections and NSs	325	-	-	-	-	3,900	-	-	-	-
Cost of Feeder Stations Including 400 kV Connection for ATFs	25,000	-	-	-	-	100,000	-	-	-	-
Cost of SFCs Including 132 kV Connection for SFCs	-	12,500	11,500	13,000	11,000	-	50,000	46,000	65,000	55,000
Cost of Power Quality Compensation Equipment, Load Balancers and Filters	2,500	100	100	100	100	10,000	400	400	500	500
<b>Total Initial Cost [£k]</b>	<b>28,000</b>	<b>12,600</b>	<b>11,600</b>	<b>13,100</b>	<b>11,100</b>	<b>116,000</b>	<b>50,400</b>	<b>46,400</b>	<b>65,500</b>	<b>55,500</b>

Table 14 Operational costs for AT and SFC systems

Description of Cost Element	Total Cost [£/year]				
	AT	SFC 4 × 40 km Synch'd	SFC 4 × 40 km Equally Shared	SFC 5 × 36.5 km Synch'd	SFC 5 × 36.5 km Equally Shared
Inspection, Maintenance and Ongoing Refurbishment	100,000	550,000	550,000	687,500	687,500
Energy	7,173,560	7,562,227	7,662,104	7,362,666	7,595,030
<b>Total Operational Cost [£/year]</b>	<b>7,273,560</b>	<b>8,112,227</b>	<b>8,212,104</b>	<b>8,050,166</b>	<b>8,282,530</b>

The capital and operational costs calculated and presented in Table 13 and Table 14 show that the initial capital cost of the AT system is approximately £50 million more than the capital cost required to install the SFC system with four SFC feeder stations on the line. It is also worth noting that the smart sharing of power reduces the rating requirement of the SFC feeder stations and consequently the capital cost for the feeder stations; however, the capital cost of purchasing and installing feeder stations does not reduce linearly as the rating reduces, due to costs such as the construction works, project management and land costs.

The yearly operational costs include the maintenance and energy usage costs as well as a yearly allowance for refurbishment and replacement of faulty parts. As indicated in Table 14, the yearly running cost of the AT system is the lowest amongst all the scenarios investigated. Compared to the next cheapest SFC system alternative, the AT system presents a 10% saving in annual operational costs. This saving comes from both the energy consumption as predicted in Chapter 5 and also the maintenance and refurbishment costs. While all systems require an annual inspection, transformer systems require comparably little reactive maintenance as the core components are generally more robust and reliable as the technology is more mature than the comparably novel power electronics in SFC-based systems.

The data presented in Table 13 indicate that all SFC scenarios investigated have a lower capital cost than the equivalent AT system. Conversely, the data presented in Table 14 show that the AT system

runs on a lower annual operation cost in comparison with the SFC scenarios. In order to provide a meaningful comparison of the technologies, it is therefore necessary to consider both the initial and cumulative costs over the duration that the system would be used. As SFCs are a developing technology, there is no example in which an SFC system has run to decommissioning; however, AT-based systems commonly have an operating life of approximately 50 years and so this has been selected for use in the following analysis. It should be noted that SFC feeder stations are modular in nature and that an annual contribution towards refurbishment and replacement of core components has been included in the operating costs.

In order to achieve this analysis, the capital cost and cumulative operational costs have been calculated and summed over the 50-year period. Results are presented graphically in Figure 70 focusing on the initial, 5-, 10-, 20-, 30- and 50-year points. This analysis indicates that the cumulative operational costs exceed the capital cost in 16 years for the AT system while it takes between 6 and 9 years for the SFC-based systems depending on the precise scenario. Due to the higher capital cost of the specified AT system, it is possible to install and operate all of the equivalent SFC systems considered for 7 to 9 years before the cumulative operational and capital cost of the SFC system reaches the initial capital cost of the AT system.

The scenarios with five SFC feeder stations using both control strategies is initially more expensive than their four unit counterparts. The annual operating costs are reduced for energy; however, they are increased for inspection and maintenance due to the larger number of feeder stations involved. The variation in annual operating costs is therefore small and consequently the overall cost over 50 years for five-SFC feeder station cases is greater than that for four-SFC feeder station scenarios.

In the four-SFC feeder station scenario, the equal sharing of power approach allows the individual units to have lower ratings and thus the capital cost is reduced. Due to increased energy losses, however, the operational costs are fractionally higher. The equal sharing of power approach is therefore less expensive at first, but it is anticipated that the synchronised approach would ultimately be the cheaper solution. Considering the results of the analysis, for the specified scenarios with four SFC feeder stations, this

transition would not occur until year 41 of operation. The equivalent transition for the scenarios with five SFC feeder stations occurs in year 44.

Considering all of the results over the estimated 50-year operational life of the AT systems, the analysis shows that even with the greater annual operational costs, the total cost for deployment of the specified SFC-based scenarios does not exceed that of the AT system. This is primarily due to the significance of the difference in the initial capital cost. Extending the analysis beyond the estimated 50-year life of the AT-based system, the point at which the AT system's reduced operating costs make it the cheaper solution comes between 75 and 79 years for the four-SFC feeder station scenarios, and between 60 and 66 years for the five-SFC feeder station scenarios.

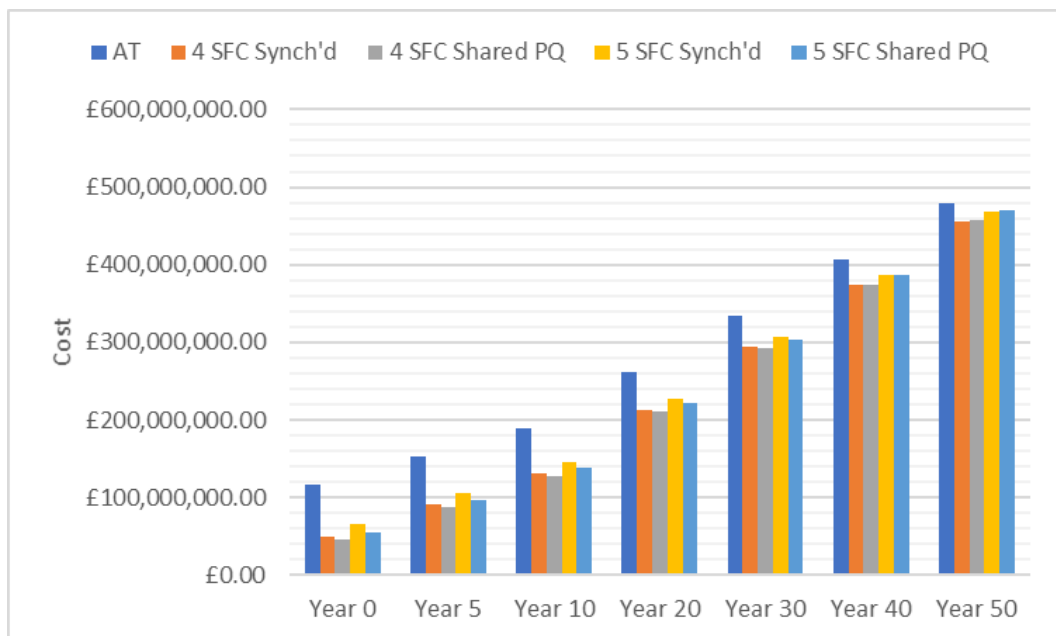


Figure 70 Capital and cumulative annual operation cost

This analysis has been carried out disregarding the depreciation of the value of the assets over time for immediate comparability. However, Section 7.5 presents the cost analysis study using the Discounting Technique.

## 7.5 COST ANALYSIS USING DISCOUNTING TECHNIQUE

This cost analysis, however, is not fully representative of the real life as it does not consider the reduction in the current value of expenditure (and income) in the future. In order to indicatively quantify this

effect, the 'Discounted Cash Flow' technique is used and presented in Figure 71 and Figure 72. According to "The Green Book" published by HM Treasury (HM Treasury, 2018), "Discounting is a technique used to compare costs and benefits occurring over different periods of time on a consistent basis. Discounting should be applied to all future costs and benefits. Discounting in appraisal of social value is based on the concept of time preference – that generally people prefer to receive goods and services now rather than later." In order to find the current value of the cost of different scenarios in this thesis, the Net Present Value for these scenarios has been calculated using the equation below (Jory et al., 2016):

$$NPV = \sum_{i=0}^n \frac{CF_i}{(1+r)^i}$$

Where NPV is the Net Present Value, n is the number of periods (in this case, years), CF is Cash Flow within the period and r is the Discount Rate.

The cash flow for year zero is the capital cost for each scenario and the cash flow from year one to year fifty is the operational cost in that year. The calculated NPV therefore represents the Net Present Value of the total cost of each scenario.

For long term analyses, 30 years and over, an change in the Discount Rate should be considered. HM Treasury suggests a current (2018) Discount Rate of 3.5% for the first thirty years followed by a Discount Rate of 3% for the later years (HM Treasury, 2018). For comparison purposes, a historic Discount Rate has also been considered. The historic Discount Rate is 7.5% for the first 30 years and 7% for the following 20 years.

Figure 71 and Figure 72 show the result of the cost analysis with consideration of current and historic Discount Rates respectively. These graphs show the cumulative Net Present Values of cost for each scenario for year zero (Capital cost), 5, 10, 20, 30, 40, and 50.

The use of the Discounting Technique shows that the real value of the cost of the projects are significantly lower for all scenarios than the calculated cumulative costs without consideration of Discount Rates.

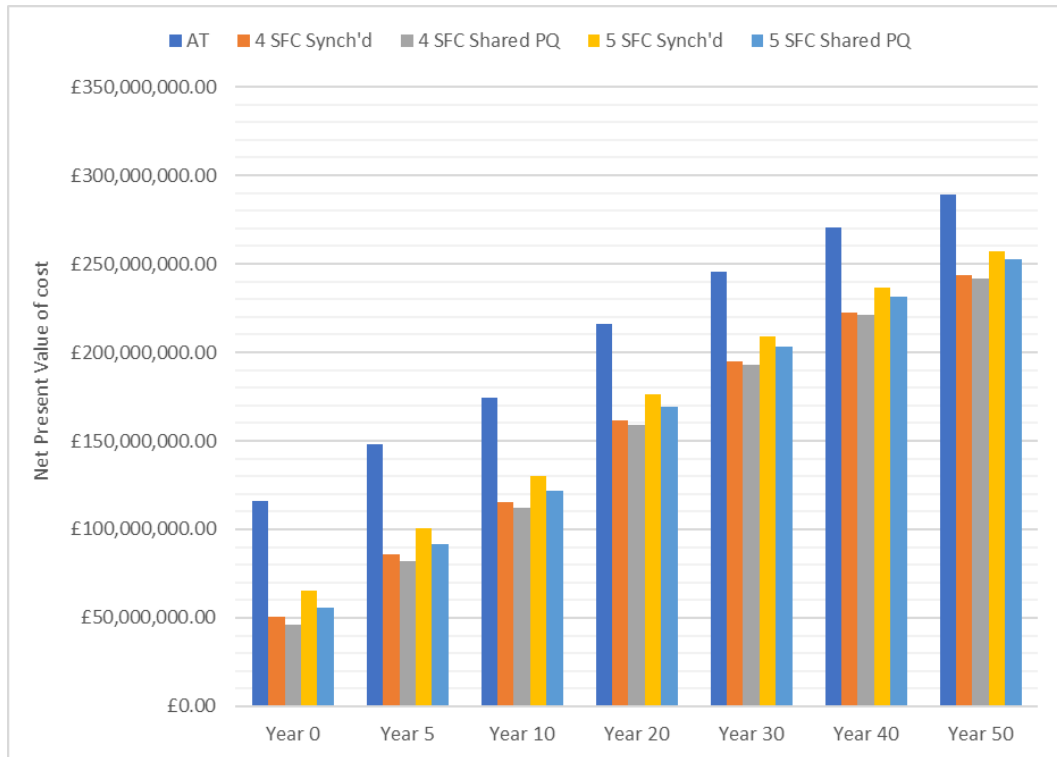


Figure 71 Capital and cumulative annual operation cost with current Discount Rates (3.5%)

The cost analysis with consideration of Discount Rates shows a larger gap between the cost of the AT based Scenario and the cost of the SFC based scenarios. The AT based scenario’s Net Present Value of cost is higher using the historic Discount Rates as it is a higher percentage.

The use of Discount Rates emphasises the greater effect of capital costs on the cost of each scenario and consequently favours the SFC based cases substantially. For the same reason, the scenarios with five SFC feeder stations on the line are less cost effective than the scenarios with four SFC feeder stations. In both cases, the SFC scenarios with smart equal sharing of active and reactive power are more cost effective than their respective synchronised control arrangements. The most cost-effective case is the scenario with four SFC feeder stations with equal sharing of active and reactive power. This is different from the result of the cost analysis presented in Section 7.4 which showed the cheapest scenario as the four SFC feeder-stations scenario with synchronised control.

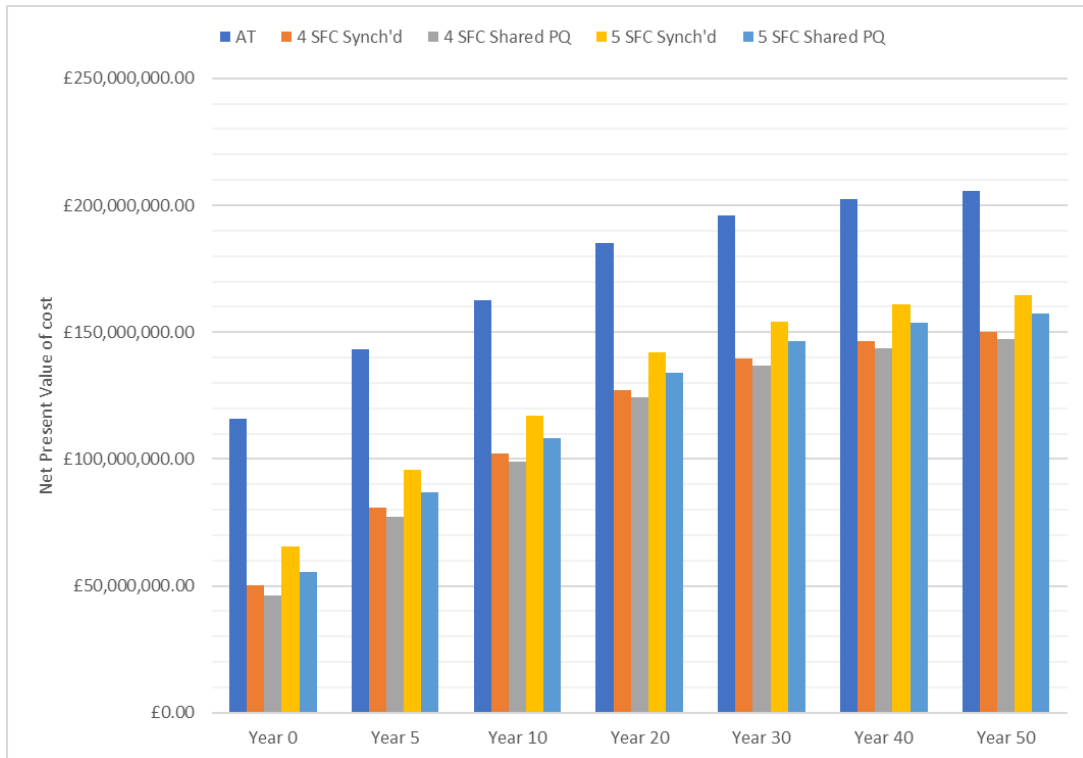


Figure 72 Capital and cumulative annual operation cost with historic Discount Rates (7.5%)

## 7.6 CONCLUSIONS

In this chapter, the capital and operational costs are compared amongst five different arrangements and control strategies as described in Section 7.4. This study considers the SFC feeder station arrangements most comparable with the AT system previously discussed in Chapter 5 and the most energy efficient arrangements as previously established in Chapter 6.

This chapter discusses the derivation of the capital and operational costs as well as considering non-monetary quantifiable benefits associated with the new SFC solutions, such as dual and mesh-feeding abilities due to the controllability and lack of neutral sections, adaptability, scalability and flexibility of connections to the national power grid.

The chapter goes on to consider the cumulative capital and operations costs, allowing evaluation both of the SFC technologies against conventional AT systems, and internal comparisons between different SFC deployments.

This chapter has confirmed previous assumptions around the balance of capital and operational costs between AT- and SFC-based systems and indicates that over a 50-year operational life the capital costs of the AT system would still result in a more expensive solution than one featuring SFCs despite the lower operational costs. The calculations of the Net Present Value of the cost for each scenario, presented in Section 7.5, a more realistic view of the cost of each scenario and further emphasises the effect of capital cost on the total cost of each scenario, which works in favour of the SFC scenarios.

Technology is moving all the time and while AT systems have been improved and investigated over many decades, SFCs are still a developing technology. This makes the judgement between these cases particularly challenging. The price of power electronics is predicted to fall, and the efficiency of the systems is predicted to increase as the technology of the power electronics used to build SFCs and the structural topologies improve. The cost of energy has a great impact on the results presented in this study. As discussed, future energy prices are unknown and could be volatile, and any changes would have a significant impact on the overall operational cost comparisons between these systems. SFCs offer benefits that are not measurable financially, such as flexibility in feeding arrangements, but which would have huge impacts on the possibility of improving, expanding and utilising the railway lines to their best during their long lifetimes. Their use may also support a more robust and reliable railway which is becoming increasingly important.

This chapter has made certain assumptions about the development of supporting technologies which will have an impact on the costs and suitability of deploying SFCs going forward. The following chapter will consider some of the factors affecting the wider environment as well as potential innovative solutions to enable development of the SFC technology and the formation of a railway smart grid. Such a solution would provide a power system capable of accepting multiple sources of energy including renewables and benefiting from energy storage systems.

# 8 RAILWAY SMART GRID TECHNOLOGY ROADMAP

## 8.1 INTRODUCTION

Since the introduction of ATs to the rail network, there has been relatively little in the way of innovation of the methods of transmitting and utilising power across the network. Many incremental improvements have been made, but for the railway to continue to grow and serve the wider economy, it must be prepared to undertake a more systematic update of its power distribution infrastructure.

SFCs are ideally placed, with their simple, modular design and precise controllability, to begin to replace legacy transformer-based systems and provide significant benefits in terms of both flexibility and load balancing across the grid.

Moving forward, there are a number of potential improvements which could be made to the power generation and distribution grid for the railway which would allow the adoption of a railway smart grid by 2050.

A railway smart grid would be one in which the production, distribution and regeneration of power can be controlled to a level which allows the grid to work more efficiently as a mesh network than as a hub-and-spoke network, giving greater reliability and ensuring that the least power possible is wasted.

With the current use of transformer feeder stations, it is not possible to have a fully interconnected network, due to the requirements of neutral sections and issues regarding the power quality and load imbalance on the system, as discussed extensively in Chapter 2. Therefore, utilising greater numbers of SFCs in place of transformers for feeder stations will allow further interconnection of the existing islands of power, leading to the potential for having an optimised route with regards to power distribution.

Care must be taken to ensure that the adoption of new technology in the rail network does not produce areas in which there is incompatibility between the existing technology and the newly installed technology. Of paramount importance is the smooth functioning of the network, and so it is vital that the overall system is considered when technologies of different capabilities and maturity levels are introduced. Additional integration testing can be performed where necessary to ensure the existing capabilities are maintained.

The global focus is currently around the reduction of energy losses and increase in clean energy usage, with an eye to the eventual decarbonisation of the transportation network. Railway travel, while already being one of the most efficient method of transportation (European Commission, 2017a), needs to do its part to help achieve these goals, and make use of these technologies to create a fully modernised smart grid which will make a considerable step towards decarbonisation of the railways and the most efficient use of the energy generated.

A roadmap is presented in Figure 73 which describes the potential development of the railway power network based on SFCs being introduced into the system. This roadmap considers the ultimate goal of having a railway smart grid as a step towards decarbonisation of the railway. The figure shows how the smart grid would incorporate multiple energy sources and storage systems connected into the railways' power system. A railway smart grid has never before been an option for AC railways due to the lack of controllability for transformer feeder stations and the requirement for isolation sections which breaks the systems' continuity.

The roadmap is divided into four swim-lanes each focused on a technology theme identified as core to the development of the railway smart grid. The adoption of the smart grid itself appears as the vertical integrating elements occurring on a fifteen-year time-horizon. The four technology themes are:

- Power electronics – which underpins the SFC technology and developments in which will have knock-on effects on SFC performance;
- Static Frequency Converters – both in terms of their development and application where demonstrated systems will facilitate improved adoption of the technology;
- Renewable Energy – which represents the increasing development and adoption of renewable power sources;
- Energy Storage – which includes developments both on the vehicle and lineside and which is essential for the energy redistribution at the core of the railway smart grid.

Each swim-lane will be considered in depth later in this chapter.

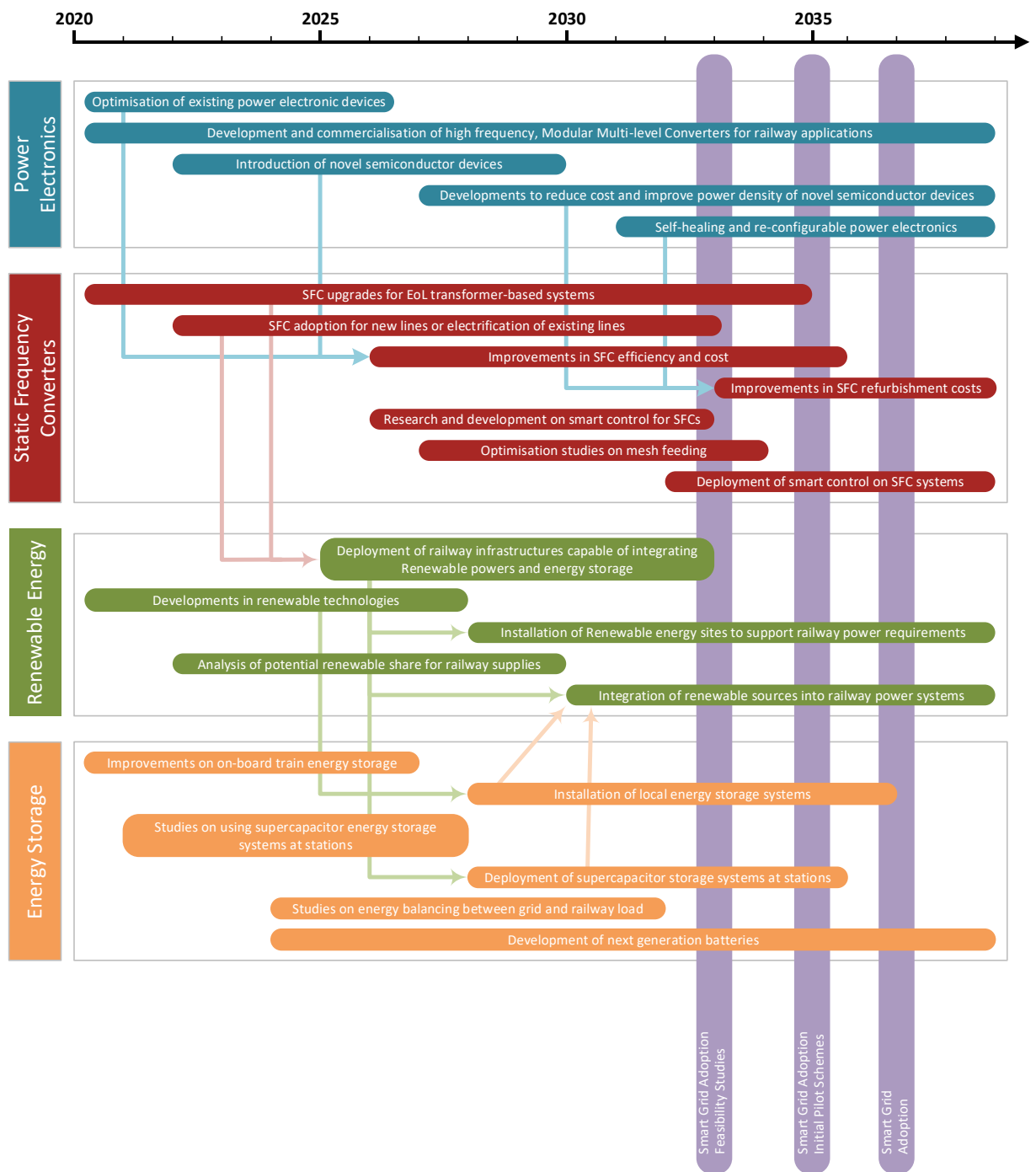


Figure 73 Potential roadmap for the adoption of a railway smart grid

## 8.2 POWER ELECTRONICS

SFC feeder stations are converters built using power electronic devices as described in Section 2.2.2.

The use of power electronic devices for high-power density converters is a new and immature technology and consequently developments and advances made in the coming years will have a great impact on the efficiency and cost of these systems.

Currently, improvements in the state-of-the-art IGBT/MOSFET material and designs can result in performance improvements and a reduction in the cost and size of the feeder stations. Introduction of new materials, such as Silicon Carbide and Gallium nitride (Advanced Propulsion Centre UK (APCUK), 2017), and new methods into power electronic manufacturing and design will improve the endurance of power electronic devices against temperature rises and increase the reliability of their use. By increasing the scale of use of these new power electronic devices, the cost will naturally go down and make the use of modern power electronic devices increasingly feasible.

While the devices used in SFC feeder stations are of significance, innovation in the architectural design of these converters has a considerable role in improving the use of available devices. Soft-switching technology for high-frequency applications (Heuvelmans et al., 2014), adaptive power inverters alongside higher frequency PWM (Xia and Ayyanar, 2018), resonant converters (Bhuvaneshwari and Babu, 2016) and multi-level converters (Gruber and O'Brien, 2014) are amongst the innovations which will maximise the potential of power electronic converter devices.

One of the biggest concerns with the use of power electronic converters is the cost of refurbishment and the limited repairability of the devices; however, a new material created by an international team has proven to be able to function automatically after multiple hardware failure / reset incidents. This will greatly improve the durability of power electronic devices which will result in a reduction in refurbishment and operational costs (Tan et al., 2018).

## 8.3 SFCs

Over the next 15 years, as more transformer feeder stations begin to reach the end of their life, it is anticipated that the vast majority will be replaced by SFCs. This will give an initial capital saving over

replacement with AT systems, although they are more expensive to run due to higher operations costs as previously discussed in Chapter 7. The higher operational costs for SFC-based systems are mainly due to the technology being less mature in comparison with AT systems; however, this is expected to change by the mid-2020s as the underlying power electronics improve, and more SFC systems are commissioned and economies of scale will reduce the capital and refurbishment costs of SFC feeder stations.

On top of this, as improvements are made to all aspects of power electronic devices and SFCs adopt the use of power electronics and microprocessor control and benefit from innovative designs and solutions, rapid advances will be made fuelled by both consumer and industrial needs in other sectors. This should allow generally improved functionality, rapid decreases in power loss, increases in efficiency, and the ability to control the outputs of the system more precisely.

Consequently, if a new line is about to be built, or an existing line updated it should be possible to relatively easily develop a business case to install SFCs in place of transformer feeder stations. This would be based on their significantly lower capital costs (as indicated in Chapter 7). Additionally, in a scenario where there is a failure of an existing transformer feeder station, it may be beneficial for it to be replaced with an SFC, rather than another transformer feeder station. This would prevent the requirement of replacing a transformer-based feeder station before the end of its life in the future should the rest of the line be updated. Although the SFC in this case may not work with maximum efficiency, it would be able to provide the required power in place of the failed transformer feeder station and have the potential to be integrated into a full SFC scheme in the future.

The next stage of grid control facilitating the use of a smart grid is the development of smart control for SFCs as discussed and investigated extensively in this PhD. Smart control will allow dynamic load sharing across feeder stations, to better balance the power drawn from the feeder stations at any given time. This PhD thesis has proved through mathematical modelling and simulation that this concept is achievable. Such an approach will reduce the required size of the SFC feeder stations as well as enabling

optimised solutions for fault scenarios and facilitation of integration of other types of power into the system.

#### 8.4 RENEWABLE ENERGY

With the ever-increasing customer demand, whether imposed by governments to reach carbon emission targets (DECC, 2016) or by individuals as the awareness of climate change increases, improvements in the technologies, innovative ideas and further collaboration in the renewables industry are making significant advances. These advances pave the way for significant cost competitiveness which enables a phase of growth in this industry. With renewable power becoming more readily available and more cost-effective to use, and the railway industry developing an infrastructure which can accept the integration of renewable energy into the system, new doors will open in consumer markets and innovative design developments.

Replacement of conventional transformer-based power systems for railways by SFC feeder stations will create an infrastructure which is capable of using multiple power sources and storage units to provide the power required for the railways. With more stringent decarbonisation targets set by the governments around the world (United Nations, 2015) and the future availability of modular and extensible infrastructure, it is crucial to consider and plan for the integration of sources of clean energy into railway power systems (Pilo De La Fuente et al., 2014).

The railways, usually one of the largest load entities on national grids (European Commission, 2017b), are an obvious target to move to using sustainable energies, and there is huge potential for improving the carbon footprint of this system. With the railways going over long distances and mostly through land, which is not densely populated, it is possible to install renewable energy harvesting alongside the railways. Having the renewable resources nearby improves the efficiency of transmission greatly. Extensive studies will have to be carried out in order to find appropriate resources available for harvesting and the locations they can be installed at as well as to estimate the potential contribution renewable energy can have and consequently the potential carbon footprint improvements it can make.

The unpredictability of the output power produced by these renewable sources, however, requires an adaptive system which can take advantage of these resources when available but provide the energy required by other means when they recede (Muttalib et al., 2012). Extensive research and analysis should be carried out to understand these uncertainties and design potential solutions. Energy storage devices can play a significant role in stabilising a multi-resource power system. This can be done by implementing a smart grid where multiple sources are interconnected and intelligently controlled to keep the railways operating in the most efficient way (Nikhil et al., 2015).

## 8.5 ENERGY STORAGE

According to published energy storage roadmaps (Automotive Council and the Advanced Propulsion Centre, 2017), significant improvements in power density, efficiency, and the cost of batteries are due in the next decade. Energy storage devices have played a significant role in the application of renewable energy and implementation of smart grids in the past decade. In the railway industry, on-board energy storage systems have been implemented in both AC and DC railways to utilise the recovered braking energy. In order to provide solutions for running trains through sections of discontinuous electrification, hydrogen fuel cells and batteries are the most commonly used on-board energy storage technologies.

On-board energy storage is limited by space and the added weight which results in inefficiency (Gao et al., 2019). Consequently, local (lineside) energy storage units supported by renewable resources can be an efficient and maintainable addition to a railway power system (Pilo De La Fuente et al., 2014). This solution could potentially provide a regulated and reliable source; however, it requires extensive research and analysis.

As previously discussed in Chapters 5 and 6 of this PhD thesis, the greatest requirement for power, and consequently a great percentage of losses, happens at the station locations due to the trains accelerating. Feeder stations are designed with larger ratings to address the surges in load when trains accelerate. It may, therefore, be possible to use supercapacitors to provide the support required at stations where trains require maximum power to accelerate. According to a study conducted by RSSB (Rail Safety and Standards Board (RSSB), 2009; Rail Safety and Standards Board (RSSB), 2010), they are generally more

robust, have a longer life and can operate with frequent discharging at substantial discharge rates which would make them an ideal solution for this issue. Consequently, due to the fast discharge requirements and the frequent use, installation of supercapacitor energy storage systems could greatly help the optimisation of the railway power network.

With studies identifying optimisation scenarios considering a balance between the railway load and the feeder station supplies connected to the grid, it is possible to identify locations where energy storage units would be best placed in order to add a smart and reliable energy storage mechanism to the railway power network and provide another step towards achieving a smart grid solution.

## 8.6 SMART GRID

Significant changes should be applied to the current railway electrification network in order to make the existing system sustainable and work towards decarbonisation goals. However, decarbonisation is not the only benefit of having a railway smart grid; a more reliable power system, reduced cost, increased consumer satisfaction and an increase in the adaptability of the system are other benefits associated with their implementation (Steele et al., 2019).

While other industries have rapidly moved towards smart grid technologies, the nature of the railway infrastructure and operation has limited this industry from moving quickly towards this common goal. As transformer feeder stations require an isolation section, the idea of a mesh network of multiple energy sources has not been easily implementable; however, with the introduction of SFC feeder stations into the railway infrastructure and their ability to eliminate isolation sections, a railway smart grid is now becoming a possibility.

In order to implement a railway smart grid efficiently, several elements should come together. Firstly, the transformer-based infrastructure is to be replaced by SFC-based infrastructure. Secondly, in order to utilise these networks most efficiently, extensive studies should be carried out to explore the capabilities and needs of the railway power network, as well as potential locations for different renewable resources and the optimised locations of the energy storage units. Finally, according to the optimisation studies

and analysis carried out, the resources and power units identified should be installed and integrated into the railway system (Advanced Propulsion Centre UK (APCUK), 2017).

## 8.7 CONCLUSIONS

This chapter presents a roadmap outlining one possible set of steps that need to be taken in order to improve and modernise the railway power network. The use of SFC feeder stations and the consequent elimination of isolation sections provides an essential foundation to implement a smart grid for railways, utilising multiple power sources and storage systems to provide a more reliable, efficient and cost-beneficial railway system.

In order for a railway smart grid to be realised by 2040, supporting multiple countries which have committed to 2050 decarbonisation targets, a number of key milestones have been identified. A range of technology areas, including the SFC-based power systems considered in this thesis, have been discussed. Early-stage milestones, such as the use of current SFC technology in refurbishment and newly commissioned railway electrification, are already being met in schemes such as those at Potteric Carr in the UK and Queensland, Australia. The next developments required are in the areas of the underlying power electronics, which will reduce cost and increase reliability, and in the control strategies such as those considered in this PhD thesis.

# 9 CONCLUSION

The writer of his PhD thesis has considered the hypothesis that the use and configuration of SFC feeder stations on a railway line, and the associated control strategy, can reduce the overall cost of railway electrification and operation, and provide additional benefits around operational robustness and flexibility.

Following a thorough literature review which considered the different methods of railway electrification, the infrastructure elements for a number of different approaches, including SFC implementation and operation, and the comparison of SFC-based infrastructure with the state-of-the-art transformer-based infrastructure, the hypothesis was explored across six technical chapters.

In order to address the hypothesis, several elements of applying SFCs in the railway network were considered. Firstly, SFCs were considered in direct comparison with existing AT systems. A novel and intelligent control system for the management of power sharing in a multi-SFC network enabling mesh feeding was then developed and compared to AT and conventional SFC systems. Secondly, to understand how SFC systems can be most effectively deployed in the real world, a unique analysis of the effect of the number and arrangement of SFCs along the line was undertaken. Finally, bringing together the results and data from both analyses and a panel of industrial experts, an economic analysis for deployment of SFCs using the conventional and novel control strategies was undertaken, and a comparison against the cost of deploying AT systems was carried out. As a developing technology which has fundamental differences to the existing railway power network, SFCs have benefits which are overlooked in a purely cost-oriented analysis. Consequently, a technology roadmap was developed to identify the potential role of deploying SFCs in the future of railway electrification.

In order to undertake the main technical evaluations described within this PhD thesis, a number of novel mathematical models and computational simulations were developed and described in Chapters 3 and 4, respectively. The computational models were used to represent: (i) an AT electrification network, (ii) an SFC-based electrification network with a conventional control strategy, and (iii) an SFC-based electrification network with a novel control strategy enabling mesh feeding. In Chapter 3, the potential for equal sharing of power amongst multiple SFC feeder stations on a railway line, using the phase angle

and magnitude of output voltage, has been mathematically demonstrated for the first time. This chapter also demonstrated a method for the implementation of such a control strategy in an SFC system.

The computational simulation described in Chapter 4 is an implementation of the work described in Chapter 3 combined with a real-world scenario. It facilitates technical investigations to support evaluation of the overall hypothesis. The real-world scenario includes the length of the line, number and location of train stations, a timetable and the number of trains required to implement it, a realistic train power profile, and the arrangement of feeder stations on the line. These elements together allow a realistic theoretical analysis of the different power network infrastructures and their comparison. The simulations developed in Chapter 4 allow the evaluation and comparison of the electrical performance of AT and SFC systems (Chapter 5), performance evaluation of different numbers and arrangements of feeder stations (Chapter 6), and an economic analysis of SFC deployment (Chapter 7), which are required in order to evaluate the hypothesis. The model developed in Chapter 4 is also demonstrated using single-train scenarios in order to showcase different infrastructure and control strategies in an easy-to-interpret format.

In Chapter 5, the model developed in Chapters 3 and 4 is used to compare the electrical performance of AT and SFC (synchronised control and equally shared power control) systems. Consideration is given to normal operating conditions as well as a fault scenario. The key findings of this investigation are:

- The AT system is the most efficient system; however, it requires the largest-rated feeder stations amongst the three cases;
- The SFC case with the equal sharing of power control strategy requires the lowest-rated feeder stations; however, it is the least efficient of the three cases;
- The SFC cases cope with the fault scenario with a smaller required feeder stations capacity margin;
- Despite the elimination of ATs in cases where SFC feeder stations are used, voltages are always retained within the limits prescribed by the standards.

The simulations undertaken as part of the investigations described in Chapter 5 are primarily to identify the energy efficiency and rated power required for the feeder stations used in different scenarios, but also therefore provide overall energy usage and feeder station capacity values for those scenarios. These data are used to calculate the cost of energy (as part of operational costs) and of infrastructure (as part of capital costs) in the economic evaluation presented in Chapter 7.

As the work presented in Chapter 5 is a comparative study, the infrastructure used in the simulations is based on existing AT system configurations. The work presented in Chapter 6 removes this limitation and considers the effect of the number and arrangement of feeder stations along the route specified in Chapter 4. Five spacings are considered for each number of feeder stations, ranging from an equal distribution with feeder stations positioned at the ends of the line, to an equal distribution where the first and last feeder stations are as far from the ends of the line as from the next feeder station. Each arrangement is considered for both synchronised and equal sharing of power, constant and variable train power demand, and from the perspective of apparent power rating required for feeder stations, transmission losses incurred, and the overall system efficiency. The data obtained through this analysis were plotted to understand the behaviour of the systems with respect to the number and arrangement of feeder stations on the line. The key findings from this chapter are:

- For each possible number of SFC feeder stations on the line, there is a distribution that maximises energy efficiency and minimises the rating required for the feeder stations;
- For the example line and operational regime used throughout this thesis, there is a non-linearity in the efficiency / number of SFCs relationship which means that five SFCs may be an optimum configuration;
- The SFC case with the new equal sharing of power control strategy requires the smallest-rated feeder stations;
- The SFC case with synchronised control strategy results in the most efficient transmission of power;

- The SFC case with the new equal sharing of power control strategy results in more predictable and less variable system behaviour;
- The overall performance of the system is highly dependent on the location of accelerations and decelerations (e.g., around stations) with respect to the location of the feeder stations. This effect is minimised through the use of the new equal sharing of power control strategy.

The results from this chapter informed the selection of scenarios considered in the economic evaluation undertaken in Chapter 7. In addition to a directly comparable replacement of an AT system with SFCs, the numerical results from the most favourable arrangement of SFCs (i.e., five feeder stations spaced 36.5 km apart) are used in operation and capital cost calculations.

Building on the technical results obtained in Chapters 5 and 6, Chapter 7 presents an economic evaluation comparing existing AT systems with SFC-based alternatives, using both the synchronised and novel control strategies. Although heavily dependent on specific deployment, indicative costs have been identified using the simulation results and input from experts in industry. Both capital and annual operational costs have been considered, and hence long-term cost estimations have been established.

The key findings of the economic evaluation are:

- The capital cost to procure and install SFC systems with the equally shared power control strategy is less than for SFCs with synchronised control, and both are significantly cheaper than the AT system;
- The annual operational cost of the AT system is less than that of an SFC system with synchronised control, which in turn is marginally cheaper than that of an SFC system with equally shared power control;
- The total combined capital and operational cost results indicate that the SFC systems are cheaper overall over the predicted 50-year life of the AT system;
- The increased maintenance requirements mean that the reduction in energy costs obtained through increasing the number of SFCs on a line from four to five makes little difference to the overall operational costs. However, this does provide increased operational flexibility.

- Considering the Discount Rates for the cost analysis, the use of SFCs with equally shared active and reactive power control provides a more cost-effective solution than both an equivalent AT based system and an SFC based system with synchronised control.

Although the costs have been identified, it is thought that SFCs will provide benefits which are not yet quantifiable due to a lack of mature application of the technology to 50 Hz railways. Additionally, it is anticipated that forthcoming advances in the technology and its support technologies will significantly alter the efficacy and cost of SFC-based systems.

While Chapters 3 to 7 consider the technical and financial feasibility of implementing SFC-based systems, they do not consider how such systems would fit into the wider railway and national power networks. Chapter 8 presents timelines for the development and adoption of key technologies in order to support a railway smart grid. Among these, SFCs will play a critical role in providing the required infrastructure capable of hosting multiple power inputs into the railway system. The flexibility of the SFC-based solutions enables integration of multiple power sources, including renewables and energy storage solutions, which will reduce the cost of operating the railway.

The writer of this PhD thesis had set out to investigate the feasibility and potential benefits of deploying SFC-based systems in a 50 Hz railway power network. Through a range of mathematical models and computational simulations, it has been shown that SFCs can indeed be deployed in this application, and that different benefits can be obtained depending on the SFC control strategy used. The author has considered both the conventional synchronised control and a novel control strategy based on equal sharing of active and reactive power amongst all SFCs on the line.

The results from the computational model show that the individual SFCs in a network using the equally shared power control strategy can be of a smaller rating (lower capital cost) and provide greater reliability and fault tolerance throughout the network. However, due to the increased transmission losses associated with power being supplied over longer distances, such systems are less energy-efficient (higher operational costs). The simulations have also shown that it is possible to make extensive energy and equipment cost savings through careful design of the deployment of SFCs onto a given line or for a

given operational regime. Results indicate that the power profile of SFC networks with equally shared active and reactive power control strategies are less influenced by variations in the timetable and the location of acceleration and deceleration points throughout the network. Such systems are therefore more tolerant to the precise installation location for the individual SFC feeder stations which may be of significant benefit in deployment planning.

Although SFC technology is evolving rapidly and limited examples of its deployment in 50 Hz railway environments exist, an economic evaluation exercise has shown that the dramatically reduced capital costs of SFC deployment easily outweigh the increased energy, maintenance and refurbishment costs in comparison with AT systems. The analysis identifies areas such as the increased flexibility and controllability of SFC deployment which may also provide additional benefits but cannot yet be monetarily quantified. A wider technology deployment evaluation and road mapping exercise has shown how SFCs are an integral part of the proposed railway smart grid architecture, and how improvements in SFC technology will support the rail industry's wider goals of reducing costs and supporting decarbonisation.

# 10 REFERENCES

ABB (2017) Static frequency converter supports 50 Hz rail network Advanced power conversion keeps Queensland Rail 's network on track ABB is upgrading the feeder station at Wulkuraka in Australia as part of a program to strengthen the rail power. *Application Note*.

ABB Traction (2018) Traction systems for locomotives and high speed applications.

Abrahamsson, L., Schütte, T. and Östlund, S. (2012) Use of converters for feeding of AC railways for all frequencies. *Energy for Sustainable Development*, 16 (3): 368–378. doi:10.1016/j.esd.2012.05.003.

Abusara, M.A., Sharkh, S.M. and Guerrero, J.M. (2015) Improved droop control strategy for grid-connected inverters. *Sustainable Energy, Grids and Networks*, 1: 10–19. doi:10.1016/j.segan.2014.10.002.

Advanced Propulsion Centre UK (APCUK) (2017) *Power Electronics Roadmap*. Available at: <https://www.apcuk.co.uk/technology-roadmaps/>.

Aeberhard, M., Courtois, C. and Ladoux, P. (2010) Railway traction power supply from the state of the art to future trends. *SPEEDAM 2010 - International Symposium on Power Electronics, Electrical Drives, Automation and Motion*, pp. 1350–1355. doi:10.1109/SPEEDAM.2010.5542093.

Agarwal, A. and Lang, J.H. (2005) *Foundation of Analog and Digital Electronic Circuits*. Burlington: Morgan Kaufmann.

Alvarez-Alvarado, M.S., Khan, Z.A., Vaca-Urbano, F., et al. (2018) Grounding points model for power flow applied to an autotransformer configuration railway. *2018 International Conference on Electrical Engineering, ICEE 2018*, pp. 1–6. doi:10.1109/ICEE.2018.8566799.

Automotive Council and the Advanced Propulsion Centre (2017) *Technology Roadmap 2017: Electrical Energy Storage*.

Banceanu, C., Aubert, S., Converters, S.F., et al. (2015) STATIC FREQUENCY CONVERTERS – A FLEXIBLE AND COST EFFICIENT METHOD TO SUPPLY SINGLE PHASE RAILWAY GRIDS.

- Barnes, R. and Wong, K.T. (1992) Unbalance and harmonic studies for the Channel Tunnel railway system. *IEE Proceedings B: Electric Power Applications*, 139 (4): 419–420. doi:10.1049/ip-b.1992.0051.
- Baxter, A. (2015) A Guide to Overhead Electrification. Network Rail.
- Behmann, U. (2013) Advantages of low frequencies in converter-supplied railway traction power systems. *Rail Technology Review*, 52: 34–37.
- Behmann, U. and Rieckhoff, K. (2011) Converter Stations in 50 or 60 Hz Traction Power Supply. *Rail Technology Review*, 51 (4): 8–14.
- Behmann, U. and Schütte, T. (2012a) Cost effectiveness of using static converters in power supply for 50 Hz railways. *Rail Technology Review*, 52: 2–5.
- Behmann, U. and Schütte, T. (2012b) Static converters-The future of traction power supply. *Rail Technology Review*, 51: 9–15.
- Bhuvaneswari, C. and Babu, R.S.R. (2016) A review on LLC Resonant Converter. *2016 International Conference on Computation of Power, Energy, Information and Communication, ICCPEIC 2016*, pp. 620–623. doi:10.1109/ICCPEIC.2016.7557268.
- Blaabjerg, F., Teodorescu, R., Liserre, M., et al. (2006) Overview of control and grid synchronization for distributed power generation systems. *IEEE Transactions on Industrial Electronics*, 53 (5): 1398–1409. doi:10.1109/TIE.2006.881997.
- Brandt, A., Saniter, C. and Electric, G. (2014) Traction power inverters for Traction power inverters for Australia, 50Hz / 50Hz. *Elektrische Bahnen*.
- British Standards (2010) BS EN 50160:2010+A1:2015 ; Voltage characteristics of electricity supplied by public electricity networks.
- Burlein, C. and Gruber, R. (2013) Dezentrale Umrichter mit neuer Umrichtertechnologie. *Umrichtertechnik*, 111: 412–416.

- Carrara, G., Gardella, S., Marchesoni, M., et al. (1992) A new multilevel PWM method: a theoretical analysis. *IEEE Transactions on Power Electronics*, 7 (3): 497–505. doi:10.1109/63.145137.
- Castro, A.J.M., Rocha, A.P. and Oliveira, E. (2014) “Chapter 20: Protection of A.C. Electrified Railways.” *In Network Protection & Automation Guide*. pp. 85–122. doi:10.1007/978-3-662-43373-7\_5.
- Celli, G., Pilo, F. and Tennakoon, S.B. (2000) “VOLTAGE REGULATION ON 25kV AC RAILWAY SYSTEMS BY USING THYRISTOR SWITCHED CAPACITOR.” *In Ninth International Conference on Harmonics and Quality of Power. Proceedings (Cat. No.00EX441)*. 2000. IEEE.
- CENELEC (2007) BS EN 50163:2004+A1:2007 - Railway applications, Supply voltages of traction systems.
- Chen, B.K. and Guo, B.S. (1996) Three phase models of specially connected transformers. *IEEE Transactions on Power Delivery*, 11 (1): 323–330. doi:10.1109/61.484031.
- Chen, C.L., Wang, Y., Lai, J.S., et al. (2010) Design of parallel inverters for smooth mode transfer microgrid applications. *IEEE Transactions on Power Electronics*, 25 (1): 6–15. doi:10.1109/TPEL.2009.2025864.
- Chen, J.H., Lee, W.J. and Chen, M.S. (1999) Using a static VAR compensator to balance a distribution system. *IEEE Transactions on Industry Applications*, 35 (5): 1177. doi:10.1109/28.793381.
- Chen, M., Li, Q., Roberts, C., et al. (2016) Modelling and performance analysis of advanced combined co-phase traction power supply system in electrified railway. *IET Generation, Transmission & Distribution*, 10: 906–916. doi:10.1049/iet-gtd.2015.0513.
- Chen, M., White, R., Fella, T., et al. (2011) “Multi-conductor train simulations for electrification systems.” *In RRUKA*. 2011. pp. 1–6.

Chen, S.-L., Li, R.-J. and Hsi, P.-H. (2004) Traction system unbalance problem—analysis methodologies. *IEEE Transactions on Power Delivery*, 19 (4): 1877–1883. doi:10.1109/TPWRD.2004.829920.

Chen, T.H. (1994) Comparison of Scott and Leblanc transformers for supplying unbalanced electric railway demands. *Electric Power Systems Research*, 28 (3): 235–240. doi:10.1016/0378-7796(94)90038-8.

Chen, T.H. (2002) Network modelling of traction substation transformers for studying unbalance effects. *IEE Proceedings - Generation, Transmission and Distribution*, 142 (2): 103. doi:10.1049/ipgtd:19951592.

Cozza, A. and Démoulin, B. (2008) On the modeling of electric railway lines for the assessment of infrastructure impact in radiated emission tests of rolling stock. *IEEE Transactions on Electromagnetic Compatibility*, 50 (3 part 2): 566–576. doi:10.1109/TEMC.2008.924387.

Czarnecki, L.S., Chen, G., Starpszyk, Z., et al. (1995) Compensators with thyristor switched inductors operated under degraded power quality: Performance and its improvement. *Proc. PQA 4th Int. Conf. Power Quality, Applications and Perspectives*. pp. 32–34.

Debnath, S., Member, S., Qin, J., et al. (2015) Operation, control, and applications of the Modular Multilevel Converter: A Review. *IEEE TRANSACTIONS ON POWER ELECTRONICS*, 30 (1): 37–53.

DECC (2016) UK Renewable Energy Roadmap - Update 2016. doi:10.1021/es00108a605.

Dehbonei, H., Nayar, C., Ko, S.-H., et al. (2006) Application of voltage- and current-controlled voltage source inverters for distributed generation systems. *IEEE Transactions on Energy Conversion*, 21 (3): 782–792. doi:10.1109/TEC.2006.877371.

Ding, G., Tang, G., He, Z., et al. (2008) New technologies of voltage source converter (VSC) for HVDC transmission system based on VSC. *2008 IEEE Power and Energy Society General Meeting - Conversion and Delivery of Electrical Energy in the 21st Century*, pp. 1–8. doi:10.1109/PES.2008.4596399.

European Commission (2017a) *Electrification of the Transport System: Studies and Reports.*, pp. 1–49. Available at: [ec.europa.eu/newsroom/horizon2020/document.cfm?doc\\_id=46372](http://ec.europa.eu/newsroom/horizon2020/document.cfm?doc_id=46372).

European Commission (2017b) *Electrification of the Transport System: Studies and Reports.*, pp. 1–49.

Feldgun, V.R., Karinski, Y.S. and Yankelevsky, D.Z. (2011) A simplified model with lumped parameters for explosion venting simulation. *International Journal of Impact Engineering*, 38 (12): 964–975. doi:10.1016/j.ijimpeng.2011.08.004.

Feng, J., Chu, W.Q., Zhang, Z., et al. (2017) Power electronic transformer-based railway traction systems: challenges and opportunities. *IEEE Journal of Emerging and Selected Topics in Power Electronics*, 5 (3): 1237–1253. doi:10.1109/JESTPE.2017.2685464.

Gao, Z., Lu, Q., Wang, C., et al. (2019) Energy-Storage-Based Smart Electrical Infrastructure and Regenerative Braking Energy Management in AC-Fed Railways with Neutral Zones.

Gruber, R. and O'Brien, D. (2014) Use of Modular Multilevel Converter (MMC) technology in rail electrification. *Use of MMC Technology in Rail Electrification*.

Hagiwara, M. and Akagi, H. (2009) Control and experiment of Pulsewidth-Modulated Modular Multilevel Converters. *IEEE Transactions on Power Electronics*, 24 (7): 1737–1746. doi:10.1109/TPEL.2009.2014236.

Hagiwara, M., Maeda, R. and Akagi, H. (2011) Control and analysis of the Modular Multilevel Cascade Converter based on double-star. *IEEE Transactions on Power Electronics*, 26 (6): 1649–1658.

Hassanpoor, A., Norrga, S., Nee, H., et al. (2012) Evaluation of different carrier-based PWM methods for Modular Multilevel Converters for HVDC application. *IECON 2012 - 38th Annual Conference on IEEE Industrial Electronics Society*, pp. 388–393.

He, X., Shu, Z., Peng, X., et al. (2014) Advanced cophase traction power supply system based on three-phase to single-phase converter. *IEEE Transactions on Power Electronics*, 29 (10): 5323–5333. doi:10.1109/TPEL.2013.2292612.

Healy, A. (2018) Notification of the overall EC4T tariffs applicable to charter operators in 2018 / 19. London: Network Rail.

Hemici, K., Zegaoui, A., Bokhtache, A.A., et al. (2015) Three-phases flying-capacitor multilevel inverter with proportional natural PWM control. *Energy Procedia*, 74: 1061–1070. doi:10.1016/j.egypro.2015.07.744.

Heuvelmans, M., Modeer, T. and Norrga, S. (2014) Soft-switching cells for high-power converters. *IECON Proceedings (Industrial Electronics Conference)*, pp. 1806–1812. doi:10.1109/IECON.2014.7048747.

Heydt, G.T., Ayyanar, R., Hedman, K.W., et al. (2012) Electric power and energy engineering: The first century. *Proceedings of the IEEE*, 100: 1315–1328. doi:10.1109/JPROC.2012.2187130.

Hill, R.J. (1994) Electric railway traction. Part 3: Traction power supplies. *Power Engineering Journal*, 8 (6): 275. doi:10.1049/pe:19940604.

Hillmansen, S. (2013) Electric railway traction systems and techniques for energy saving., pp. 19–23. doi:10.1049/ic.2012.0071.

Hillmansen, S., White, R., Weston, P., et al. (2016) Multi-conductor model for AC railway train simulation. *IET Electrical Systems in Transportation*, 6 (2): 67–75. doi:10.1049/iet-est.2013.0052.

HM Treasury (2018) *The Green Book. Central Government Guidance on Appraisal and Evaluation*. doi:http://dx.doi.org/10.1016/j.firesaf.2012.10.014.

Hornik, T. and Zhong, Q.C. (2011) A current-control strategy for voltage-source inverters in microgrids based on  $H_\infty$  and Repetitive Control. *IEEE Transactions on Power Electronics*, 26 (3): 943–952. doi:10.1109/TPEL.2010.2089471.

Hossain, M.A., Pota, H.R., Issa, W., et al. (2017) Overview of AC microgrid controls with inverter-interfaced generations. *Energies*, 10 (9): 1–27. doi:10.3390/en10091300.

Huang, C.P., Wu, C.J., Chuang, Y.S., et al. (2006) Loading characteristics analysis of specially connected transformers using various power factor definitions. *IEEE Transactions on Power Delivery*, 21 (3): 1406–1413. doi:10.1109/TPWRD.2005.864076.

Huang, S. and Chen, B. (2002) Harmonic Study of the Le Blanc Transformer for Taiwan Railway' s Electrification System. *IEEE Transactions on Power Delivery*, 17 (2): 495–499.

International Electrotechnical Commission (2008) IEC TR 61000-3-13:2008 ; Electromagnetic compatibility (EMC) - Part 3-13: Limits - Assessment of emission limits for the connection of unbalanced installations to MV, HV and EHV power systems.

International Railway Journal (2013) *Traction choices: overhead ac vs third rail dc.*, February. Available at: [https://www.railjournal.com/in\\_depth/traction-choices-overhead-ac-vs-third-rail-dc](https://www.railjournal.com/in_depth/traction-choices-overhead-ac-vs-third-rail-dc).

Ishikura, N., Hiraki, E. and Tanaka, T. (2009) A constant DC voltage control based strategy for an active power quality compensator used in electrified railways with improved response. *IECON Proceedings (Industrial Electronics Conference)*, pp. 3199–3204. doi:10.1109/IECON.2009.5415311.

Jin, B., Lee, W., Kim, T., et al. (2005) A study on the multi-carrier PWM methods for voltage balancing of flying capacitor in the flying capacitor multi-level inverter. *31st Annual Conference of IEEE Industrial Electronics Society, 2005. IECON 2005*, p. 6 pp. doi:10.1109/IECON.2005.1568993.

Jory, S., Benamraoui, A., Roshan Boojihawon, D., et al. (2016) Net present value analysis and the wealth creation process: a case illustration. *The Accounting Educators Journal*, 26 (December 2018): 85–99.

von Jouanne, A. (2005) Closure on “assessment of voltage unbalance.” *IEEE Transactions on Power Delivery*, 17 (4): 1176–1177. doi:10.1109/tpwrD.2002.805032.

Kalantari, M., Sadeghi, M.J., Fazel, S.S., et al. (2010) Investigation of power factor behavior in AC railway system based on special traction transformers. *Journal of Electromagnetic Analysis and Applications*, 02 (11): 618–626. doi:10.4236/jemaa.2010.211081.

Kang, D.-W., Lee, W.-K. and Hyun, D.-S. (2004) Carrier-rotation strategy for voltage balancing in flying capacitor multilevel inverter. *IEE Proceedings - Electric Power Applications*, 151 (2): 239. doi:10.1049/ip-epa:20040220.

Kazmierkowski, M.P., Krishnan, R., Blaabjerg, F., et al. (2002) *Control in Power Electronics: Selected Problems (Academic Press Series in Engineering)*. Cambridge: Academic Press.

Kneschke, T.A. (1985) Control of Utility System Unbalance Caused by Single-Phase Electric Traction. *Industry Applications, IEEE Transactions on*, I (6): 1559–1570.

Konishi, T., Hase, S., Okui, A., et al. (2003) “Development of PWM converter with large capacity for electric railway substation.” *In The Fifth International Conference on Power Electronics and Drive Systems, 2003. PEDS 2003*. 2003. pp. 1264–1267.

Konstantinou, G.S. and Agelidis, V.G. (2009) Performance evaluation of half-bridge cascaded multilevel converters operated with multicarrier sinusoidal PWM techniques. *2009 4th IEEE Conference on Industrial Electronics and Applications*, pp. 3399–3404. doi:10.1109/ICIEA.2009.5138833.

Krastev, I., Tricoli, P., Hillmansen, S., et al. (2016) Future of electric railways: Advanced electrification systems with static converters for ac railways. *IEEE Electrification Magazine*, 4 (3): 6–14. doi:10.1109/MELE.2016.2584998.

Kulworawanichpong, T. (2003) Optimising Ac Electric Railway Power Flows With Power Electronic Control.

Kunyu, L., Shun, T., Lei, Z., et al. (2018) A balance compensation method based on negative sequence weighted equivalent model of unbalanced load. *Proceedings of International Conference on Harmonics and Quality of Power, ICHQP*, 2018–May: 1–6. doi:10.1109/ICHQP.2018.8378945.

Kwan Lee, C., Ray Chaudhuri, N., Chaudhuri, B., et al. (2013) Droop control of distributed electric springs for stabilizing future power grid. *IEEE Transactions on Smart Grid*, 4 (3): 1558–1566. doi:10.1109/TSG.2013.2258949.

- Ladoux, P., Serbia, N., Marino, P., et al. (2014) Comparative study of variant topologies for MMC. *International Symposium on Power Electronics, Electrical Drives, Automation and Motion (SPEEDAM), 2014*, pp. 659–664.
- Lao, K., Wong, M., Dai, N., et al. (2015) A Systematic Approach to Hybrid Railway Power Conditioner Design With Harmonic Compensation for High-Speed Railway., *62* (2): 930–942.
- Lao, K.W., Wong, M.C., Dai, N., et al. (2018) Analysis of the effects of operation voltage range in flexible DC control on railway HPQC compensation capability in high-speed co-phase railway power. *IEEE Transactions on Power Electronics*, *33* (2): 1760–1774. doi:10.1109/TPEL.2017.2684427.
- Li, F. and Yang, Z. (2010) Analysis and management research on the impact of Shanghai-Nanjing intercity railway traction load on power grid. *CICED 2010 Proceedings*, pp. 1–6.
- Li, S. (2010) *Power flow in railway electrification power system*. New Jersey Institute of Technology.
- Li, Y.W. (2009) Control and resonance damping of voltage-source and current-source converters with LC filters. *IEEE Transactions on Industrial Electronics*, *56* (5): 1511–1521. doi:10.1109/TIE.2008.2009562.
- Liu, H., Dahidah, M., Naayagi, R.T., et al. (2019) Unidirectional DC/DC modular multilevel converter for offshore windfarm with the control strategy based on stationary frame. *The Journal of Engineering*, *2019* (17): 4309–4314. doi:10.1049/joe.2018.8003.
- Liu, Y.-J., Chang, G.W. and Huang, H.M. (2002) Mayr's equation-based model for pantograph arc of high-speed railway traction system. *IEEE Transactions on Power Delivery*, *22* (5): 48–51. doi:10.1109/39.999661.
- Ma, F., Luo, A., Xu, X., et al. (2013) A simplified power conditioner based on half-bridge converter for high-speed railway system. *IEEE Transactions on Industrial Electronics*, *60* (2): 728–738. doi:10.1109/TIE.2012.2206358.

- Mazin, H.E. and Xu, W. (2009) Harmonic cancellation characteristics of specially connected transformers. *Electric Power Systems Research*, 79 (12): 1689–1697. doi:10.1016/j.epsr.2009.07.006.
- Mcgrath, B.P. and Holmes, D.G. (2000) “A Comparison of Multicarrier PWM Strategies for Cascaded and Neutral Point Clamped Multilevel Inverters.” *In 2000 IEEE 31st Annual Power Electronics Specialists Conference*. 2000, pp. 674–679.
- Middleton, W.D. (2002) *When the Steam Railroads Electrified*. Bloomington: Indiana University Press.
- Mori, H. (2000) Chaotic behavior of the Newton-Raphson method with the optimal multiplier for ill-conditioned power systems. *IEEE International Symposium on Circuits and Systems. Emerging Technologies for the 21st Century*, 4: 237–240. doi:10.1109/ISCAS.2000.858732.
- Mott MacDonald (2019) *Electrifying stories*.
- Mousavi Gazafrudi, S.M., Tabakhpour Langerudy, A., Fuchs, E.F., et al. (2015) Power quality issues in railway electrification: A comprehensive perspective. *IEEE Transactions on Industrial Electronics*, 62 (5): 3081–3090. doi:10.1109/TIE.2014.2386794.
- Muttalib, S., Ariful Islam, M., Siddiqa, F., et al. (2012) Improved algorithm for estimating state variables in power system with highly integrated renewable energy sources. *2012 International Conference on Informatics, Electronics and Vision, ICIEV 2012*, (i): 267–270. doi:10.1109/ICIEV.2012.6317322.
- Network Rail (2003) *Technical plan - Section 11, Network Capability*. Available at: <http://www.networkrail.co.uk/documents3177BusinessPlan2003NetworkCapability.pdf>.
- Network Rail (2007) NR/SP/ELP/21085-Specification for the design of earthing and bonding systems for 25 kV A.C. electrified lines.
- Nikhil, K., Mishra, M.K. and Kotra, S. (2015) Power management based on the operating conditions of grid, microgrid and hybrid storage. *2015 International Conference on Renewable Energy Research and Applications, ICRERA 2015*, pp. 1437–1441. doi:10.1109/ICRERA.2015.7418645.

Otto, R.A. and Gbciv, B. (1978) Principles and applications of static, thyristor-controlled shunt compensators. *IEEE Transactions on Power Apparatus and Systems*, 75 (5): 1935–1945.

Peeran, S.M. and Kusko, A. (1985) Tuned filters for traction rectifier sets. *IEEE Transactions on Industry Applications*, I (6): 1571–1579.

Peroutka, Z., Michaílík, J. and Molnár, J. (2009) Single-phase current-source active rectifier for traction applications: New control strategy based on phase shift controller. *EPE Journal (European Power Electronics and Drives Journal)*, 19 (1): 33–39. doi:10.1109/EPE.2007.4417547.

Pilo De La Fuente, E., Mazumder, S.K. and Franco, I.G. (2014) Railway electrical smart grids: An introduction to next-generation railway power systems and their operation. *IEEE Electrification Magazine*, 2 (3): 49–55. doi:10.1109/MELE.2014.2338411.

Pilo, E., Mazumder, S.K. and González-Franco, I. (2015) Smart electrical infrastructure for AC-Fed railways with neutral zones. *IEEE Transactions on Intelligent Transportation Systems*, 16 (2): 642–652. doi:10.1109/TITS.2014.2336535.

Porcarelli, D., Spenza, D., Brunelli, D., et al. (2015) Adaptive rectifier driven by power intake predictors for wind energy harvesting sensor networks. *IEEE Journal of Emerging and Selected Topics in Power Electronics*, 3 (2): 471–482. doi:10.1109/JESTPE.2014.2316527.

Private Communication with Alan Hodge (2019).

Private Communication with Chris Wilson (2019).

Private Communications with Garry Keenor (2019).

Private Communications with Ross MacFarlane (2019).

Quesada, I., Lázaro, A., Martinez, C., et al. (2011) Modulation technique for low frequency harmonic cancellation in auxiliary railway power supplies. *IEEE Transactions on Industrial Electronics*, 58 (9): 3976–3987. doi:10.1109/TIE.2010.2102320.

Rail Industry Decarbonisation Taskforce (2019) *Final report to the minister for rail*. London. Available at: <https://www.rssb.co.uk/Library/improving-industry-performance/Rail-Industry-Decarbonisation-Task-Force-Initial-Report-to-the-Rail-Minister-January-2019.pdf>.

Rail Safety and Standards Board (RSSB) (2009) Engineering Energy storage systems for railway applications Phase 1.

Rail Safety and Standards Board (RSSB) (2010) Energy storage systems for railway applications Phase 2: OHL electrification gaps.

Ranneberg, J. (2007) “Transformerless topologies for future stationary AC-railway power supply keywords state of the art SFC for railway supply SFCs Supplying Catenary without single-phase transformer.” *In 2007 European Conference on Power Electronics and Applications*. 2007.

RIA (2019) RIA Electrification Cost Challenge., (March).

Rocabert, J., Luna, A., Blaabjerg, F., et al. (2012) Control of power converters in AC microgrids. *IEEE Transactions on Power Electronics*, 27 (11): 4734–4749. doi:10.1109/TPEL.2012.2199334.

Rochard, B.P. and Schmid, F. (2000) A review of methods to measure and calculate train resistances. *Proceedings of the Institution of Mechanical Engineers, Part F: Journal of Rail and Rapid Transit*, 214 (4): 185–199. doi:10.1243/0954409001531306.

RSSB (2007) Engineering Safety Management (The Yellow Book): Fundamentals and Guidance v. 1 and 2, Issue 4. London: Rail Safety and Standards Board.

Schmid, F., Goodman, C.J. and Watson, C. (2017) Overview of electric railway systems. *8th IET Professional Development Course on Railway Electrification Infrastructure and Systems (REIS 2017)*, 44 (0). doi:10.1049/ic.2015.0320.

Seimille, D. (2014) Design of power supply system in DC electrified transit railways - Influence of the high voltage network.

Seiphethlo, T.E. and Rens, A.P.J. (2010) On the assessment of voltage unbalance. *ICHQP 2010 - 14th International Conference on Harmonics and Quality of Power*, (1): 1–6. doi:10.1109/ICHQP.2010.5625366.

Senini, S.T. and Wolfs, P.J. (2002) “Novel topology for correction of unbalanced load in single phase electric traction systems.” *In 33rd Annual IEEE Power Electronics Specialists Conference*. 2002. pp. 1208–1212. doi:10.1109/psec.2002.1022340.

Shu, Z., Xie, S. and Li, Q. (2011) Single-phase back-to-back converter for active power balancing, reactive power compensation, and harmonic filtering in traction power system. *IEEE Transactions on Power Electronics*, 26 (2): 334–343. doi:10.1109/TPEL.2010.2060360.

Shu, Z., Xie, S., Lu, K., et al. (2013) Digital detection, control, and distribution system for co-phase traction power supply application. *IEEE Transactions on Industrial Electronics*, 60 (5): 1831–1839. doi:10.1109/TIE.2012.2190959.

Siemaszko, D., Antonopoulos, A., Ilves, K., et al. (2010) Evaluation of control and modulation methods for Modular Multilevel Converters. *The 2010 International Power Electronics Conference Evaluation*, pp. 746–753.

De Souza Ribeiro, A.L., Freijedo, F.D., De Bosio, F., et al. (2018) Full Discrete Modeling, Controller Design, and Sensitivity Analysis for High-Performance Grid-Forming Converters in Islanded Microgrids. *IEEE Transactions on Industry Applications*, 54 (6): 6267–6278. doi:10.1109/TIA.2018.2847635.

Steele, H., Roberts, C. and Hillmansen, S. (2019) Railway smart grids: Drivers, benefits and challenges. *Proceedings of the Institution of Mechanical Engineers, Part F: Journal of Rail and Rapid Transit*, 233 (5): 526–536. doi:10.1177/0954409718800523.

Steimel, A. (2012) Power-electronic grid supply of AC railway systems. *Proceedings of the International Conference on Optimisation of Electrical and Electronic Equipment, OPTIM*, pp. 16–25. doi:10.1109/OPTIM.2012.6231844.

- Sun, J., Duan, Y., Xiong, Y., et al. (2012) Study of reactive power compensation for high speed railway design. *Energy Procedia*, 17: 414–421. doi:10.1016/j.egypro.2012.02.114.
- Sutherland, P.E., Waclawiak, M. and Mcgranaghan, M.F. (2006) System Impacts Evaluation of a Single-Phase Traction Load on a 115-kV Transmission System. *IEEE Transactions on Power Delivery*, 21 (2): 837–844.
- Takeda, M., Hasuike, K., Hisamizu, V., et al. (1993) “Static power conditioner using GTO converters for AC electric railway.” *In Conference Record of the Power Conversion Conference*. 1993. pp. 641–646.
- Tan, P.C., Loh, P.C. and Holmes, D.G. (2005) Optimal impedance termination of 25-kV electrified railway systems for improved power quality. *IEEE Transactions on Power Delivery*, 20 (2 II): 1703–1710.
- Tan, Y.J., Wu, J., Li, H., et al. (2018) Self-Healing Electronic Materials for a Smart and Sustainable Future. *ACS Applied Materials and Interfaces*, 10 (18): 15331–15345. doi:10.1021/acsami.7b19511.
- Tayab, U.B., Roslan, M., Hwai, L.J., et al. (2017) A review of droop control techniques for microgrid. *Renewable and Sustainable Energy Reviews*, 76 (May 2016): 717–727. doi:10.1016/j.rser.2017.03.028.
- Taylor, P., Mcfadden, G., Railway, S., et al. (2010) *Dc Regenerative Braking in the Uk*.
- Tinney, W. and Hart, C. (1967) Power flow solution by Newton’s method. *IEEE Transactions on Power Apparatus and Systems*, PAS-86 (11): 1449–1460. doi:10.1109/TPAS.1967.291823.
- Trias, A. (2018) *Fundamentals of the Holomorphic Embedding Load-Flow Method*. Boston: Now Publishers Inc. Available at: <http://arxiv.org/abs/1509.02421>.
- Ufert, M. (2016) “Static frequency converters for use in 50 Hz railway traction power supply substations.” *In 15 International Conference on Railway Engineering Design and Operation*. 2016. pp. 203–212. doi:10.2495/CR160191.
- United Nations (2015) *PARIS AGREEMENT*.

- Ward, J.B. and Hale, H.W. (1956) Digital computer solution of power-flow problems. *Transactions of the American Institute of Electrical Engineers. Part III: Power Apparatus and Systems*, 75 (2): 398–404. doi:10.1109/AIEEPAS.1956.4499318.
- White, R.D. (2008) *AC 25 kV 50 Hz electrification supply design.*, pp. 7–7. doi:10.1049/ic:20050623.
- White, R.D. (2010) “INTERFACING ELECTRIFICATION AND SYSTEM RELIABILITY.” *In IET Conference on Railway Traction Systems*. 2010.
- Wong, C.K., Dai, N.Y., Wong, M.C., et al. (2012) Hybrid power quality conditioner for co-phase power supply system in electrified railway. *IET Power Electronics*, 5 (7): 1084–1094. doi:10.1049/iet-pel.2011.0292.
- Wu, C., Luo, A., Shen, J., et al. (2012) A negative sequence compensation method based on a two-phase three-wire converter for a high-speed railway traction power supply system. *IEEE Transactions on Power Electronics*, 27 (2): 706–717. doi:10.1109/TPEL.2011.2159273.
- Xia, Y. and Ayyanar, R. (2018) Naturally Adaptive, Low-Loss Zero-Voltage-Transition Circuit for High-Frequency Full-Bridge Inverters with Hybrid PWM. *IEEE Transactions on Power Electronics*, 33 (6): 4916–4933. doi:10.1109/TPEL.2017.2734638.
- Xie, J. and Schmidt, R. (2004) Control of network coupling inverters for directly supplying the 16 2 / 3 Hz traction catenary network Keywords 2 . Basic principle for Control of the decentral inverter stations., pp. 1–6.
- Yu-quan, L., Huang-sheng, H., Guo-pei, W., et al. (2011) Research for the effects of high-speed electrified railway traction load on power quality LIU. *Electric Utility Deregulation and Restructuring and Power Technologies (DRPT)*, pp. 569–573.
- Zhang, J., Li, L., Dorrell, D.G., et al. (2019) Modified PI controller with improved steady-state performance and comparison with PR controller on direct matrix converters. *Chinese Journal of Electrical Engineering*, 5 (1): 53–66. doi:10.23919/cjee.2019.000006.

Zhang, Z., U, B., Kang, J., et al. (2009) A multi-purpose balanced transformer for railway traction applications. *IEEE Transactions on Power Delivery*, 24 (2): 711–718.  
doi:10.1109/tpwr.2008.2008491.